PARAMETRIC SOIL-STRUCTURE MODELING FOR RAPID CLIMATIC DISASTER RESPONSE

A THESIS IN
Civil Engineering

Presented to the Faculty of the University
of Missouri—Kansas City in partial fulfillment of
the requirements for the degree

MASTER OF SCIENCE

by
Rahul Tripathi
B.Tech University College of Engineering, Kota, India, 2011

Kansas City, Missouri
2014

PARAMETRIC SOIL-STRUCTURE MODELING FOR RAPID CLIMATIC DISASTER RESPONSE

Rahul Tripathi, Candidate for the Master of Science Degree

University of Missouri—Kansas City, 2014

ABSTRACT

Global climate changes have seemly caused acerbating impacts on coastal environments in terms of severe meteorological hazards, such as hurricanes and their induced storm surges, flooding, and heavy precipitation. Recent disasters of these types, such as HurricaneSandy, have afflicted millions in coastal communities and resulted in billion dollars of losses. Given disasters at such scales, field-based reconnaissance has become ever demanding than before. In the context of structural and geotechnical damage inspection, it calls for efficient tools that can analyze coastal structures that take a system modeling approach. Such a system approach should consider structuresthat are subjected to a combination of extreme forces and changes of boundary conditions, which may include hydrodynamic wave effects, hydraulic buoyancy, debris impact, and foundation scour.

The objective of this thesis to develop a rapid tool for assessing the vulnerability of coastal structures subjected to climatic impacts. Similar tools have been widely used in Structural and Earthquake Engineering for design and loss assessment, such as the use of a fixed oscillator model characterized by a single parameter of Tn (the natural period of the structure). The direct hazardous impacts considered in this thesis are extreme

hydraulic forces and local foundation scouring that may ultimately cause failure of coastal structures (i.e. collapse). The criteria of success of this tool emphasize that it should be as simple as the oscillator model in Earthquake Engineering and is parametric in terms of a few key (intrinsic) parameters to model the nonlinear behavior of a structure subjected to hydraulic storm surges and foundations scour.

To precede, two research components are conducted. The first is a hypothesis-driven physical modeling experiment, in which a flume-based modeling is conducted to prove that storm surges can attack a structure by simultaneous surging and scouring. In the hydraulic flume, a generic foundation-structure system is placed and is subjected to forced vibration for probing the dynamic properties of the structure model. Test result successfully revealed the formation of foundation scour, the failure of structure, and the progressively modified dynamic characteristics of the soil-structure system.

The second, based on the above flume-based evidence, is to computationally model such the failure of building systems in a reduced order subjected to the combined hazards of storm surges and foundation scour. In this thesis, Ibuild afinite-element (FE) based model using Abaqus software. In this model, the structural system response has been resolved from prototype models to simplified dimensionless model consisting of a single degree of freedom (SDOF) oscillator founded on a square foundation. The footing is embedded in near-field soil modeled using inelastic soil under an undrained condition.

The two primary intrinsic parameters identified in this thesis. The first is theratio of the vertical foundation load N in comparison with the ultimate vertical capacity N_u, expressed through the ratio $\chi = N/N_u$. The second is defined as $a_o = \omega H / v_s$where ω is the

circular frequency of the fixed base structure, H is the height of superstructure and v_s is the shear wave velocity.

Rocking response of the (SDOF) system on nonlinear soil is examined through the general-purpose finite element software Abaqus to perform the parametric analysis, and to establish the failure mechanism of the system. Lightly loaded oscillators tend to uplift from the supporting soil whereas heavily loaded oscillators tend to accumulate settlement and soil yielding is intense. The structural response corresponding to moment-rotation settlement under monotonic loading at the mass center, under loading has been designed to output. The Python-based Abaqus scripting interface is used to realize a client-based model input, which is an extension of the Python object-oriented programming language.

APPROVAL PAGE

The faculty listed below, appointed by the Dean of the School of Computing and Engineering have examined a thesis titled “Parametric Soil-Structure Modeling for Rapid Climatic Disaster Response”, presented by Rahul Tripathi, candidate for the Master of Science degree, and certify that in their opinion it is worthy of acceptance.

Supervisory Committee

ZhiQiang Chen, Ph.D., Committee Chair
Department of Civil and Mechanical Engineering

Jerry Richardson, Ph.D.,
Department of Civil and Mechanical Engineering

Gregory W. King, Ph.D.,
Department of Civil and Mechanical Engineering

TABLE OF CONTENTS

LIST OF ILLUSTRATIONS

Figure Page

LIST OF TABLES

Table Page

ACKNOWLEDGEMENTS

I would like to express my deepest gratitude to my adviser, Dr. ZhiQiang Chen, for his excellent guidance, patience and providing me with excellent atmosphere for doing research. I am sure it would have not been possible without his help. His research attitude and method is truly inspirational. He always encourages me to explore novel ways of doing research. He has invested a lot of time and energy in guiding through my thesis here at University of Missouri-Kansas City.

I would also like to thank my committee members, Dr. Jerry Richardson and Dr. Gregory Kingfor their support and interest in my thesis.

I would like thank Xuan Guo, Jianfei Chen (Max), and Ryan Holmes who as friends were always willing to help and discuss problems with me. It would have been a lonely lab without them.

Finally, and more importantly, I wish to thank my parents, Ajay Kumar Tripathi, Vijay Laxmi Sukhwal, my brother Siddharth Tripathi, for their encouragement, patience and trust in me throughout my studies abroad.

CHAPTER 1

IMPACT OF CLIMATE CHANGES ON CIVIL INFRASTRUCTURE

In this chapter, a brief review climate changes and their impacts on civil infrastructure are discussed with an emphasis on buildings and bridges. Then impact of storm surge Sandy on civil infrastructure is discussed. Finally the goal of this research and the organization of this thesis are stated.

1.1 Climate Changes& Coastal Hazards

Global climate change is expected to affect rate of rising sea level, temperature, precipitation patterns, and the frequency of hurricane and tropical storms. These factors are expected to have substantial impacts on coastal wetland patterns. A variety of coastal systems produce a large number of goods and services that are valuable to society. This diversity has influenced many people to migrate towards coastal area, and even to places that are susceptible to hazards such as storm surges and coastal erosion [1]. Climate change is expected to have important impacts on coastal zones. Many climate factors have relevance to the coast, most notably sea level and the frequency and intensity of extreme events such as cyclones and storm surge.Extensive research has shown that today's hazard potential for many coastal zones will increase because of climate change. Sea level rise produces range of impacts on coastal community that includes inundation and displacement of wetlands and lowlands, erosion and degradation of shorelines and increased coastal flooding during storms [2].

1.2 Impact on Civil Infrastructure

General Description

Road, railways, airport runways, shipping terminals, canals and bridges are examples of structure used for mobility from one place to another. Climate and weather affects the planning, design construction, service life span of these facilities. Transportation system is designed according to local weather and climatic conditions. Every mode of the transportation will be altered from the climatic changes such as flooding of roads, transit systems and airport runways in coastal areas. Climate change impacts transportation mainly through changes in weather extremes such as hot/cold days, severe storms, intense precipitation events and extended droughts and sea level rise. Moderate changes in the climate have little impact on the transportation infrastructure because it is built to accommodate changing weather conditions. However extreme changes in the weather and climate conditions have a considerable impact on transportation, when the limit exceeds the design considerations[3].

Impact on BuildingStructures

Flood damage at the areas close to shoreline is due to waves, velocity flow and flood borne debris, while at areas far from shoreline is due to storm surge. Flood damages to the buildings away from the breaches and within the levee-protected area are due to slow rising water which inundates houses for long period. Most low-rise residential buildings are constructed on shallow foundation with some in deeply embedded pile or column foundation. All these foundations are effective for protecting buildings where waves and surge remains below the floor system, erosion and scouring has no or little influence on the foundation. However when surge and waves exceeds the floor elevation, buildings are subjected to the effect of scouring. Residential buildings such as apartments, reinforced concrete and steel framing

buildings sustains less structural damage as compared to light framed wood or masonry construction as displayed in Figure 1.1 (a &b), but will undergo some damage such as wall collapse when wave action is present [4].

Apart from waves from storm surge and flooding, flood borne debris including small pieces of destroyed buildings, vehicles and shipping container increase the damage in some areas, in some other areas large piles of debris could have sheltered landward buildings from damaging waves.For light framed wood and unreinforced masonry residential structures the effect of storm surge was catastrophic. In coastal communities only ground floor slab and piles of debris of high water mark, remains as evidence of residential construction [5].

(a) (b)

Figure 1.1 (a) Apartment damaged by storm surge and wave action (Biloxi), (b) Condominium building's lowest floor damage due to waves and storm surge [4].

The extent of damage to commercial building depends on the location and flooding conditions. Low rise buildings close to the Gulf were destroyed by the combined effect of storm surge, waves and floating debris. Steel framed commercial buildings performed better due to structural integrity of frame and roof but curtain walls and contents were destroyed.

Flood damage to historic structures is caused due to velocity flow, inundation or rising waters. Historically many buildings were designed near the waterways, and included elevated floors or selected materials that stood up to floodwaters. Elevated foundation allows water to pass underneath and they were impacted only by rising water and not by wave or debris impact. In coastal areas the survivability of the building is checked due to the high velocity flow impact on the buildings. Numerous historic buildings were destroyed by waves and flood borne debris. Damage to historic buildings depends on their elevation, structural system, foundation type. Historic buildings near the open coast were often damaged by waves and flood borne debris [6].

Impacts on Bridge Structures

Hurricane induced storm surge causes most damage to the bridges due to the combination of many forces like wave force acting on the superstructure and substructure of the bridges, buoyancy and uplift force when the bridge becomes inundated, horizontal force due to debris and barges, and scour of foundations. Storm induced loading causes most damage to the bridges built near the water. Damage includes unseating of decks and breaking of parapets due to storm surge. Damage depends upon the connection between decks and bents. Damage due to debris impact is also seen on many bridges. Severe storm surge in the form of combination of buoyant forces and pounding by waves in low elevation spans leads to excessive longitudinal or transverse motion of the bridge decks which leads to unseating of the individual spans. Deck displacement or unseating leads to displaced position between superstructure and sub structure which leads to

loss of support and hence damage. Fixed connection also leads to damage through dowelling which leads to more impact of lateral wave and wind forces resulting in more displacement of the bridge decks. Both moving bridges have a swing and fixed type bridges having continuous or simply supported spans, undergoes lot of damage due to storm surge, with the damaged span being the one with low lying span of the bridge or having elevation at or below the estimated peak storm surge level. For example Figure 1.2 shows the US-90 St. Louis Bridge suffered damage due to the combination of surge and wave loading, which had strong transverse force to unseat majority of the spans. This concrete bridge simply supported by high steel type bearings underwent severe damage due to the surge induced loading, the storm surge force lead to unseating of all western half of the bridge and were submerged in the bay. We need to reconsider the design as these forces were not considered during the design of the bridge which led to human life loss and loss of millions of dollars [7].

Figure 1.2 Span unseating due to storm surge induced loading for US- 90 Biloxi Bridge [7]

Effects of Coastal Vegetation on Hazard Mitigation

Hurricane induced storm surge damages the coastal area if coastal bio-shield (planting a vegetation belt along coastlines) is not present. Coastal bio shield reduces erosion, blocks debris and helps in reducing damage to the structures. It reduces water flow and inundation water depth, while the drawbacks are that they may be ineffective against a catastrophic event, and themselves can become destructive forces to surrounding houses and hurt people if cut down by storm surges. The effectiveness of coastal vegetation in reducing the damage caused by storm surge depends on the forest width, tree density, tree diameter, tree height, ground elevation. Coastal vegetation reduces damage to the structure through the reduction in wave energy of the incoming storm surge. It also helps in reducing the damage to the structures as dense vegetation helps in reducing the intensity of the storm surge when it hits the structures, Coastal vegetation can build elevation by accumulating sand and organic materials, areas surrounded by vegetable coast contains low mound, which helps in reducing the effect of large waves across coastal topography. Coastal vegetation acts as buffer zone by protecting inland areas from woody debris, rocks, and ships. Dense vegetation across coastal region tends to decrease coastal erosion. It can be a source of hazard as woody debris in underwater can cause deaths and damage to human beings [8].

1.3 Case Study: Hurricane Sandy Impact on Civil Infrastructure

HurricaneSandy reminded that United States is vulnerable to significant weather hazards and intense storm events can cause significant damage and disruption to property and infrastructure. Sandy was not notable for its wind intensity rather extremely low atmospheric pressure, and the astronomical high tide combined with other weather systems amplified

flooding consequences and economic and transportation disruption. Hurricane Sandy referred as hurricane sandy, damaged physical infrastructure, coastal infrastructure by the wave action combined with storm surge and high winds. The storm damaged coastal protection structures, bridges, underground utilities, roadway tunnels. Sandy started in the southwestern Caribbean Sea, and moved along the US east coast. The coastlines of the New York and New Jersey was severely affected by the slow movement of the storm coincided with the astronomical high tide devastating storm surge. Flooding is caused due to this storm surge in the ocean level that extends above normal tide level [9].

Impact on Bridges

The entire east coast was flooded from Florida northward to States of New Jersey, New York, and Connecticut underwent highest impact due to greatest inundation and storm surge. Assessment of 8 bridges is done after the storm event, and it was found that except "Mantoloking Bridge" other bridges performed well and were able to remain serviceable immediately after the storm event. Mainly identified impact observed was impact to drawbridge electrical system from flooding, and erosion of soil at bridge approaches and abutments. For Mantoloking Bridge the abutment damaged and was unserviceable for a prolonged period of time. The damage assessment due to hurricane sandy on some notable bridges is as follows [10]

Route 35 – Cheesequake River Drawbridge

The route 35 drawbridge over Cheesequake connects old bridge and Sayreville in Middlesex. Due to storm surge it underwent erosion along the southeast abutment wing wall.

Figure 1.3 Erosion at the southeast abutment wall [10]

Railroad Draw Bridge-Manasquan River

The railroad bridge shown in Figure 1.4was at a low elevation with stringers 3-4 feet above the water, and it had no damage on the north abutment but the south abutment or the moving part of the drawbridge had mechanical damage.

Figure 1.4 Railroad draw bridge at Manasquan River, [10]

Route 35-Manasquan River Draw Bridge

It is located about quarter mile west of the railroad draw bridge and connects Brielle and Point Pleasant beach shown in Figure 1.5. Similar to the railroad bridge there was no damage on the north abutment.

Figure 1.5 North abutment of route 35 Draw Bridge over Manasquan River, [10]

Route 70-Manasquan River Bridge

It connects the towns of Brielle to the north and Brick to the south. It is a large elevated structure with the bridge abutments and piers of concrete or concrete-faced shown in Figure 1.6

Figure 1.6 Route 70 bridges over the Manasquan River, [10]

Impact on Buildings

The damage due to Hurricane sandy mainly consists of damage caused because of inundation and shallow flooding. Lower levels and basement were flooded which resulted in increase of damage. One and two story timber frame houses sustained major damage. Lateral shifting and lifting of foundation occurred which resulted in damage. Scour was particularly observed along father Capodanno Boulevard in midland beach. Streets, curb line, sidewalks, utility poles and house foundation were undermined by sinkholes. Concrete masonry unit block

foundation was damaged, resulted in collapse of timber- frame house above. Due to storm debris in the form of timber decks, trees, cars, deposited inland. Buckling or breaking of Concrete masonry unit walls resulted in tilt, collapse or detachment of the overlying structure. For houses adjacent to the oceans CMU piers performed poor, as compared to inland where they performed better most likely because opening between piers allowed flood water to move through the foundation without building hydrostatic pressure. Sand dunes appeared to have reduced flooding and protected inland neighborhood. Concrete piers get partially damaged and several cracking was observed in reinforced concrete piers and scouring was also observed as shown in Figure 1.7

Figure 1.7 Scouring and cracking observed in concrete piers, [10]

Somehow, vegetation beach and dumes helped to protect home, the damage to the homes was less as compared to the places where these natural features were not present. A vegetation beach buffer protects homes.

Figure 1.8 Damage due to scouring on street, curb, sidewalk and utilities, [10]

1.4 Research Motivation & Objective

Experiments and theory are necessary for predicting the damage caused by extreme climate events on civil infrastructure. In design philosophy, the forces due to combination of many forces such as buoyancy uplift, debris impact and scour of foundationsare not accounted and in term of the response of civil infrastructure to withstand extreme loads coming from the aforementioned multi-hazard strikes. There is a need to understand the structural response when acted by rapid climate action.

This thesis will carry out to develop an efficient tool with a system modeling approach that can analyze structural response when certain key structural response parameters are varied to fully understand the response of structures,soil and interaction that exist in between soil and structure known as soil-structure interaction. The scope of this study is to shed some light on the plastic response of Single Degree of Freedom (SDOF) oscillator in case of static pushover

analysis taking into account the non-linear soil-structure interaction, with variation of two control parameters which affect the system response, in other words perform a parametric study using (SDOF) and finite element method to develop moment-rotation for fully embedded foundation in inelastic soil. The idea for this thesis is to generate large data using parametric variation of control parameters using a solver and then the python based tool can be implemented which provides rapid field based decision making.

1.5 Problem Statement

Given a generic surging event and a fluid-structure interaction instance, hydrostatic force, buoyancy force, hydrodynamic force and debris impact force displayed in Figure 1.9 are the four major forces. In the meantime, due to foundation scouring, there is a modification to the soil-foundation-structure configuration.

The combined effects of hydraulic impact and scouring on modification of structural characteristics have not been fully understood in the literature. Thus it is necessary to study and develop tools for understanding the behavior of simplified soil-structure models using hydraulic loads and scouring conditions. In this thesis (1) Perform hydraulic flume based modeling to develop understanding on the formation of foundation scour, the failure of the structure and progressively modification of the soil-structure system; and (2) Computational Finite-element modeling to provide realistic soil-structure modeling tool.

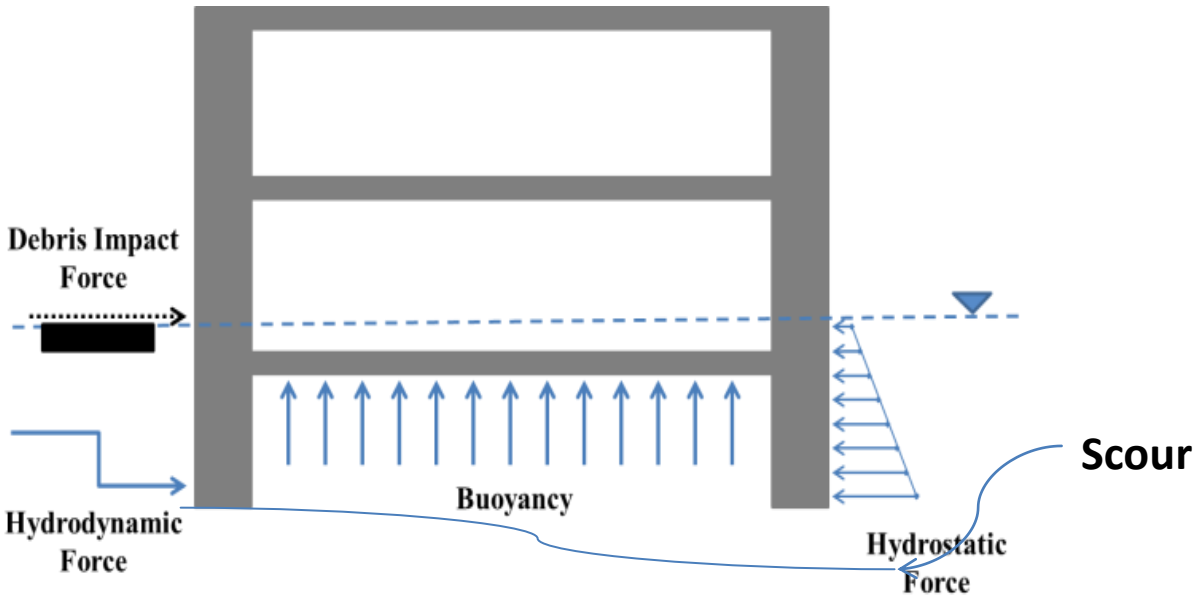

Figure 1.9 Illustration of forces acting on a typical structure subjected to stormsurge and scour.

1.6 Thesis Organization

This thesis is organized as follow

- Chapter1 introduces the subject of this thesis which is about impact of extreme climate on civil infrastructure due to combination of many forces.
- Chapter 2 discusses the forces induced due to storm surge on civil infrastructure and the basic soil-structure interaction impedance functions.
- Chapter3 gives the details of physical modeling method using hydraulic flume and system identification for extracting modal response.
- Chapter4 provides the details of available soil material models in finite element program (FEP).

- Chapter 5 gives the details on numerical modeling of SDOF slender structure on inelastic soil using finite element software abaque cae and the variation of contour parameters using parametric study and extraction of solver's result using python programming.
- Chapter 6gives insight on conclusions drawn fromthis thesis research and future research recommendations.

CHAPTER 2

LITERATURE REVIEW

In this chapter impact of forces induced due to storm surge on civil infrastructure are discussed, and soil-structure interaction impedance function is also

2.1 Introduction

Storm surge and floods as natural disaster has affected coastal community and leads to incalculable economic losses. Floods can be categorized in two main types: riverine and coastal. Riverine floods are caused mainly by the overflow of channels and can be produced by accidental situations such as breaking of dams. Coastal floods are a result from storm surges, unusually high tides, or tsunamis. The impact of forces generated due to storm surge on civil infrastructures needs to be address and the notable forces are hydrostatic and hydrodynamic forces, buoyancy, debris impact and waves on buildings [11].

Flood hazards in coastal areas occur as a result of storm surges and unusually high tides. Riverine flood differs in character from coastal floods due to the difference between current flow and wave action.

2.2 Storm-Surge Induced Forces

Hydrostatic forces

Hydrostatic forces are results from vertical and lateral forces that act on a building from standing or slow moving water. Lateral hydrostatic forces are applied to a building face at a point 2/3 below the depth of the Stillwater elevation and are generally not sufficient to cause deflection or displacement of a building unless there is difference in water elevation on opposite sides of

the wall in contact with the floodwater. Figure 2.1 shows an example of a building failure due to lateral and vertical hydrostatic forces. Structure was detached from the foundation and moved during the flood event.

$$F_s = \int \rho g h dA \qquad 2.1$$

Where ρ is the mass density of water.

g is the gravitational acceleration.

h is the depth of floodwater.

A is the surface area of the wall in contact with water.

Figure 2.1 Failure due to hydrostatic forces [12]

Hydrodynamic forces

Hydrodynamic forces are the forces which act on a structure due to moving water around exterior walls. These loads impacts all sides of the building: directly to the exterior wall perpendicular to the flow of water, drag along the exterior walls parallel to the flow of water and

suction along the exterior walls opposite to the seaward face.These forces are a function of floodwater velocity and the building geometry. The location of a building within a floodplain predicts whether or not it will be acted by the hydrodynamic forces. The hydrodynamic force can impact a building at localized points when the flow velocity is increased unevenly around a building.

The most common means of reducing the damage to buildings due to hydrodynamic forces is by elevating the floor of the structure so that it is above the expected design flood elevation and anchor it properly to an open foundation [12].

$$F_D = 0.5 \int C_D \rho V^2 \, dA \qquad 2.2$$

Where

h = height of the wall.

V = intensity of the velocity component orthogonal to the object.

C_D = drag coefficient which varies with building geometry and flow conditions.

Debris Impact Force

The force acting on a building by objects carried by moving floodwater is termed as Debris impact force. The magnitude of debris impact is difficult to predict due to uncertainties including floodwater velocity, velocity of the waterborne object, geometry and weight of the object, section of the building and duration of the impact.Figure 2.2 shows an example of impact and damage due to debris onEstimation of the debris impact force F is equated using the expression of impulse-momentum in equation 2.3.

Figure 2.2 Damage as a result of debris impact [12]

$$F_D = \int d\,(m_d V) \qquad 2.3$$

Where:

m_d = mass of the debris

t = contact time between object and wall.

Buoyancy Force

Buoyancy force is the net result of hydrostatic forces acting in a vertical direction on the bottom of buildings, these uplift forces can result in the building or parts of its structure to float if the building is not properly anchored. In addition to these uplift forces, lateral pressures may then displace the floating building or part of the structure causing damage, destabilization or even complete destruction. The buoyancy force acting on the bottom area is determined as

$$F_B = \int \rho g h \, dA_b \qquad 2.4$$

Where

ρ is the mass density of water

g is the gravitational acceleration

h is the depth of floodwater

A_b is the bottom surface area of the wall in contact with water

2.3 Scour

Scour is defined as the erosive action of flowing water, excavating and carrying away material from the bed and banks of streams and from around the piers and abutments of bridges. Scouring action is predominantly more in loose granular soils as compared to the cohesive or cemented soil.It involves removal of material from around piers, abutments, spurs, and embankments. It is caused by an acceleration of flow and resulting vortices induced by obstructions to the flow. The basic mechanism causing the local scour at piers or abutments is the formation of vortices called as horseshoe vortex along their base. The horseshoe vortex results acceleration of flow around the nose of the pier or abutment die to the pileup of water on the upstream surface of the obstruction. The removal of the bed material around the base of the obstruction is due to the action of the vortex. The transport rate of sediments away from the base region is greater as compared to transport rate into that region and consequently a scour hole develops. The strength of the horseshoe vortex reduces due to the increase in the depth of the scour, thereby reducing the transport rate from the base region. For clear-water scour, scouring ceases when the shear stress due to the horseshoe vortex equals the critical shear stress of the sediment particles at the bottom of the scour hole [13].

In addition to the horseshoe vortex around the base of a pier, there are vertical vortices downstream of the pier called the wake vortex. Both vortex horseshoe and wake removes material from the pier base region, however the intensity of wake vortices reduces as the distance downstream of the pier increases. The factors that affect the magnitude of local scour depth at piers and abutments are

- Velocity of the approach flow.
- Depth of flow.
- Width of the pier.
- Discharge intercepted by the abutment.
- Length of the pier if screwed to flow.
- Size and gradation of bed material.
- Angle of attack of the approach flow to a pier or abutment.
- Shape of a pier or abutment.
- Bed configuration.
- Ice formation or jams and debris.

Local scour at piers is a function of bed material, bed configuration, flow characteristics, fluid properties, and the geometry of the pier and footing. Bed materials are characterized by granular or non-granular, cohesive or non-cohesive, erodible or non-erodible rock. The velocity, depth at the upstream of pier, the angle the velocity vector makes with the pier and the free surface or pressure flow are the flow characteristics of interest for local pier scour. Pier geometry characteristics are its type, dimensions, and shape. Piers can be single column, multiple columns, or rectangular; with or without friction. The important dimensions are the diameter for circular piers or columns, spacing for multiple columns, and width and length for solid piers.

Local Pier Scours

The determination of pier scours for both live-bed and clear-water is based on the prediction of maximum pier scour depths. The equation is

$$\frac{y_s}{y_1} = 2.0 K_1 K_2 K_3 K_4 \left(\frac{a}{y_1}\right)^{0.65} Fr_1^{0.43}$$

2.5

Where

y_s = Scour depth

- y_1 = Flow depth directly upstream of the pier
- K_1 = Correction factor for pier nose shape from Table 2.1
- K_2 = Correction factor for angle of attack of flow from Table 2.2
- K_3 = Correction factor for bed condition from Table 2.3
- K_4 = Correction factor for armoring by bed material size
- a = Pier width
- L = Length of pier
- F_{r1} = Froude number directly upstream of the pier
- V_1 = Mean velocity of flow directly upstream of the pier
- g = Acceleration due to gravity.

Table 2.1Correction Factor, K_1 for Pier Nose Shape [13]

Shape of Pier Nose	K_1
Square nose	1.1
Round nose	1.0
Circular cylinder	1.0
Group of Cylinders	1.0
Sharp nose	0.9

The correction factor K_2 for angle of attack of the flow is calculated using the following equation

$$K_2 = (Cos\theta + \frac{L}{a} Sin\theta)^{0.65} \quad 2.6$$

Table 2.2 Correction Factor, K_2 for Angle of Attack of the Flow [13]

Angle	L/a = 4	L/a = 8	L/a = 12
0	1.0	1.0	1.0
15	1.5	2.0	2.5
30	2.0	2.75	3.5
45	2.3	3.3	4.3
90	2.5	3.9	5.0

Table 2.3 Increase in Equilibrium Pier Scour Depths, K_3 for Bed Condition [13]

Bed Condition	Dune Height	K3
Clear-Water Scour	N/A	1.1
Plane bed and Antidune flow	N/A	1.1
Small Dunes	3 > H > 0.6	1.1
Medium Dunes	9 >H >3	1.2 or 1.1
Large Dunes	H > 9	1.3

2.4 Soil-Structure Interaction Concepts

The influence of seismic waves during earthquake deforms soil which carries deformation dynamically with the foundation and supporting structure. The inertial force induced in superstructure generates dynamic stresses at the foundation that are transmitted into the supporting soil. Thus, superstructure-induced deformations develop in the soil while the additional wave deforms the soil-foundation interface. The above phenomenon occurs simultaneously and is separated into two successive phenomena referred to as Kinematic interaction and inertial interaction [14].

Assessment of Foundation Springs and dashpots

During earthquake the first step for soil-structure interaction is to determine the foundation impedance corresponding to each mode of vibration. For rigid foundation, there are six modes of vibration: three translational (dynamic displacements along the axes x, y and z) and three rotational (dynamic rotations around the same axes). For each mode, soil can be replaced by a dynamic spring of stiffness K and by a dashpot of modulus C. Figure 2.3 displays the

vertical spring and dashpot of an embedded foundation subjected to harmonic vertical force with amplitude P_z and frequency$\boldsymbol{\omega}$.

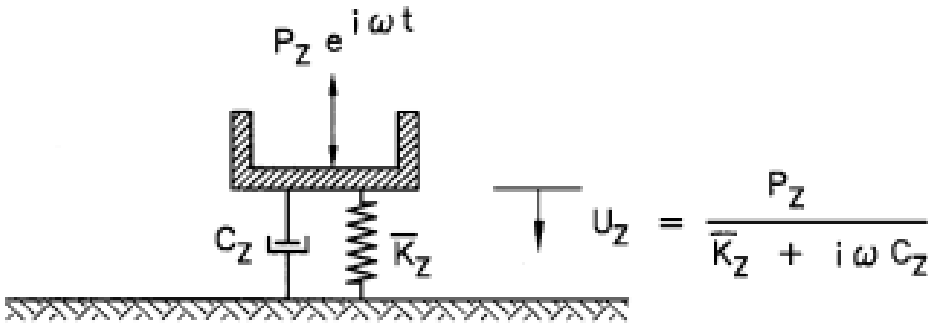

Figure 2.3 Interpretation of dynamic spring and dashpot in vertical mode of vibration [14]

Due to the force the foundation experiences a harmonic steady-state displacement which has the same frequency but is out-of-phase with the force. Thus the displacement can be expressed as

$$u_z(t) = u_z \cos(\omega t + a + \phi) \qquad 2.7$$

Alternatively it can be written as

$$u_z(t) = u_1 \cos(\omega t + a) + u_2 \sin(\omega t + a) \qquad 2.8$$

Where the amplitude u_z and phase angle are related to the in phase u_1 and out of phase component u_2 as

$$u_z = \sqrt{u_1^{\,2} + u_2^{\,2}} \qquad 2.9$$

$$\tan\phi = \frac{u_2}{u_1} \qquad 2.10$$

In complex notation

$$P_z(t) = \overline{P}_z \exp(i\omega t) \quad 2.11$$

$$u_z = \overline{u}_z \exp(i\omega t) \quad 2.12$$

Where P_z and u_z are complex quantities

$$\overline{P}_z = P_{z1} + iP_{z2} \quad 2.13$$

$$u_z = u_{z1} + iu_{z2} \quad 2.14$$

With P_z and u_z being out of phase, the dynamic vertical impedance (force-displacement ratio becomes

$$\kappa_z = \frac{\overline{P}_z}{\overline{u}_z} \quad 2.15$$

$$\kappa_z = \overline{k}_z + i\omega C_z \quad 2.16$$

Both stiffness and dashpot are the functions of frequency. The spring constant K_z, termed as dynamic stiffness, reflects the stiffness and inertia of the supporting soil, the dashpot C_z reflects two types of damping (radiation and material) damping generated in the system. Similarly the impedance function can be written for each of the other five modes of vibration. For example the lateral impedance is the ratio of the horizontal harmonic force over the resulting harmonic displacement in the same direction.

$$\kappa_y = \frac{\overline{P}_y}{\overline{u}_y} \quad 2.17$$

$$\kappa_y = \overline{K}_y + i\omega C_y \quad 2.18$$

Static Impedance

The most important geometric and material factors affecting the dynamic impedance of a foundation are the foundation shape (circular, strip, rectangular, arbitrarily), the type of soil

profile (deep uniform or multi-layer deposit, shallow stratum or rock), and the embedment depth (surface foundation, embedded foundation or pile foundation).

Surface foundation on homogeneous half space

For a rectangular foundation having dimensions of 2B by 2L impedance for six modes of vibration can be computed using the following parameters

- Ab, I_{bx}, I_{by}, I_b are area, moment of inertia about x, y, and polar moment of inertia about z, of the actual soil foundation contact surface.
- B and L are the semi-width and semi length of the circumscribed rectangle.
- G, υ， V_s, and V_{La} are the shear modulus , Poisson's ratio, shear wave velocity, and "Lysmer's analog" wave velocity which is related to the shear wave velocity as

  $$V_{La} = \frac{3.4}{\pi(1-\upsilon)} V_s$$

- $\boldsymbol{\omega}$ is the cyclic frequency in rad/s.

Table 2.4 Stiffness for foundation of rectangular shape on homogeneous half space surface[14]

Response mode	**Static Stiffness**	
	Rectangle (B/L =2)	Rectangle (B/L = 4)
Vertical	$K_z = \frac{3.3GL}{1-\upsilon}$	$\frac{2.55GL}{1-\upsilon}$
Horizontal, y (lateral direction)	$K_y = \frac{6.8GL}{2-\upsilon}$	$\frac{5.54GL}{2-\upsilon}$
Horizontal, x (longitudinal direction)	$K_x = \frac{4.9(1-1.4\upsilon)}{(2-\upsilon)(0.75-\upsilon)}GL$	$\frac{3.9(1-1.4\upsilon)}{(2-\upsilon)(0.75-\upsilon)}GL$
Rocking, r_x (around x axis)	$K_{rx} = \frac{0.82GL^3}{1-\upsilon}$	$\frac{0.2GL^3}{1-\upsilon}$
Rocking, r_y (around y axis)	$K_{ry} = \frac{2.46GL^3}{1-\upsilon}$	$\frac{1.62GL^3}{1-\upsilon}$
Torsional	$K_t = 3.5GL^3$	$2.1GL^3$

2.5 Basic Soil-Structure Formulation

The objective of system identification is to find the unknown properties of a system using a known input into and output from that system. For buildings system identification is used to estimate modal frequencies, damping ratio, mode shapes and participation factors. Non parametric system identification in frequency domain estimates the ratio of output/input motions; the locations of the peaks are used to identify modal periods and the width, height depicts the damping. Parametric system identification use discrete time domain data and transforms it into Laplace domain, where a transfer function can be evaluated that represents the ratio of output/ input motions. Modal periods and damping ratios are related to the location of the peaks of the transfer function [15].

In this experiment the excitation is imposed at the top of the structure by a shaker mounted at the top of the structure, the equation of motion for the system subjected to forced vibration at the top is derived in Laplace domain, the structure is considered to have a mass matrix m, a stiffness matrix k and a damping matrix c the relative displacement in the structure relative to the base is described by vector u, with corresponding velocity and acceleration vectors. The well-known equation of motion of the superstructure is [16]:

$$m\,\ddot{u}\,(t) + c\,\dot{u}\,(t) + k\,u(t) = F\,(t) \tag{2.19}$$

The concept of idealizing a soil- structure system with a 2-D single or multiple degree of freedom oscillator supported on a rigid, shallow foundation was initiated in the 1970's. Figure 2.4 consists of a general soil-structure model, which follows this idealization concept. The model consists of a centered mass, which is located at the top of a superstructure with a specified height and a specified translational stiffness. The superstructure rests on a rigid, massless foundation which is located on a linear elastic half space that represents the soil, the soil foundation is considered to rest on mechanical springs with damping dashpots, the corresponding stiffness and damping is related to the impedance function using complex variables $\tilde{K} = K + i\omega C$ where K is the foundation stiffness, C is the foundation damping coefficient and ω is the driving frequency and the basic foundation impedance sets for the modes are represented as K_h and C_h foundation sliding and K_ϕ and C_ϕ foundation rocking.

"The period lengthening ratio" (PLR) is defined as ratio of the first mode period of the fixed base structure to the natural period of the soil- structure system. The classical solution to compute (PLR) for the oscillator is [17].

$$\frac{f_1}{\tilde{f}} = \sqrt{1 + \frac{k_1}{k_f} + \frac{k_1 h^2}{k_\theta}} \tag{2.20}$$

Where k_f and k_Θ are the foundation stiffness in the sliding and rocking directions.

Besides the fixed base superstructure frequency, two additional system frequencies can be defined for the basic soil-structure interaction modes: (i) the rigid body system frequency due to foundation sliding f_f, and (ii) the rigid body system frequency due to foundation rocking f_Θ. Using these definitions the following relation is obtained [18].

$$\frac{1}{\tilde{f}^2} = \frac{1}{f_f^{\,2}} + \frac{1}{f_\theta^{\,2}} + \frac{1}{f_1^{\,2}} \qquad (2.21)$$

Another important aspect of soil-structure interaction is the system damping contributed by the foundation damping, [19] provides an approximation of the soil structure system damping due to augmentation of foundation damping:

$$\tilde{\xi} = \left(\frac{\tilde{f}}{f_f}\right)^3 \xi_f + \left(\frac{\tilde{f}}{f_\theta}\right)^3 \xi_\theta + \left(1 - \left(\frac{\tilde{f}}{f_1}\right)^2\right) \xi_{mat} + \left(\frac{\tilde{f}}{f_1}\right)^3 \xi_1 \qquad (2.22)$$

Where ξ_f and ξ_Θ denote the foundation damping ratios due to the foundation sliding and the foundation rocking, respectively; ξ_{mat} is the soil damping ratio as a result of hysteresis and ξ_1 is the material damping ratio of the superstructure.

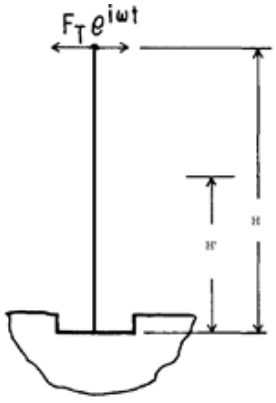

Figure 2.4 Simplified Soil Structure interaction model

2.6 Types of Nonlinearity in Soil-Structure Foundation Response

Sliding at the soil-foundation interface- This type of nonlinearity would take place whenever the transmitted horizontal force exceeds the frictional resistance at the interface. Earthquake has oscillatory nature of shaking, only short period of exceedance usually exist in one direction and hence sliding is not associated with failure, but with permanent irreversible deformations, the magnitude of deformation due to sliding should be very small and should not be structurally detrimental. Due to large value of coefficient of friction at soil footing interface, its practical significance for foundation is limited.

Separation and uplifting of the foundation from the soil. This would happen when the overturning moment at foundation due static force produce net tensile stress at the edge of the foundation. Rocking oscillations in which uplifting takes place involve primarily geometric nonlinearities. As compared to overturning, the vertical settlements due to vertical load may be minor. In some cases footing uplifting is beneficial as it help reduce ductility demands on columns.

Mobilizations of bearing capacity failure mechanism in the supporting soil- In static geotechnical analysis large factor of safety are introduce to ensure that bearing capacity modes of failure are not even approach. Inelastic deformation means permanent rotation needs to be checked for bearing capacity failure case [20].

2.7 Available Soil-Structure Analysis Methods

Impedance Method

Impedance function represents the frequency-dependence stiffness and damping characteristics of foundation-soil interaction. It calculates the foundation stiffness and damping for horizontal, translational and rotational vibration modes.

Introduction

Soil-structure interaction (SSI) has a significant effect on the response of structures. The main step involved in the SSI analysis is the evaluation of soil impedances. Foundation displacement predictions are based on impedance functions. These impedance functions are used to create a model of soil in which foundation rests as an equivalent system of springs and dampers.Dimensionless frequency is used as the basic parameter to show the variation of impedance functions and damping for a structure with a fixed base frequency the impedance function is represented by

$$\bar{K}j = k_j(a_o, v) + i\omega c_j(a_o, v) \tag{2.23}$$

Herein, j denotes deformation mode or rocking mode, ω is the angular frequency, a_o is the dimensionless frequency defined as $a_o = \omega r / V_s$, r is the foundation radius Vs is the shear wave velocity and υ is the soil Poisson ratio. Foundation radii are computed for translational and rotational deformation modes, with the actual foundation. The real stiffness and damping of the translational and rotational springs and dashpots are expressed by

$$k_u = \alpha_u K_u \; ; \; c_u = \beta_u \frac{K_u r_u}{V_s} \tag{2.24}$$

$$k_\theta = \alpha_u K_\theta \; ; c_\theta = \beta_\theta \frac{K_\theta r_\theta}{V_s} \tag{2.25}$$

Herein, α_u, β_u represents the frequency dependence of the impedances terms and K represents the static stiffness of a disk on a half space [21].

Embedded Foundations

The impedance of embedded foundations can be modeled either by coupling the increased static stiffness of embedded foundations with frequency dependent terms for surface foundation or by using analytical solutions for the impedance of a rigid foundation embedded into a half space that account for soil interaction effects. The static stiffness of shallowly embedded foundations (e/r < 1) in a half space is approximately as follows:

$$(K_u)_E = K_u (1 + \frac{2}{3}\frac{e}{r}); \; (K_\theta)_E = K_\theta \, (1 + 2\frac{e}{r}) \tag{2.26}$$

For small embedment ratios (i.e foundation embedment/radius, e/r <0.5), coupling impedance terms are small relative to displacement and rocking stiffness terms.

Cone Model

Soil-Structure has considerable effects on the response of structures. Various numeric techniques solutions are already developed by many researchers to calculate the response of foundation. Alternative way to the rigorous solutions is the advancement of some simplified models such as Cone Models which are relatively simple when compared to numerical techniques. Cone models were developed based on the work done by, where cones were used to model a foundation on the surface of a homogeneous half space for vertical and horizontal motions. The treatment of material discontinuities at the interface of a layer to the half space was explained[22]. At boundaries of the layers to a half space were traced by their own cones with cross-section properties increasing in the wave propagation direction.

Cone models can capture vertical, horizontal and torsional dynamic stiffness of a soil layer, for example for a disk lying on a half-space, the vertical dynamic stiffness whose area increases with depth. The dilatational wave propagates from the surface to infinity along the bar axis. For an infinitesimal element the equilibrium equation can be solved both directly in time and frequency domain and hence the equivalent spring stiffness and damper constants can be determined. Soil can be then replaced by a spring and a damper in the vertical direction. Cone models can be used for both surface foundation and embedded foundation for all degree of freedom.

Winkler Model

The response of caisson embedded foundation in an elastic half space was captured by Winkler model, wherein the Winkler spring stiffness and damping parameters were obtained. The major limitation of that model is that nonlinear behavior of soil was not taken into account, and that the caisson assumed to remain in complete contact with the surrounding soil. Due to complex interaction of soil-caisson interaction involving complex material and geometric non linearity's such as soil inelasticity, separation of caisson and the soil, base uplifting and even loss of soil strength. Moreover the caisson periphery generates waves leading to radiation damping which is influenced by such nonlinearities [23]. The problem of caisson embedded in cohesion less or cohesive soils subjected to lateral loading is shown as

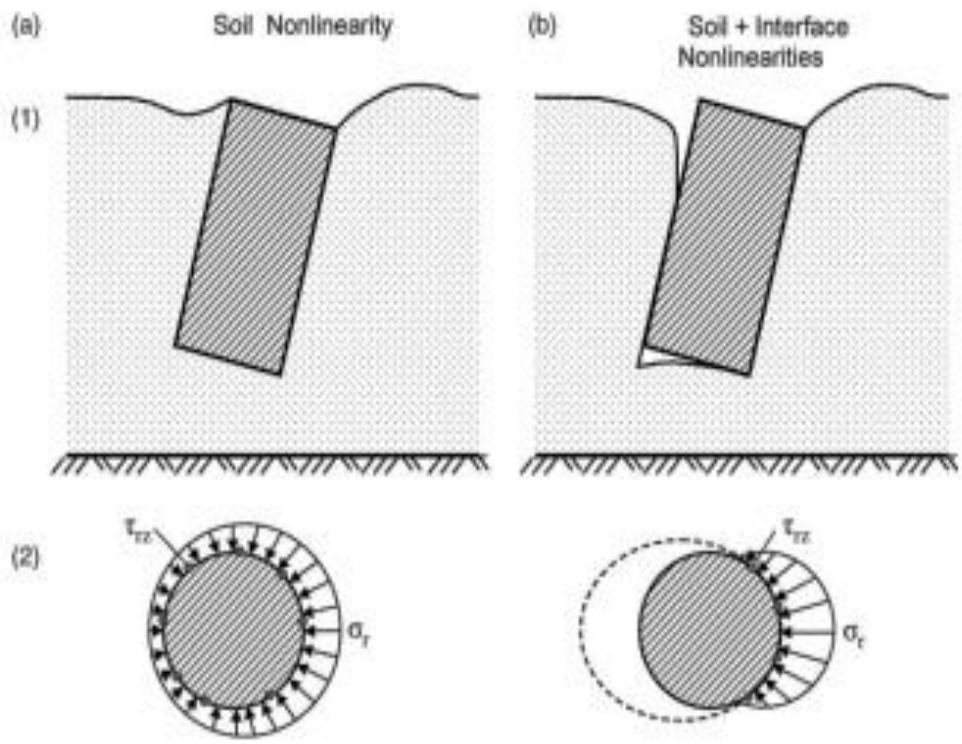

Figure 2.5 General problem of caisson embedded in a cohesionless (left) and in a cohesive soil and subjected to lateral loading, (1) caisson lateral displacement (2) distribution of normal and vertical shear near caisson section. [23]

Winkler Multi Spring Model

A static and dynamic Winkler model incorporates distributed lateral translational and rotational springs along the height of caisson and shear and moment inelastic springs at the base of the caisson. For dynamic problem viscoplastic dashpots are attached in parallel with each spring. The horizontal soil reaction on the side of the caisson is associated with the nonlinear lateral translational springs and dashpots. The separation of the caisson from the soil is modeled with these springs and dashpots. The moment produced by the vertical shear stresses on the perimeter of the caisson is associated with nonlinear rotational springs, which also models slippage at the caisson-soil interface. The horizontal shearing force on the base of the caisson is associated with a nonlinear base shear translational spring and dashpot. A nonlinear base

rotational spring and dashpot represents the moments produced by normal pressures on the base of the caisson, which indeed also models the uplift at the caisson base [24]. The proposed Winkler model is shown as

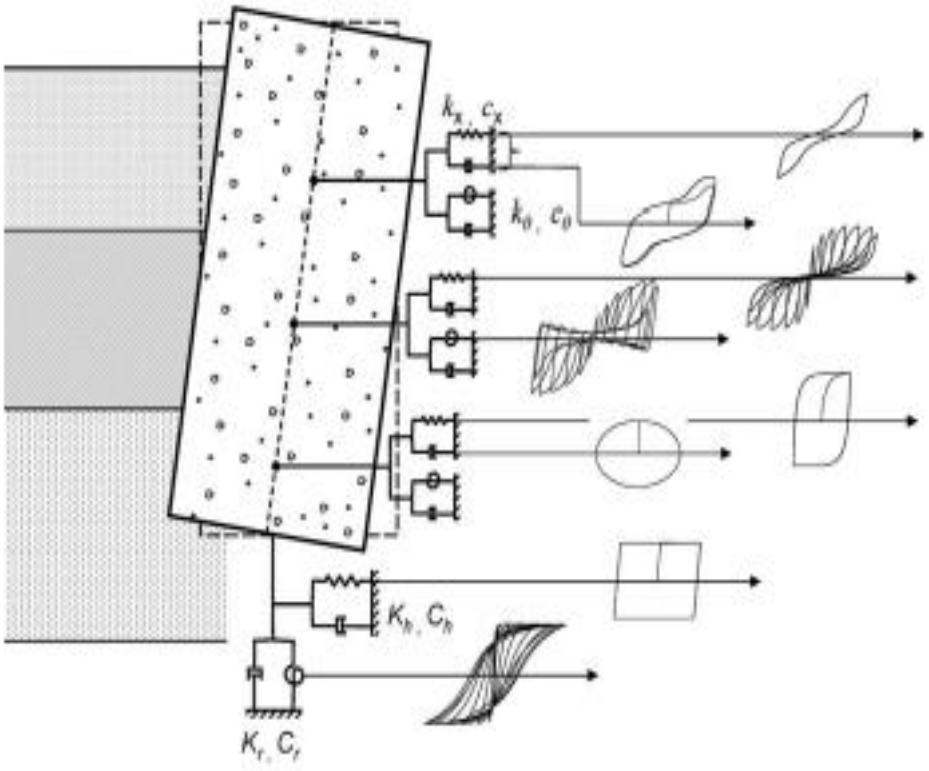

Figure 2.6 Nonlinear Winkler Model [23]

Macro element Approach

A non-linear soil-structure macro-element for shallow foundation represents the behavior of foundation under cyclic loading representing the material non-linearity of the soil under the foundation yielding as well as geometrical non-linearity at the soil-structure interaction. Foundation Uplift reduces the forces in the structure; macro element represents an efficient tool in designing a structure-foundation system [25]

Proposed Macro-Element Model

Assuming the foundation to be a rigid body, its movement is described by the foundation center, the response of soil-foundation system is thus modelled through the forces at the base of foundation and through kinematic displacements i.e. vertical, horizontal and rotational displacement at the center. Macro-element is built around two models one in plasticity and one in uplift, separated but coupled. The reduction of the foundation width in contact during uplift induces stresses in the foundation, which in turn modifies the uplift behavior of the foundation leading to larger soil yielding. The vertical, horizontal and rotational displacements are calculated for a given forces by adding the different components elastic and plastic displacements issued from the plasticity model and uplift displacement issued from the uplift model. Foundation uplift induces rotation and vertical displacement which are deducted from the uplift model for an elastic soil. They are then coupled with plasticity, and due to coupling the uplift becomes partially irreversible and moment becomes a function of the foundation bearing capacity [26].

Macro-element Components

The basic p-y method (beam on elastic foundation) approach does not address the specified aspects such as gapping and elastic reloading and unloading cycles. Macro-element as single degree of freedom is used to incorporate these aspects whereas sub elements are modeled for a specific interaction and are assembled into a composite element.

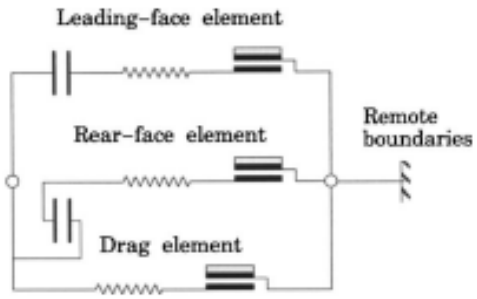

Figure 2.7 Macro element and its components [25]

Basic Elements

The interaction element shown in above figure is an assembly of various basic sub elements. The drag element models the frictional forces along foundation-soil interface. It possesses a parameter defining ultimate drag stress and frictional stiffness, which determines the shear displacements between the foundation and the surrounding soil. The governing equation of this element is identical to the classical rate independent, elastic perfectly plastic element.

The Gap element is used to model the gap contact arises due to gapping in foundation soil under cyclic loading resulting in inelastic deformations, gap accrue at their interface. Gap opening and closing can be achieved with a projection operator which maps a transmitted stress through a gap, when the gap is open no stress is transmitted and stress is perfectly transmitted when the gap is closed.

Two Dimensional Fully embedded Finite element Model

The main target to develop different models is to capture accurately the soil impedances for a wide variety of vibration frequencies. The formulation of relatively more complex discrete models leads to achieve acceptable matches for impedance functions over a wide range of excitation frequencies. A new discrete model is proposed for structures supported on a foundation embedded in a more advanced developed modified cam clay soil material model [27].

Proposed Discrete Model

A single-degree of freedom oscillator on a foundation supporting an elastic tall system embedded in modified cam clay soil model is being proposed, the modulus of elasticity of beam element is so chosen to achieve a structure with a fixed base natural period. A horizontal load is applied on the top of the structure which induces primarily an overturning moment and a secondary shear force, the footing eventually uplifts from the soil, inducing strong inelastic soil response, under progressively increasing lateral loads the foundation uplifts from the ground and failure mechanism develops in the modified cam clay soil model [28].

CHAPTER 3

PHYSICAL MODELING METHODOLOGY AND SYSTEM IDENTIFICATION

In this chapter hydraulic flume test is performed to capture the key response due to forces discussed in previous chapter. The experimental verification is performed usingcomparison of the numerical Eigen data (natural frequencies and mode shapes) with the Eigen data acquired from the modal tests. System identification is done to extract the system's modal characteristics such as natural frequencies, mode shapes.

3.1 Experimental Plan and Results

Model Structure and Forced-Vibration Method

A small-scale foundation structure system was designed in this effort ('Model'). The Model meets several pre-established parameters. The tower portion consists of a non-corrosive 304 Steel Alloy, while the baseplate is 316 Steel Alloy. Since the entire baseplate would be submerged, higher grade steel was chosen to prevent corrosion. The baseplate was affixed to the superstructure using 4 bolts, so as to provide a rigid connection. Second, the size must accommodate four accelerometers (EVAL-ADXL345Z, Analog Devices Inc.) and one shaker-motor (ROB-09238, Sparkfun Electronics). Figure 3.2 shows the setup position for sensors, circuit board, and motor where the sensors are aligned in the x direction parallel with the axil of the motor. Lastly, the design must maintain some scalability to a generic structure but is not to represent any particular structure. A cylindrical column of 13.5 inches tall with a diameter of 2.5 inches connected to a rectangular baseplate (3.5 x 3.5 x 0.75 inches) was chosen such that the bearing load on the soil was 1.78 psi (12.1 kpa) and is about $1/20^{h}$ the bearing stress of a pier. So under 20-g conditions, the bearing stress would be the same. Using a more general approach, a

universal and scientific approximation can be determined which can then be compared to existing models for cylindrical piers.

Flume and Test Setup

The rectangular flume design for this experiment had the dimensions of 4 inches wide with an 18 inch long segment filled with sand where the structure was to be placed. The base of the entirety of the flume is made of steel, save for the sand trap, to which the sand was filled level with the existing steel. Just as Figure 3.1 displays, the flume was horizontally leveled in order to reduce flow velocities to be similar with open channel flow. Sufficient length of flow was also provided to reduce turbulence and promote laminar flow [29].

Figure 3.1Flume setup and design prior to first test and (b) closed view of the Model with the motor and sensors [29]

The focus of this study was clear water scour over coarse grain soils. Scour formation completes itself when the critical shear caused by the horseshoe vortex equilibrates with the sediments critical shear at the bottom of the scour hole (HEC-13). Coarse grained soil was chosen to remove consolidation from the variables of localized displacement and because the

scour associated with storm surge would be less of a cyclical process and closer to bridge pier flooding.

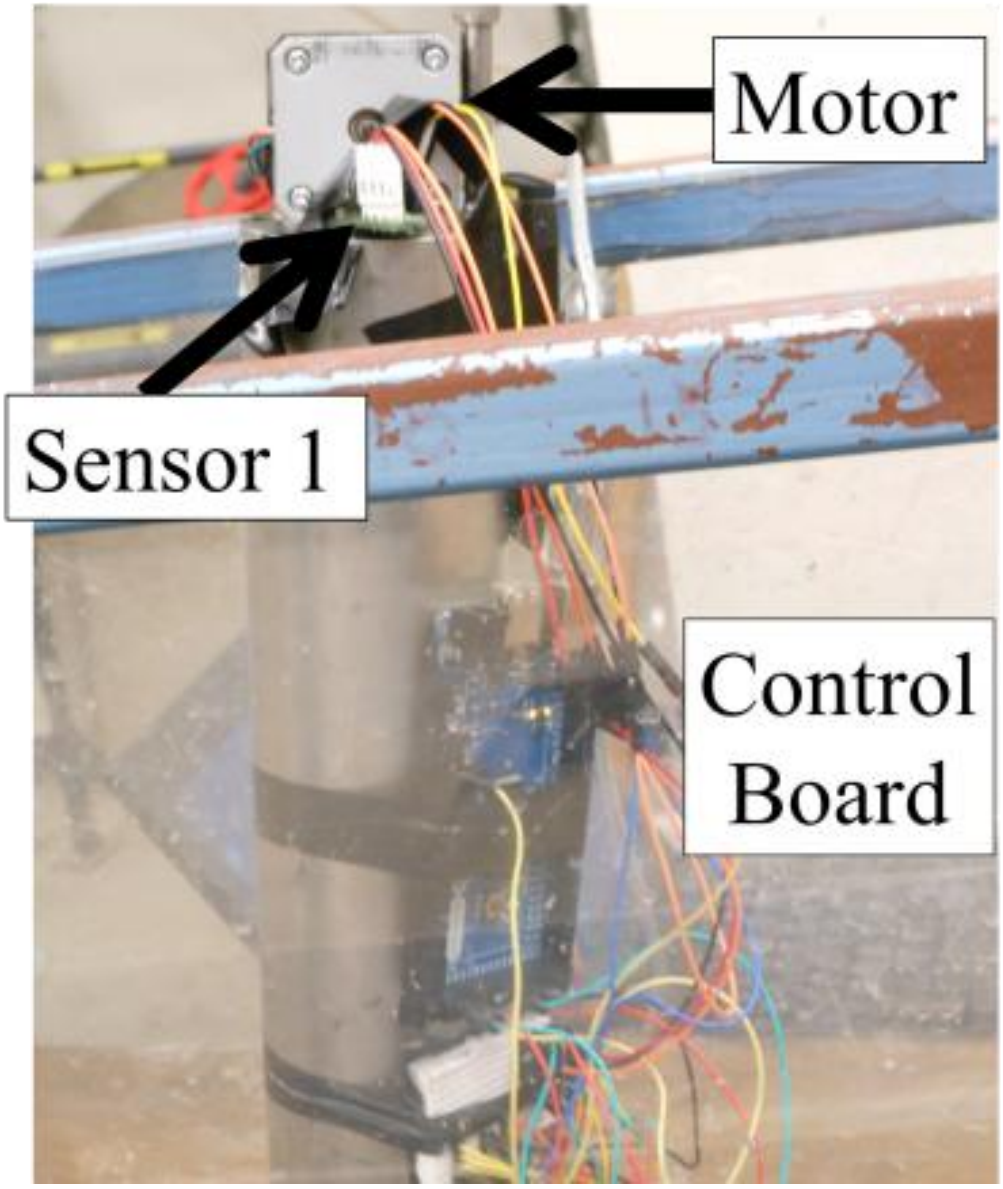

Figure 3.2 View of the Model with the motor and sensors.

Table 3.1 Testing design sequence for the Model [28]

Phase	Description
Pre-flow	Place structure in soil so base sensors are level with sand Using proctor hammer stabilized surface soil with 10 blows around structure Leveling soil surface and measuring relative heights of soil and flume depth. Shake and record data for 2 cycles (4 min), recording continues until end of test
Zero-time	Start water flow until stabilized at desired depth (2-3.5in)
During-flow	Measure relative flow heights of water Shake sequence at 5, 10, 20, 30 min or until structure fails. Angle of displacement measurements taken with every shake cycle.
Post-flow	Assess scour depth

Testing Scenarios

Testing the apparatus consisted of three basic steps beginning with verifying the functionality of the sensors and motor. Essentially making sure the sealant and waterproofing measures are functional and consistent. Secondly the calibration of the sensors, on the most ground level floor without any induced vibration, allowed for electronic drift and any possible residual structural signal interference to be reduced that would be inherent to the location or alignment of the sensors. The stepper motor was programmed to ramp up in 18 steps to the desired frequency and remain at that vibration state for approximately 2 min then step back down to the base frequency of 0.5 Hz. This cycle was designed to mimic, on a small scale, possible external vibrations a structure might experience and translate to the Model. Once ready, the testing could commence in three phases as well, pre-flow, zero-time, and during/post flow according to Figure 3.3.

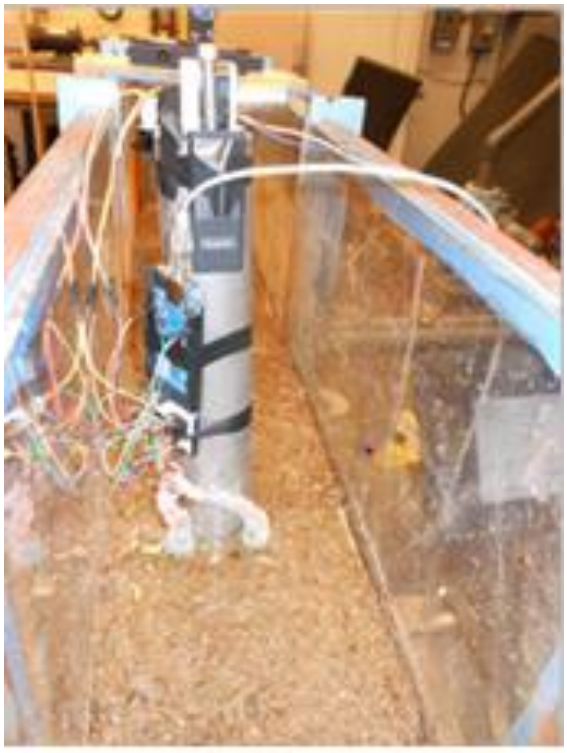

(a)

(b)

(c)

Figure 3.3Photographic descriptions of major stages in each test. From top to bottom: structure stabilized in soil prior to water flow; induced surge event occurs; scour reconnaissance and measurements recorded [28]

Throughout this entire process, a constant monitoring of total leaning (or angle of displacement at the top of the model) was measured through use of a laser (Quartet 84501 Laser Pointer) affixed to the side of the structure, pointing to a meter stick attached to the ceiling in parallel with the direction of flow. Using simple trigonometry, the angle of displacement was determined with the measured distance from laser to ceiling of 61.25 inches.

Table 3.2 Hydraulic properties for Test [28]

Position-test	Water Height, m	Velocity, m/s	Froude number
A-1	0.024	0.455	0.937
B-1	0.037	0.295	0.490
C-1	0.031	0.352	0.638
A-2	0.019	0.740	1.714
B-2	0.054	0.260	0.358
C-2	0.035	0.402	0.685

Test Formulation

The following test was performed in which four sensors were used to record the data in the time domain and sensors were labeled as 1,2,3,4 respectively. System identification was performed considering the input as the top sensor 4 attached to the motor placed at the top of the aluminum structure embedded in the soil domain. Two tests were performed pre-surging and post-surging , the frequency of motor varied from minimum to maximum in the time step of 2 minutes, the maximum frequency of revolution being 15 Hz. Data were collected in the constant time interval of 5,10 minutes.

Different conditions are analyzed as pre surge and post surge, where flow of water is varied by using venturimeter, notably transfer functions are plotted for input and output in the lateral and vertical direction respectively. Calibrated, DE trended, resampled data is changed from time domain to frequency domain and are converted into signals which are then analyzed by performing fast Fourier transform and filtering of data, and more precisely signals are done by using Butterworth filter which gave consistent results in removing the noise caused by the sound or any distraction aroused because of the incoherence. The resulting transfer function plots describes basically the first mode of the system, the peak can be considered as the peak for the first mode of vibration, at the low frequency interestingly the higher modes may be due to the noise or due to the amplification of the signal, notably the transfer function output in lateral and

vertical directions varied a lot primarily because the shaking takes place in the lateral direction due to which the frequency response has higher value as compared to the frequency response in the vertical direction. The transfer function is plotted considering input at the top where sensor 4 is located and output at the bottom which is the combination of sensor 1, 2, 3 and it can be considered that only those values will be considered which will give fairly consistent results in the transfer function plot in the lateral and vertical directions.

Benchmarking using Dry Soil Initial Condition Data

From Initial dry condition before Test1 will be used as case studies demonstrating application of the proposed framework. The case dry condition which is a representative of earthquake motion when the soil is dry , representing higher shear strength and better resistance to the earthquake motion, the measured acceleration at the top and bottom is measured by means of sensors. Prior to performing system identification, three digital pre-processing steps are applied to the recorded data to increase the stability and accuracy of the ensuring identification procedure: i) Resampling, ii) detrending, iii) selection of significant duration. The data was filtered using a ninth-order Butterworth filter with a frequency band of 0 to 10 Hz. The significant durations for the seismic inputs are selected according to the maximum disturbance produced in the time span data recorded by the respective sensors.

3.2 Soil-Structure Transfer Function Formulation

The corresponding force and moment equation are

$$F_b = m(u_h'' + u_\varphi'') + K_h u_h + C_h u_h' \qquad (3.1)$$

$$F_b H = m(u_h'' + u_\varphi'' \frac{H_c}{H}) H_c + \frac{K_\varphi u_\varphi}{H} + \frac{C_\varphi u_\varphi'}{H} \qquad (3.2)$$

Substituting

$$m \rightarrow 1, K_h \rightarrow \frac{\omega_h^2}{m}, C_h \rightarrow 2\,\xi_h\,\omega_h \;\&\; K_\varphi \rightarrow \omega_\varphi^2\,H^2\,, C_\varphi \rightarrow 2\,\xi_\varphi\,\omega_\varphi\,H^2 \;\&\; F_b \rightarrow A_f$$

Where ω_h and ξ_h are the system circular frequency and damping ratio due to the foundation sliding, respectively and ω_ϕ , ξ_ϕ are similarly defined due to the rocking mode:

$$A_f = u_h\,\omega_h^2 + u_h'\,2\,\xi_h\,\omega_h + (u_h'' + u_\varphi'') \qquad (3.3)$$

$$A_f\,H = u_\varphi\,\omega_\varphi^2\,H + 2\,u_\varphi'\,\omega_\varphi\,\xi_\varphi\,H + H_c\,(u_h'' + \frac{H_c}{H}\,u_\varphi'') \qquad (3.4)$$

Equation 2.7 and 2.8 can be converted from the time domain to the Laplace domain using the Laplace transform g(t) = g(s) e^{st} , (where s is the complex variable)

Substituting

$$A_f \rightarrow -A\,s^2\,e^{st}\,, u_h'' \rightarrow u_h\,s^2\,e^{st}\,, u_h' \rightarrow u_h\,s\,e^{st}\,, u_h \rightarrow u_h\,e^{st}\,, u_\varphi'' \rightarrow u_\varphi\,s^2\,e^{st}$$

$$\frac{s^2\,(u_h + u_\varphi) + u_h\,\omega_h\,(2\,s\,\xi_h + \omega_h) + A\,s^2}{m} = 0 \qquad (3.5)$$

$$A\,H\,s^2 + H_c\,s^2\,u_h + \frac{H_c\,s^2\,u_\varphi}{H} + H\,u_\varphi\,\omega_\varphi\,(2\,s\,\xi_\varphi + \omega_\varphi) = 0 \qquad (3.6)$$

$$A\,H\,s^2 + H_c\,s^2\,u_h + \frac{H_c\,s^2\,u_\varphi}{H} + H\,u_\varphi\,\omega_\varphi\,(2\,s\,\xi_\varphi + \omega_\varphi) = 0 \qquad (3.7)$$

Rearranging this equation system:

$$(s^2 + 2\,s\,\xi_h\,\omega_h + \omega_h^2)\,u_h = -(A + u_\varphi)\,s^2 \qquad (3.8)$$

The input is $(A + m^2\,u_\varphi)$, the output is u_h)

$$\left(\frac{H_c\,s^2}{H} + 2\,s\,\xi_\varphi\,\omega_\varphi + \omega_\varphi^2\right)u_\varphi = -\left(A + \frac{H_c\,u_h}{H}\right)s^2, \qquad (3.9)$$

The input is $(A + \frac{H_c\,u_h}{H})$ the output is $\frac{u_\varphi\,H_c}{H}$ (3.10)

Contribution of Harmonic excitation force is also considered.

Solving these two equations for u_h and u_ϕ we get

$$u_h = \frac{A\,H\,s^4 - A\,s^2\left(\frac{H_c^{\,2}\,s^2}{H} + H\,\omega_\varphi\,(2\,s\,\xi_\varphi\,\omega_\varphi)\right)}{H_c\,s^4 - (s^2 + 2\,s\,\xi_h\,\omega_h + \omega_h^{\,2})\left(\frac{H_c^{\,2}\,s^2}{H} + H\,\omega_\varphi\,(2\,s\,\xi_\varphi\,\omega_\varphi\right)} \tag{3.11}$$

$$u_\varphi = \frac{A\,H\,s^2\,(-H_c\,s^2 + H\,(s^2 + 2\,s\,\xi_h\,\omega_h + \omega_h^{\,2}))}{H\,H_c\,s^4 - H^2{}_c\,s^2\,(s^2 + 2\,s\,\xi_h\,\omega_h + \omega_h^{\,2}) - H^2\,(s^2 + 2\,s\,\xi_h\,\omega_h + \omega_h^{\,2})\,\omega_\varphi\,(2\,s\,\xi_\varphi + \omega_\varphi)} \tag{3.12}$$

These two equations are solved above for u_h and u_ϕ respectively and transfer function is defined as

Case 1: Considering both rocking and sliding modes

$$TR = \frac{u_h + u_\varphi + F_b}{F_b} \tag{3.13}$$

Case 2: For rocking mode

$$TR = \frac{u_h + u_\varphi + F_b}{u_h + F_b} \tag{3.14}$$

Case 3 For Sliding mode

$$TR = \frac{u_h + u_\varphi + F_b}{u_\varphi + F_b} \tag{3.15}$$

3.3 System Identification Results

Considering linear elastic soil-structure system, a simple transfer function plot represents the existence of SSI effects by comparing the dominant frequencies of the transfer function between the input and the output. TR1 represents the transfer function corresponding to the frequencies between the top responses to the foundation induced response. For the output at the base, Sensor 1 and 3 are used and averaged to obtain either the lateral (X) or the vertical output (Z). Sensor 4 which measures the vibration of the top motor is used as the input signal. Based on equation the system is essentially a rigid model in the soil, the modal parameters of the system are largely determined by the near field soil property around the model.

Test 1-Dry test data before the commencement of actual test

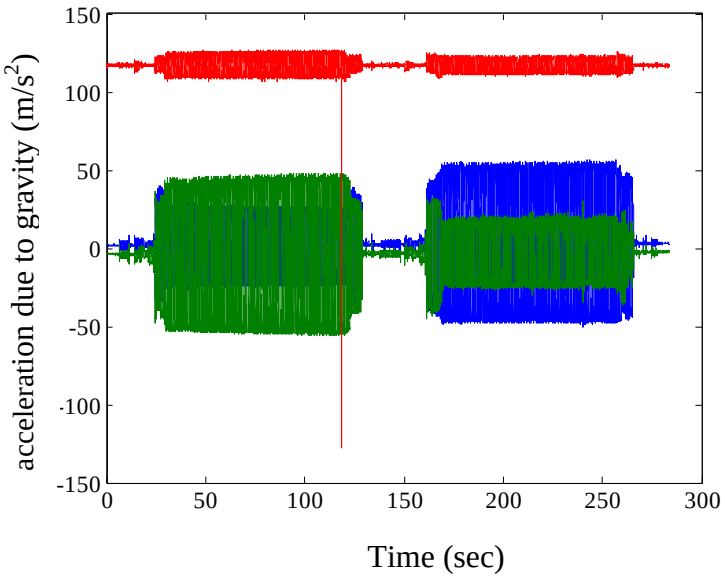

Figure 3.4 Time recorded data from input (Sensor 4)

Structural vibration can be measured by electronic sensor that converts vibration motion into electrical signals. Figure 3.4 shows time domain analysis as signal is analyzed as a function of time, the maximum vibration or peak level is recorded and for this condition those time step are selected for which the acceleration response is maximum from the input i.e. shaking of structure takes place. Those time step data are converted into frequency domain and corresponding Fast Fourier transform which is the discrete Fourier Transform of block of time signal, and represents the frequency spectrum of the time signal is plotted in lateral and vertical direction. Transfer function plots are represented for that duration, the peak of those signifies the modes of structure for the disturbed output/ input ratio.

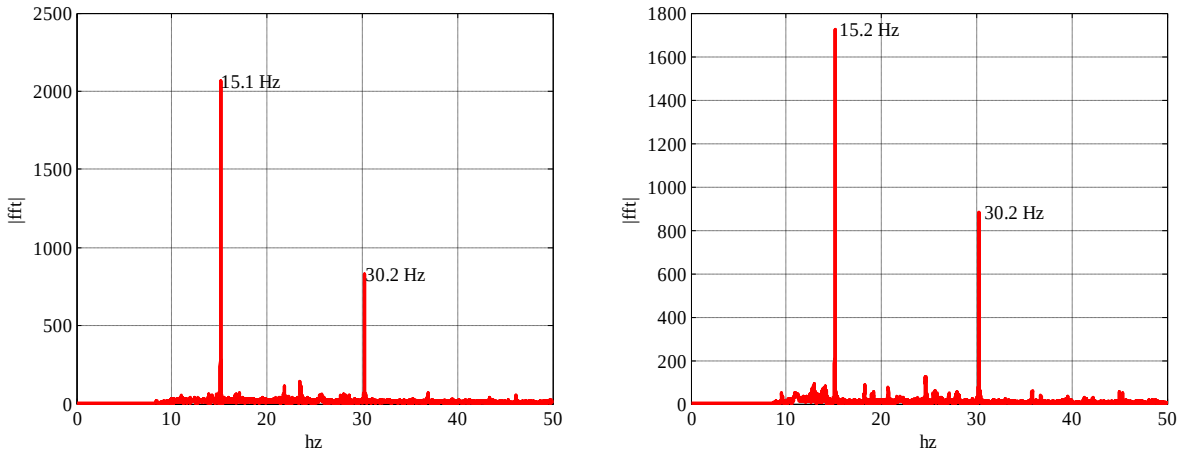

Figure 3.5FFT plots for the input and the output with the model embedded on the dry sand during strong disturbance in sensor 4in the vertical direction for (a) input signal; (b) output signal.

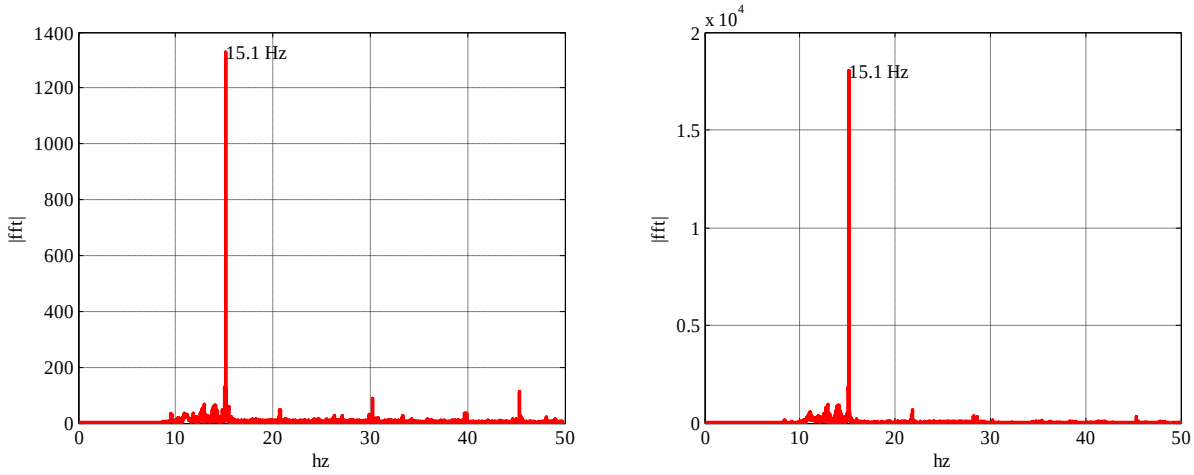

Figure 3.6 FFT plots for the input and the output with the model embedded on the dry sand during strong disturbance in sensor 4 in the lateral direction for (a) input signal; (b) output signal.

FFT curve as displayed in Figure 3.5 for vertical direction reveals that most of the amplitude or energy is at frequency 15.1 Hz, and at harmonic of 15.1 i.e. at 30.2 Hz, predominant frequency being 15.1 Hz, the same in the case of lateral direction as displayed in Figure 3.6 for which the predominant frequency that contains maximum energy or amplitude is 15.1 Hz.

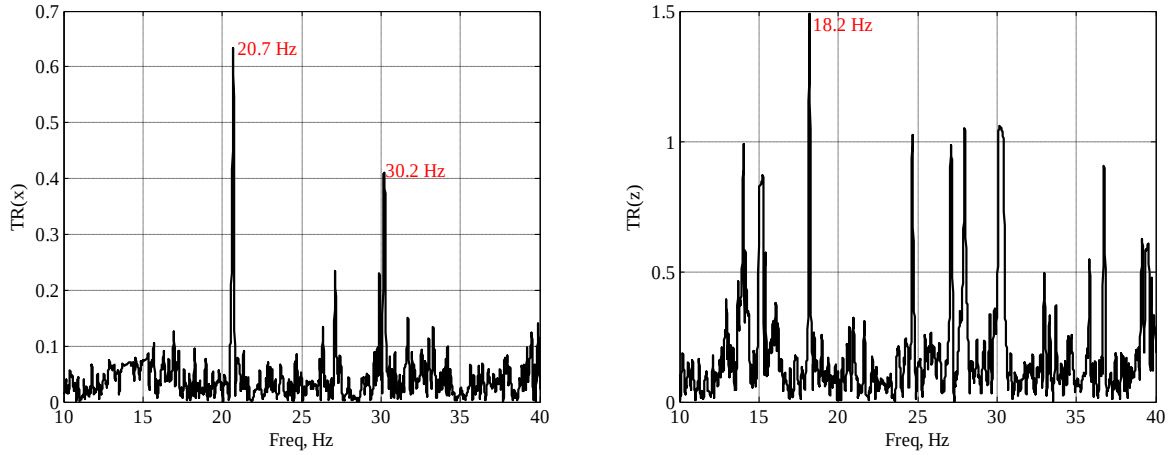

Figure 3.7Transfer Function between the input and the output with the model embedded on the dry sand during strong disturbance in sensor 4 (25-128s), (a) in the lateral direction; (b) in the vertical direction

From the transfer function plot as displayed in Figure 3.7the trend in lateral direction is showing first mode to be at 20.7 Hz, and the dominant frequencies being 20.7 and 30.2 Hz for the vertical direction the first mode for the system is at 18.2 Hz.

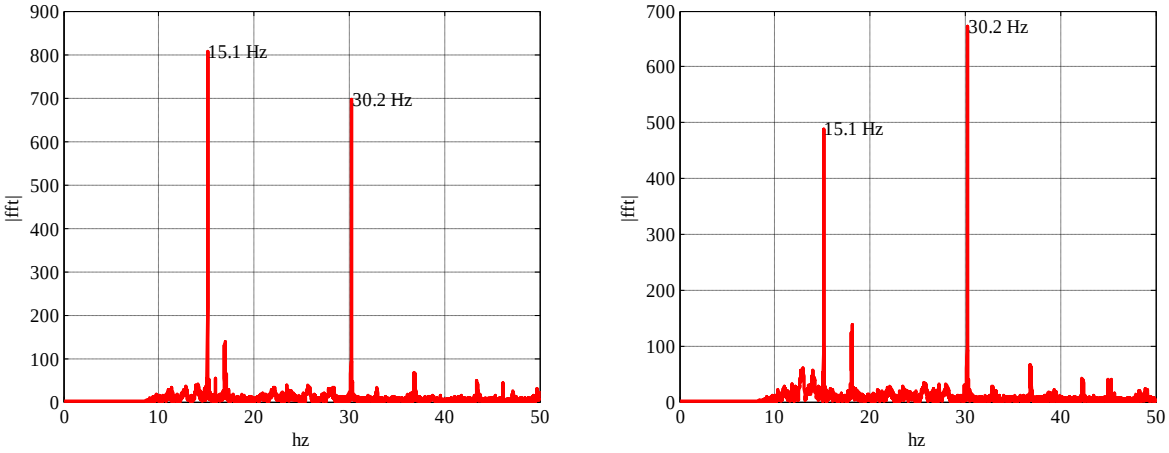

Figure 3.8 FFT plots for the input and the output with the model embedded on the dry sand during strong disturbance in sensor 4in the vertical direction for (a) input signal; (b) output signal.

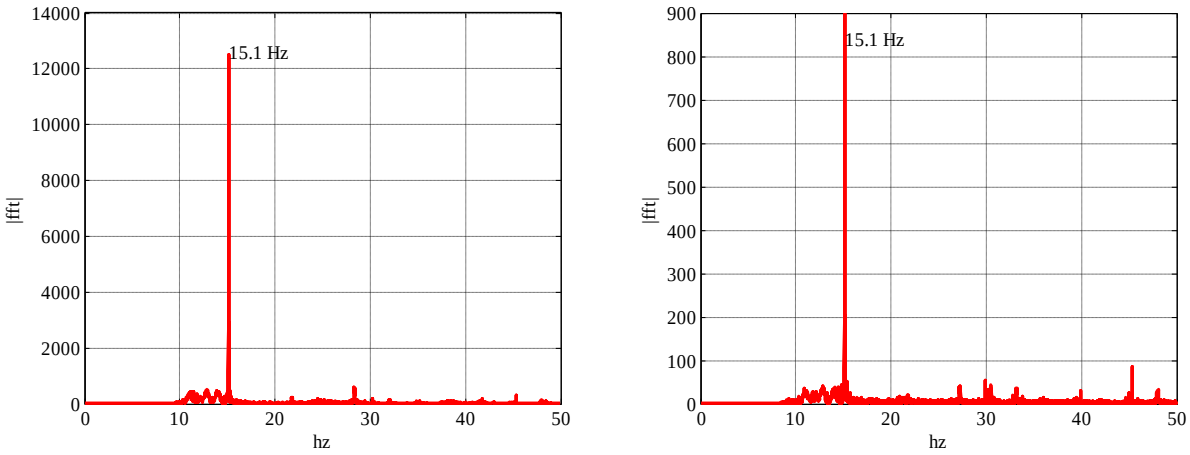

Figure 3.9 FFT plots for the input and the output with the model embedded on the dry sand during strong disturbance in sensor 4in the lateral direction for (a) input signal; (b) output signal.

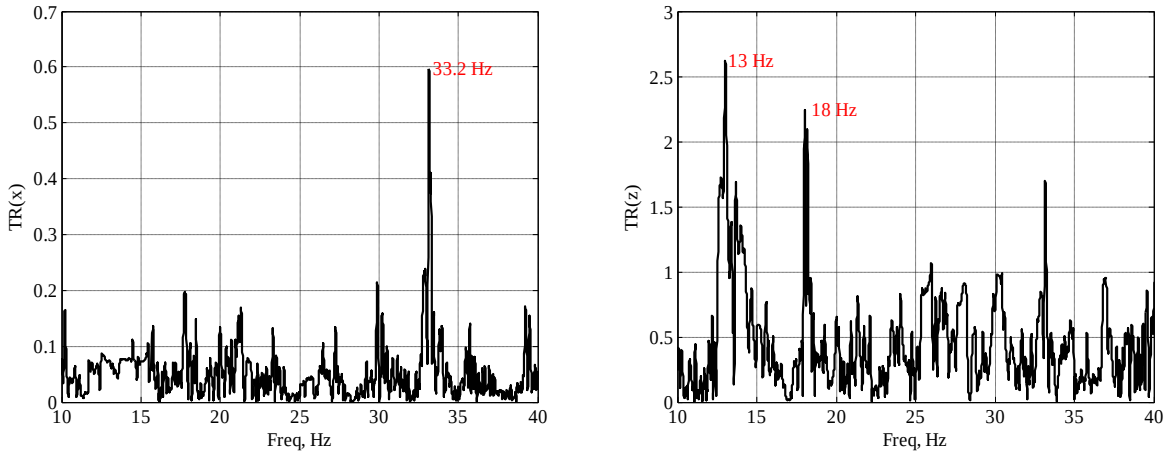

Figure 3.10 Transfer Function between the input and the output with the model embedded on the dry sand during strong disturbance in sensor 4 (168-265s): (a) in the lateral direction; (b) in the vertical direction.

As illustrated in Figure 3.10 the transfer function in the vertical and the lateral direction, respectively before the test starts (i.e., the sand in the flue is dry and dense). It can be seen that the lateral first mode is at about 33.2 Hz which is close to the 3- dimensional simulation result, for latter phase of time whereas in the initial phase the first mode is fairly close to the 22 Hz & the vertical mode is at about 18.1 Hz, which is consistent for the initial and final phase.

Test 2-Pre surging

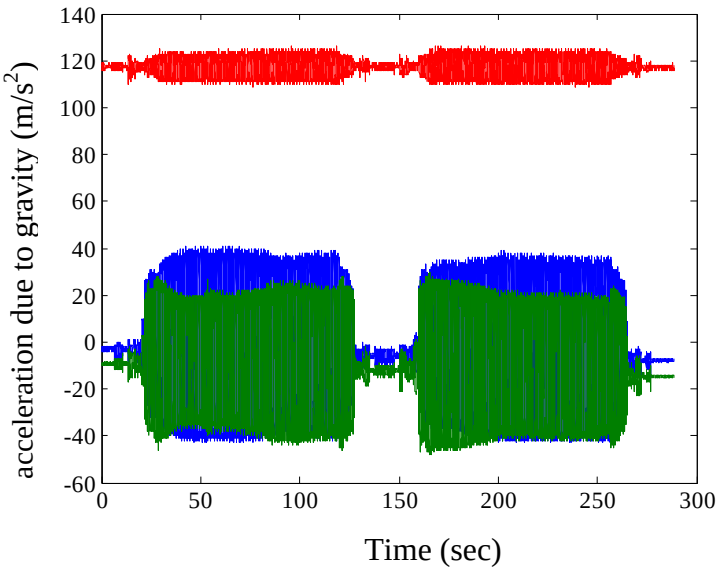

Figure 3.11Time recorded data from input (Sensor 4)

After taking the reading for model embedded in the dry soil, for the wet condition the same test is repeated and as illustrated Figure 3.4 shows time domain analysis as signal but this time the soil is wet. The shaking response is considered for the cases in which the input has most disturbances. Using the time domain data those intervals are considered and corresponding FFT and Transfer function plots are plotted for the recorded data having maximum disturbance.

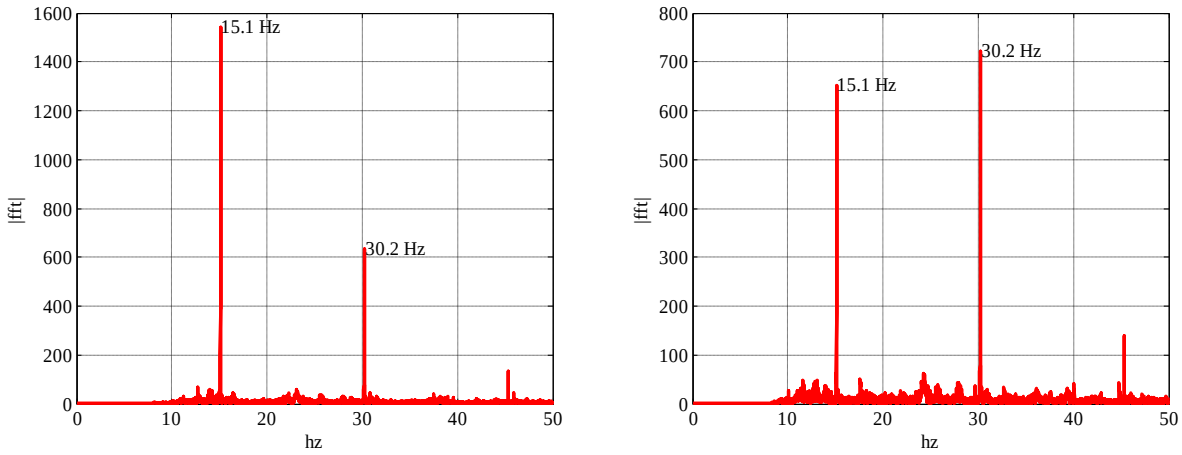

Figure 3.12 FFT plots for the input and the output for wet sand (pre – surging) during strong disturbance in sensor 4 in the vertical direction for (a) input signal; (b) output signal

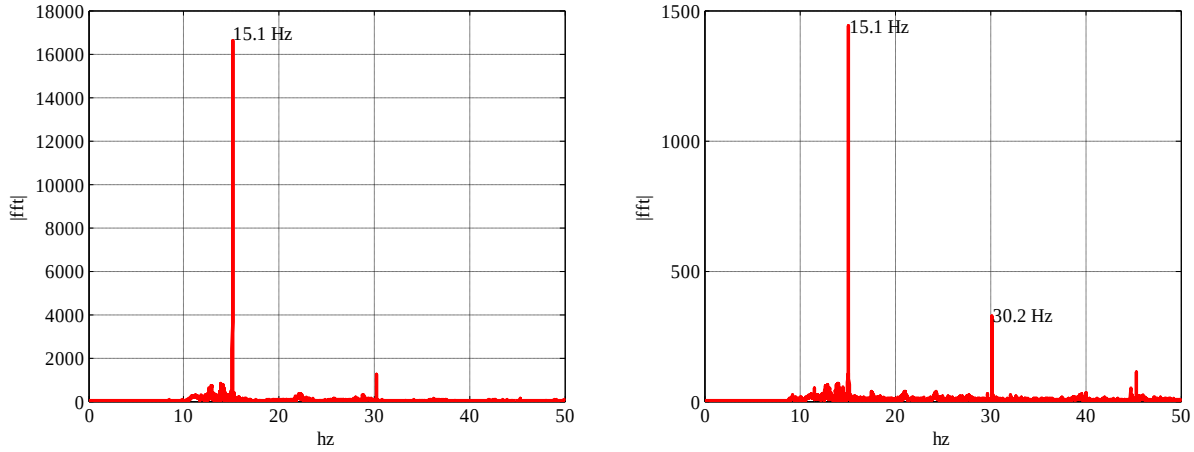

Figure 3.13FFT plots for the input and the output for wet sand (pre- surging) during strong disturbance in sensor 4 in the lateral direction for (a) input signal; (b) output signal

The corresponding FFT curves as illustrated in Figure 3.13 reveals that the maximum energy for the input in the lateral and vertical direction is at 15 Hz, while for the output in lateral and vertical direction the maximum energy is at 30.2 Hz and 15.1 Hz.

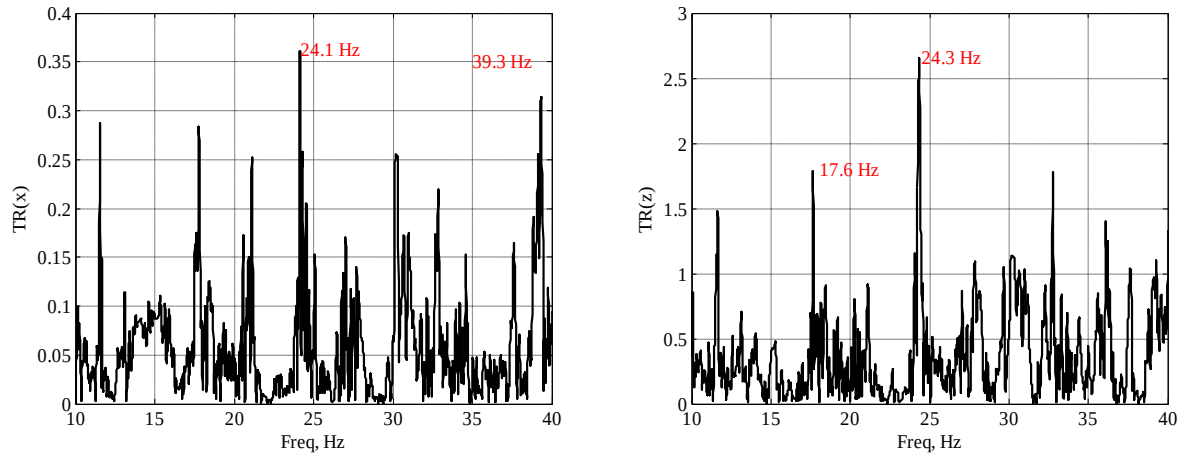

Figure 3.14 Transfer Function between the input and the output for wet sand (pre- surging) during strong disturbance in sensor 4 (25-127s): (a) in the lateral direction; (b) in the vertical direction.

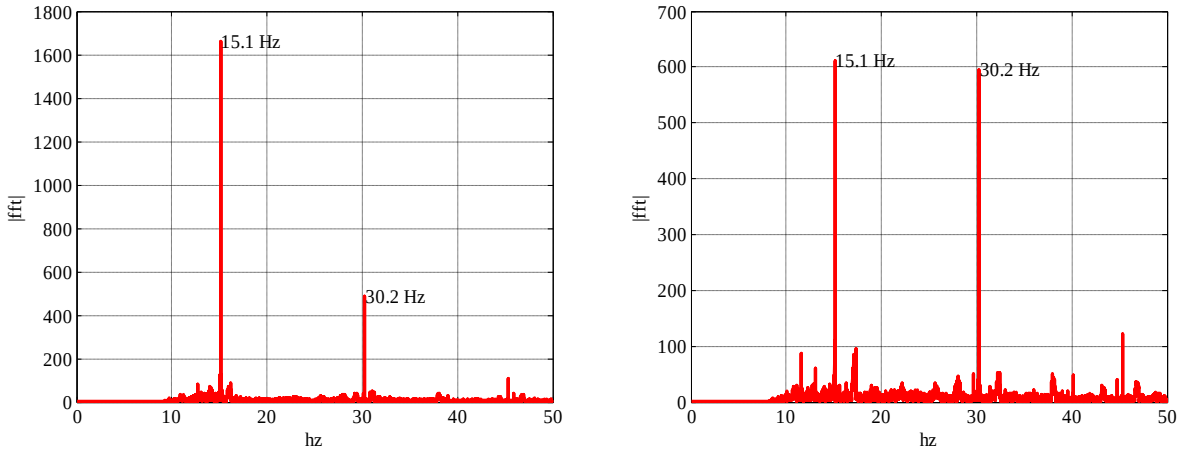

Figure 3.15 FFT plots for the input and the output for wet sand (pre- surging) during strong disturbance in sensor 4 in the vertical direction for (a) input signal; (b) output signal

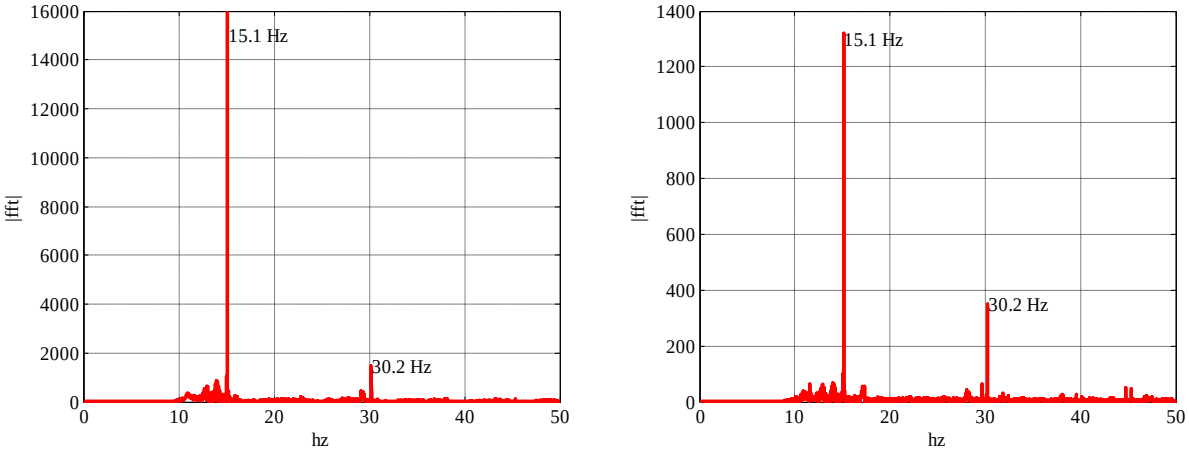

Figure 3.16 FFT plots for the input and the output for wet sand (pre –surging) during strong disturbance in sensor 4 in the lateral direction for (a) input signal; (b) output signal

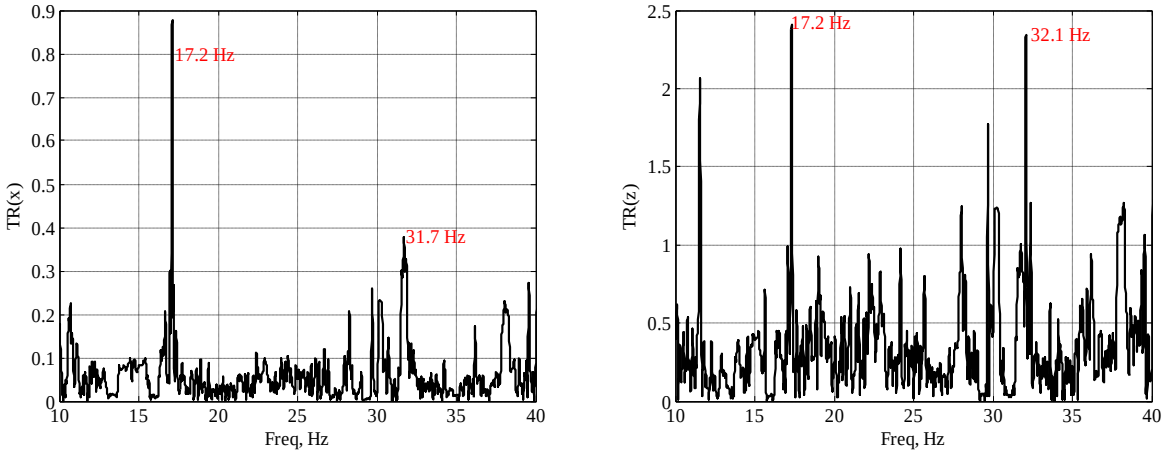

Figure 3.17 Transfer Function between the input and the output for wet sand (pre – surging) during strong disturbance in sensor 4: (a) in the lateral direction; (b) in the vertical direction

From FFT plots as illustrated in Figure 3.16 still the frequency of interest is 15.1 Hz in both lateral and longitudinal direction, but for the transfer function plot as illustrated in Figure 3.17 in the lateral direction the first mode or the dominant frequency is 17.2 Hz and it is the same for the vertical direction.

Test 2-Post surging

Case 1for the post surging condition the data is divided into two time interval data as the length of recording of data is too large.

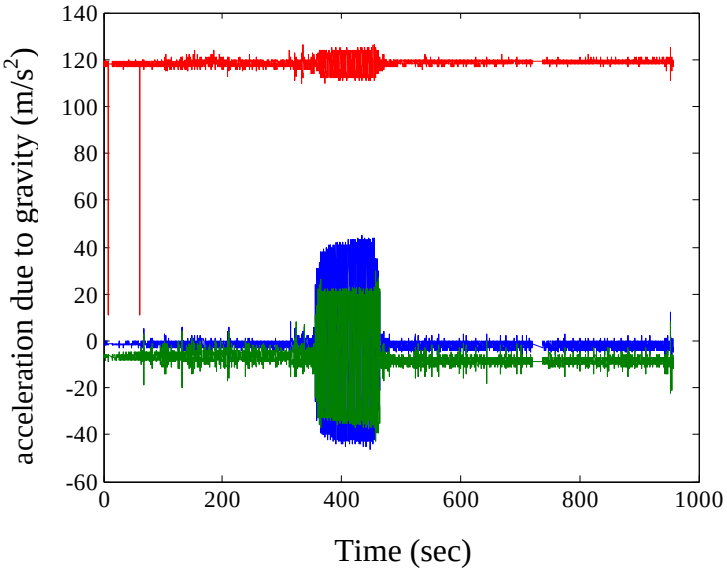

Figure 3.18Time recorded data from input (Sensor 4)

After taking the reading for model embedded in the wet soil, for the post surge condition the same test is repeated and Figure 3.18 shows time domain analysis as signal. The shaking response is considered for the cases in which the input has most disturbances. Using the time domain data those intervals are considered and corresponding FFT and Transfer function plots are plotted

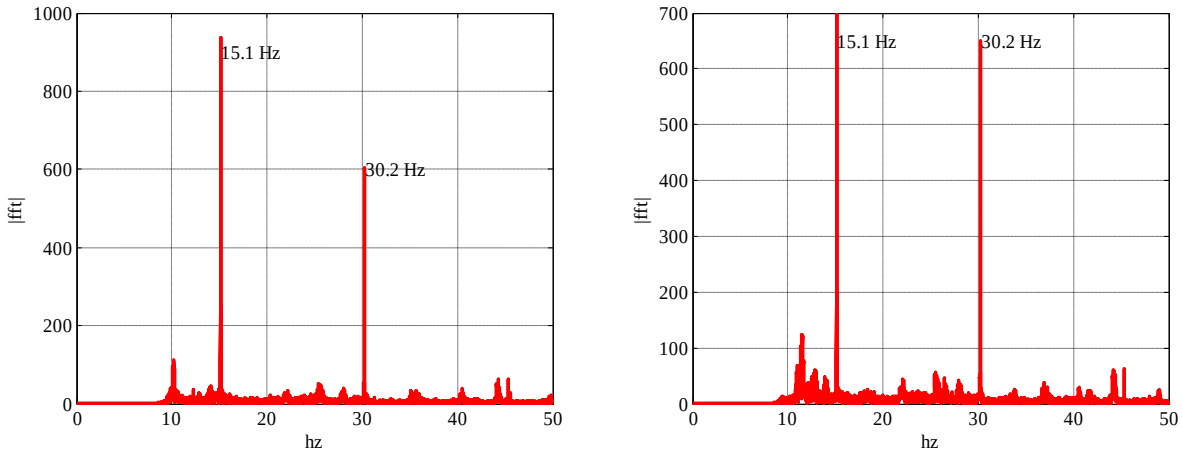

Figure 3.19 FFT plots for the input and the output for post - surge during strong disturbance in sensor 4 in the vertical direction for (a) input signal; (b) output signal.

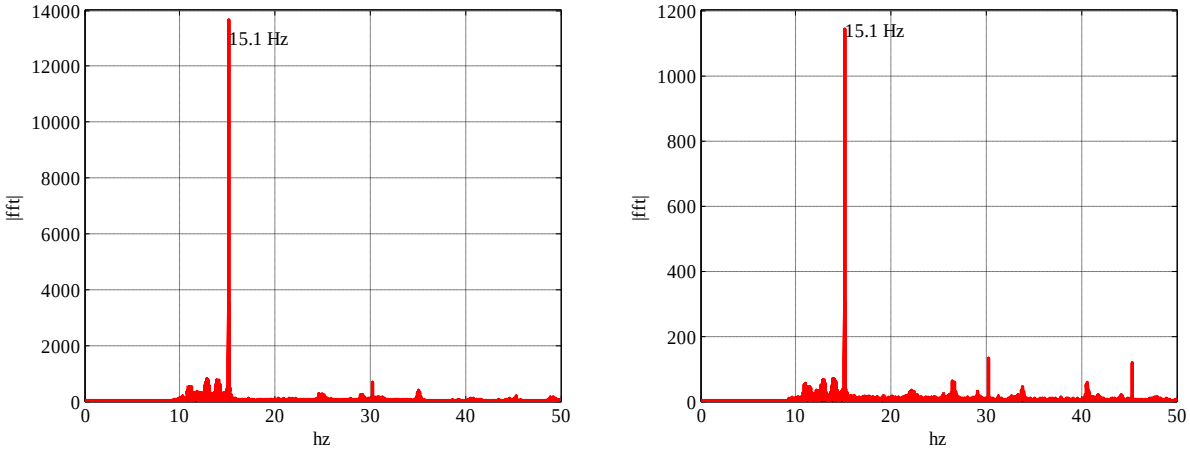

Figure 3.20 FFT plots for the input and the output for post - surge during strong disturbance in sensor 4 in the lateral direction for (a) input signal; (b) output signal.

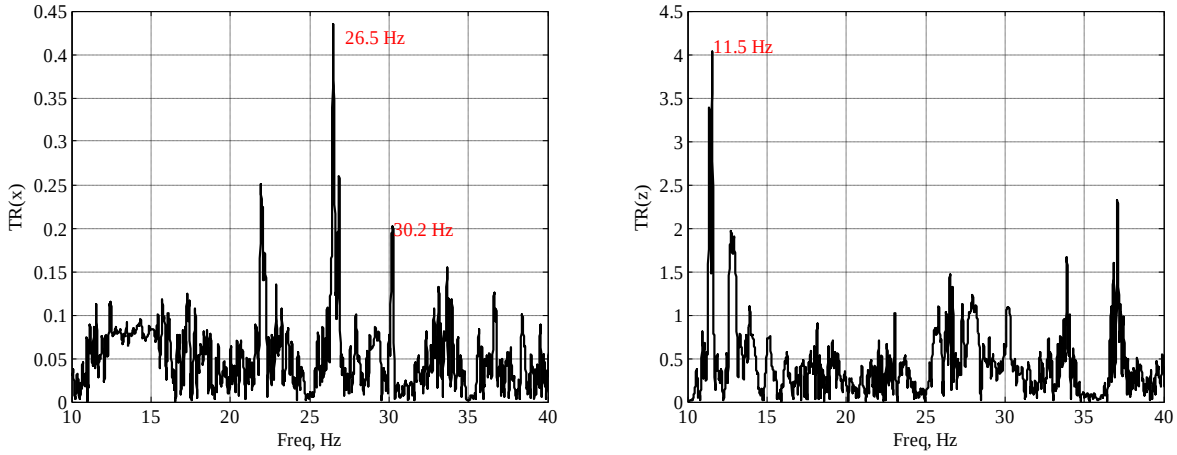

Figure 3.21Transfer Function between the input and the output for post – surge during strong disturbance in sensor 4: (a) in the lateral direction; (b) in the vertical direction

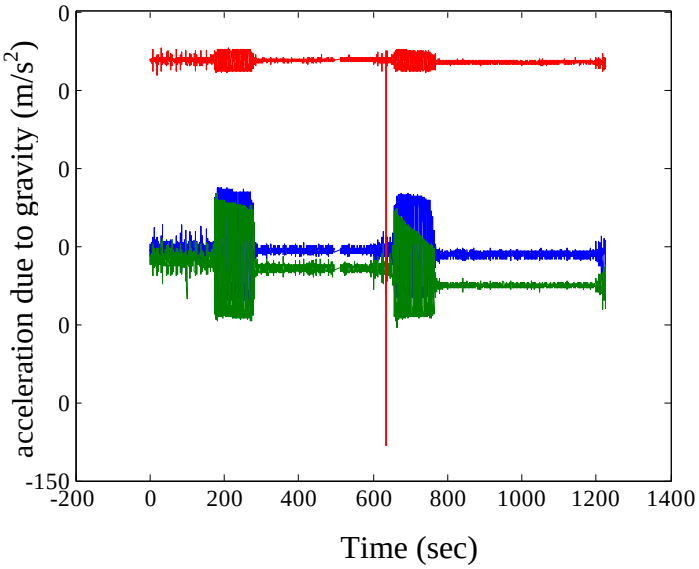

Figure 3.22Time recorded data from input (Sensor 4)

After taking the reading for model embedded in the wet soil, for the post surge condition the same test is repeated and Figure 3.22 shows time domain analysis as signal.. Using the time domain data those intervals are considered and corresponding FFT and Transfer function plots are plotted.

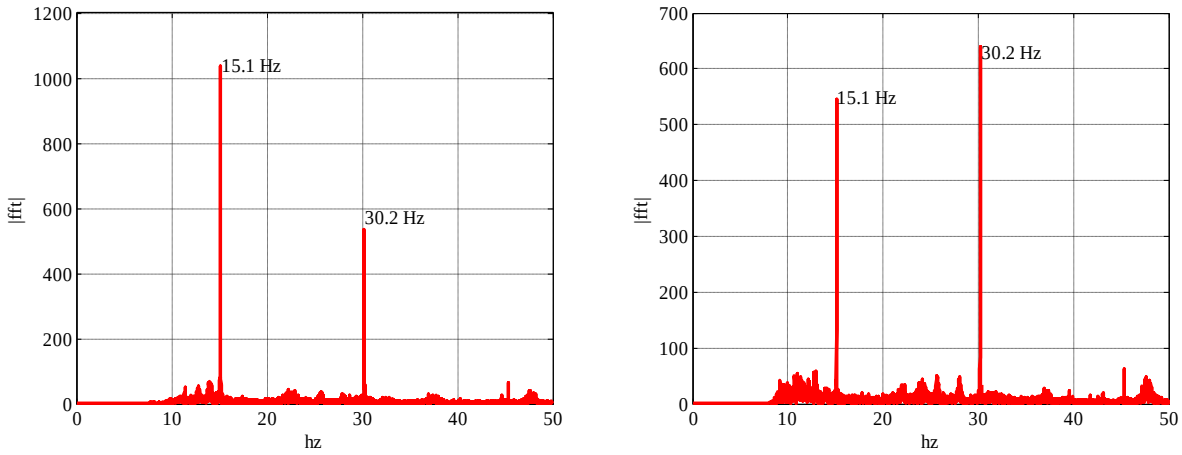

Figure 3.23 FFT plots for the input and the output for post - surge during strong disturbance in sensor 4 in the vertical direction for (a) input signal; (b) output signal.

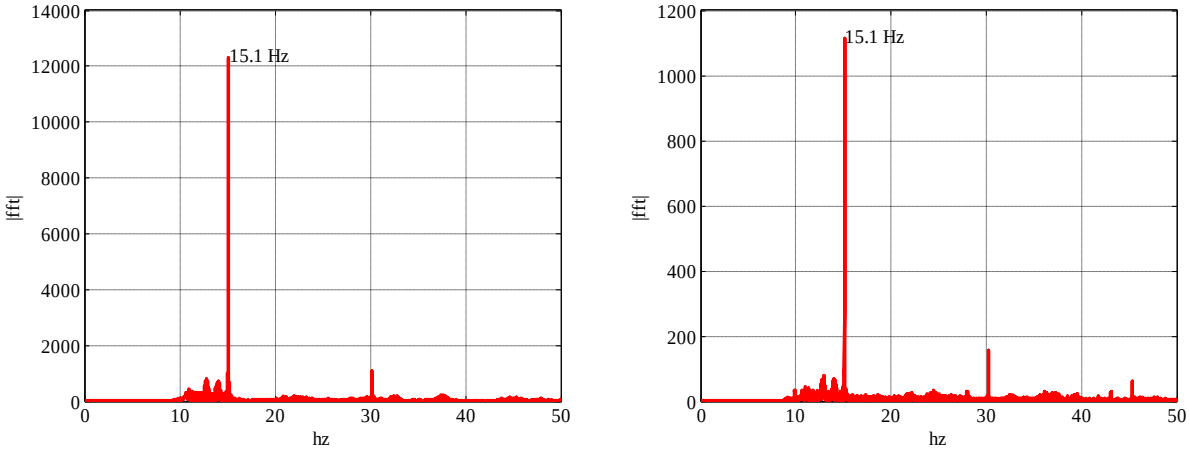

Figure 3.24 FFT plots for the input and the output for post - surge during strong disturbance in sensor 4 in the lateral direction for (a) input signal; (b) output signal

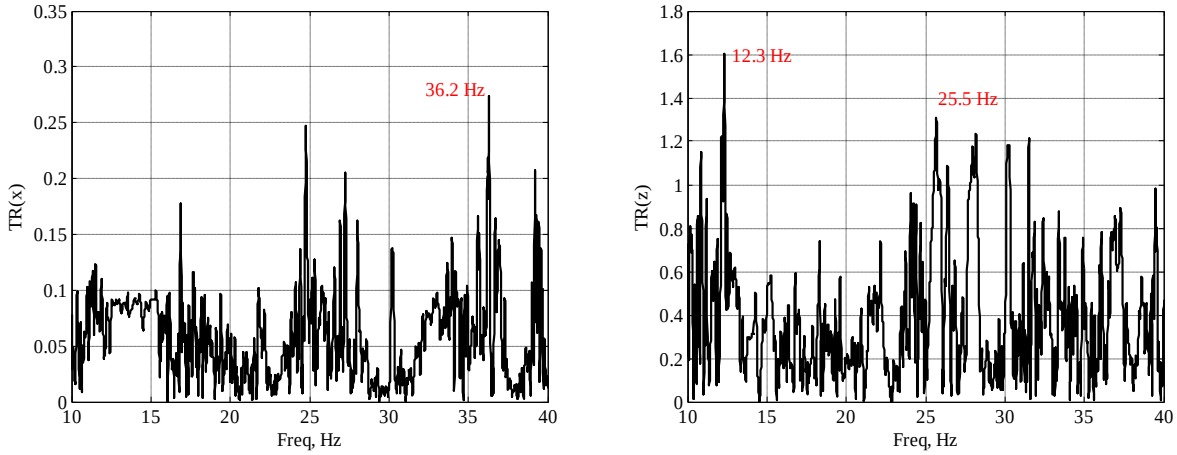

Figure 3.25Transfer Function between the input and the output for post – surge during strong disturbance in sensor 4: (a) in the lateral direction; (b) in the vertical direction

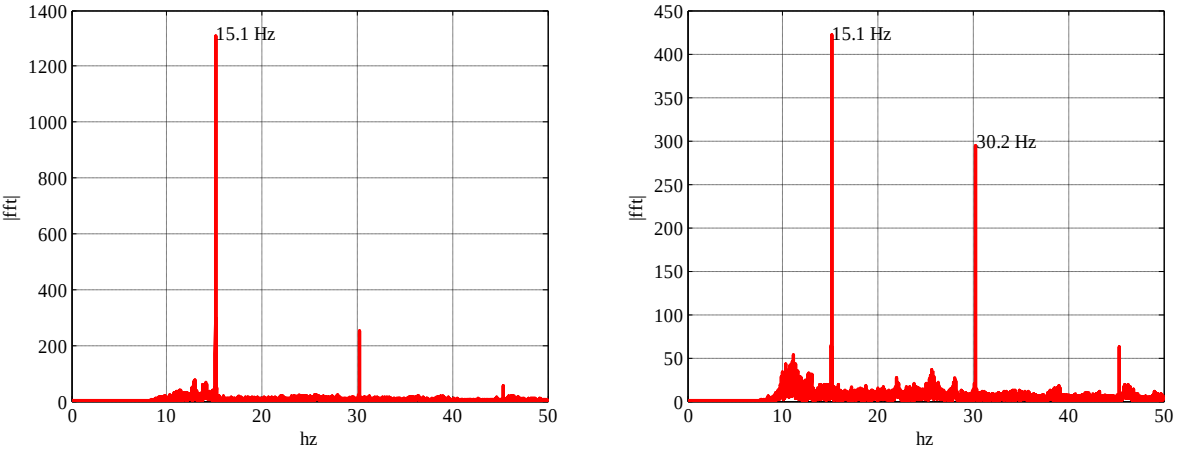

Figure 3.26 FFT plots for the input and the output for post - surge during strong disturbance in sensor 4 in the vertical direction for (a) input signal; (b) output signal.

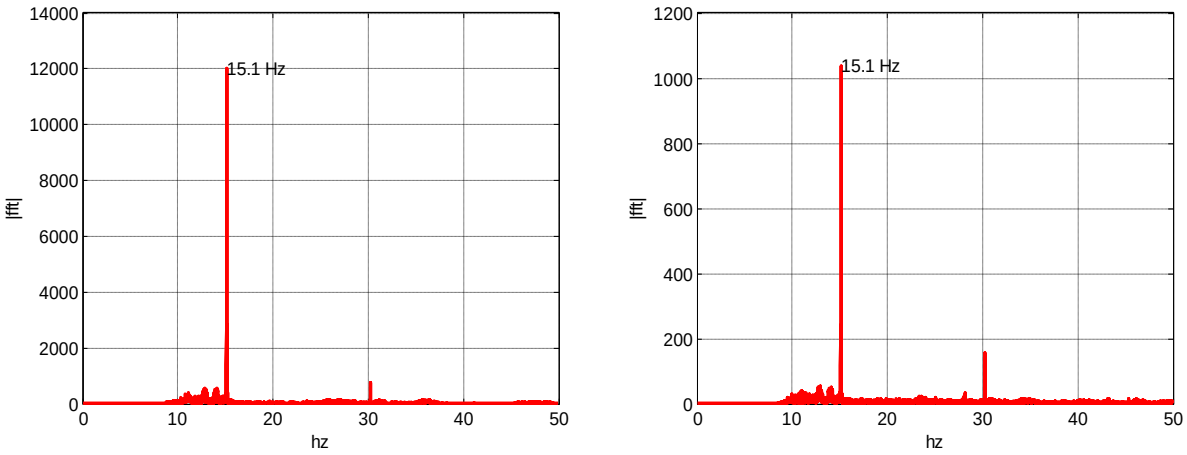

Figure 3.27 FFT plots for the input and the output for post - surge during strong disturbance in sensor 4 in the lateral direction for (a) input signal; (b) output signal.

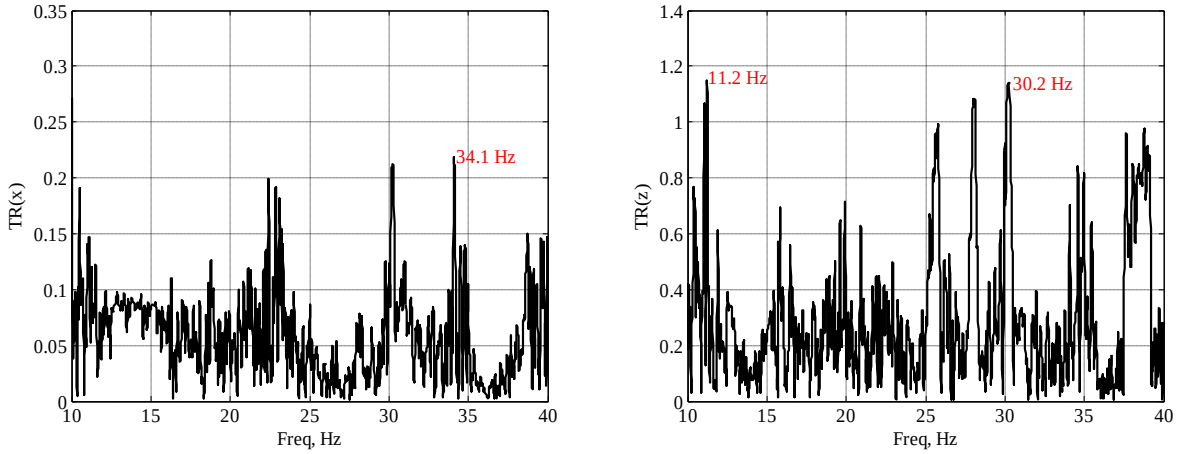

Figure 3.28Transfer Function between the input and the output for post – surge during strong disturbance in sensor 4: (a) in the lateral direction; (b) in the vertical direction.

As the test go, the transfer function, during the maximum surge are illustrated, as illustrated in Figure 3.25 and Figure 3.28 for vertical mode the test data reveals the fact that the first mode slightly gets decreased from 12.3 Hz to 11.2 Hz, which shows that the shear strength of the soil is decreased. But the trend for the lateral direction is irregular as displayed in Figure 3.25 where the first mode is hard to predict as the curve is not showing regular trend, it may be

attributed because of noise or any disturbance, for the last transfer function plot displayed in Figure 3.28 the lateral direction first mode becomes consistent with 34 Hz frequency.

Test 3-Pre surging

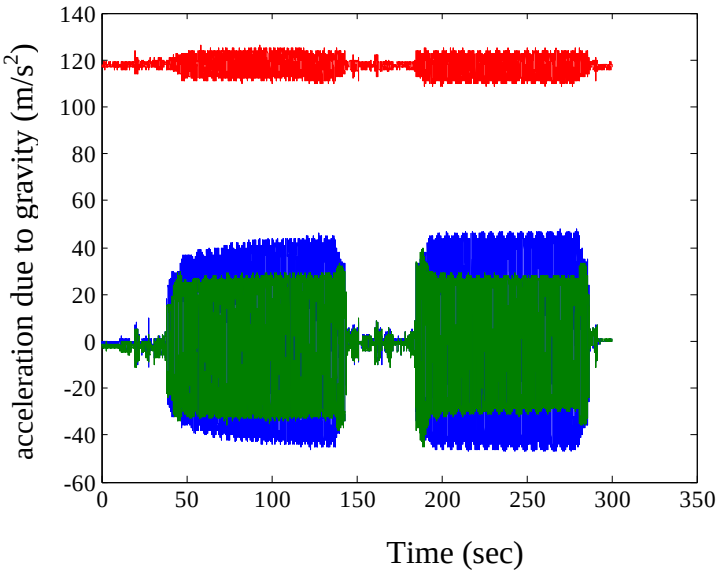

Figure 3.29Time recorded data from input (Sensor 4)

After taking the reading for model embedded in the dry soil, for the wet condition the same test is repeated and Figure 3.29 shows time domain analysis as signal. The shaking response is considered for the cases in which the input has most disturbances. Using the time domain data those intervals are considered and corresponding FFT and Transfer function plots are plotted.

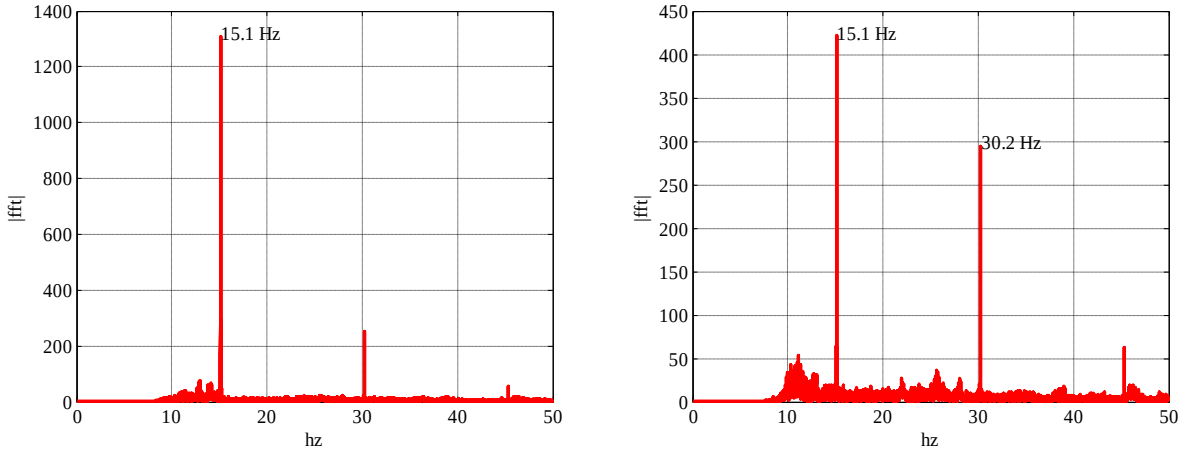

Figure 3.30 FFT plots for the input and the output for pre - surge during strong disturbance in sensor 4 in the vertical direction for (a) input signal; (b) output signal

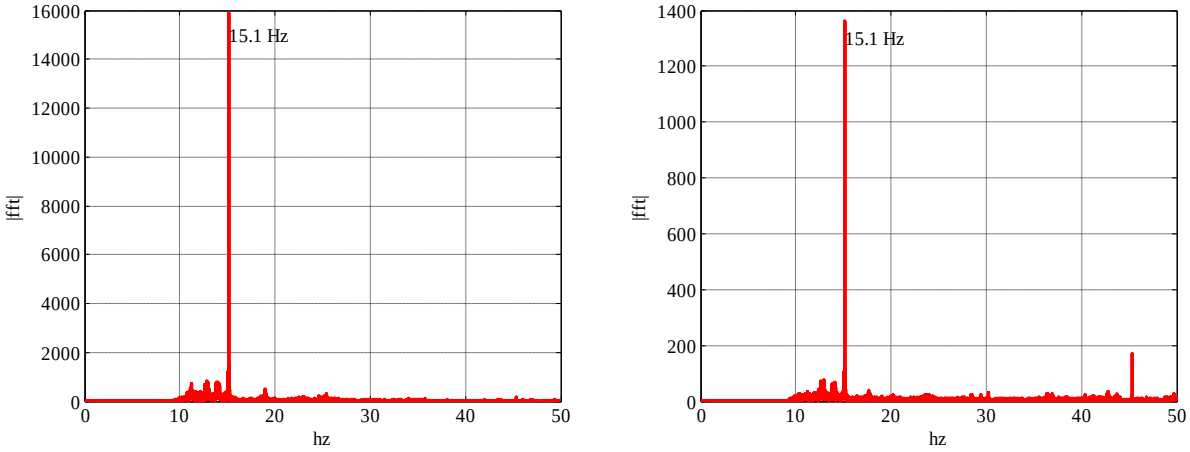

Figure 3.31 FFT plots for the input and the output for pre - surge during strong disturbance in sensor 4 in the lateral direction for (a) input signal; (b) output signal

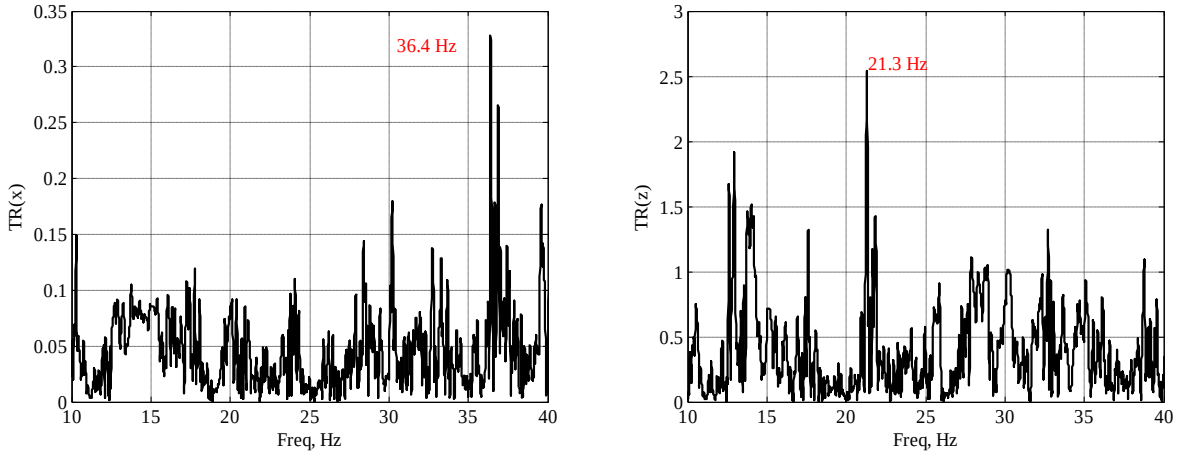

Figure 3.32 Transfer Function between the input and the output for pre – surge during strong disturbance in sensor 4: (a) in the lateral direction; (b) in the vertical direction

As the test go, the transfer function in Test 3, before the maximum surge for vertical mode as displayed in Figure 3.32 reveals the fact that the first mode getsincreased from 11.2 Hz to 21.3 Hz. But the trend for the lateral direction is irregular where the first mode is hard to predict as the curve is not showing regular trend, it may be attributed because of noise or any disturbance, for the last transfer function plot as displayed in Figure 3.32 the lateral direction first mode becomes consistent with 36.4 Hz frequency.

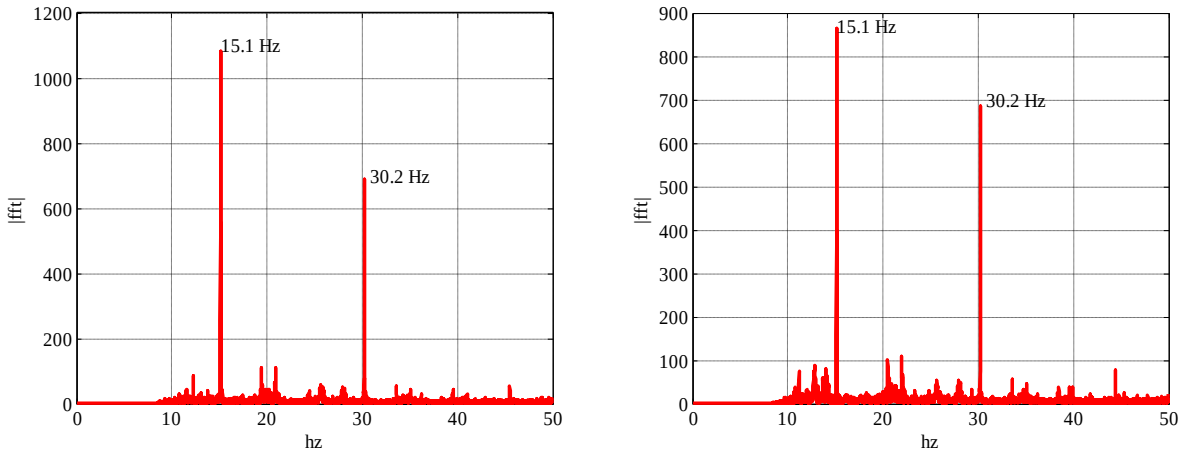

Figure 3.33 FFT plots for the input and the output for pre - surge during strong disturbance in sensor 4 in the vertical direction for (a) input signal; (b) output signal.

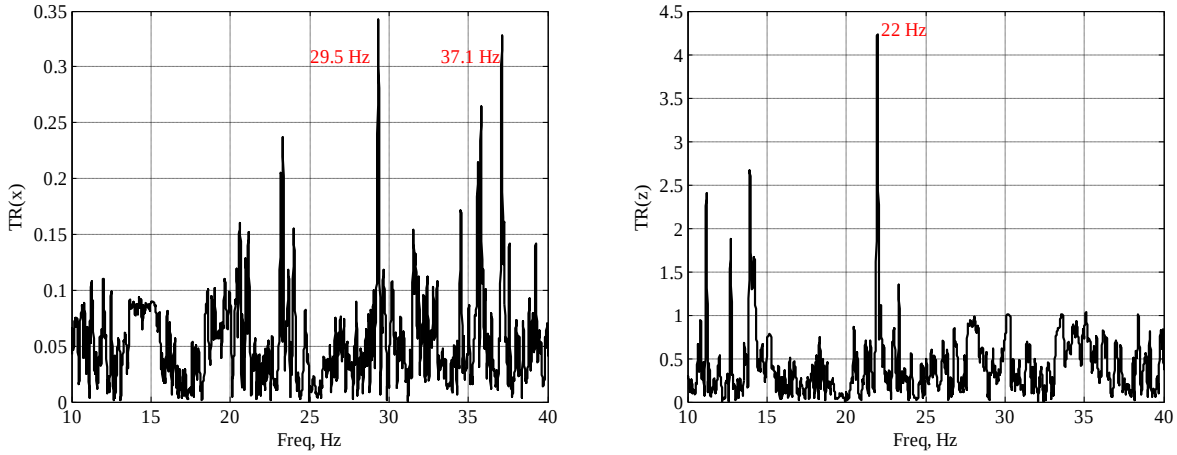

Figure 3.34Transfer Function between the input and the output with the model embedded on the dry sand during strong disturbance in sensor 4 (185 - 285s): (a) in the lateral direction; (b) in the vertical direction.

As the test go, the transfer function in Test 3, before the maximum surge for vertical mode as displayed in Figure 3.34 throughout the test data reveals the fact that the first mode getsincreased from 11.2 Hz to 22 Hz, which is consistent with the Case1 result. But the trend for the lateral direction as illustrated in Figure 3.34 is irregular where the first mode is hard to predict as the curve is not showing regular trend, it may be attributed because of noise or any disturbance, for the last transfer function plot the lateral direction first mode becomes consistent with 29.5 Hz frequency, decrease from 36.4 Hz as compared to case 1 result.

Test 3-Post surging

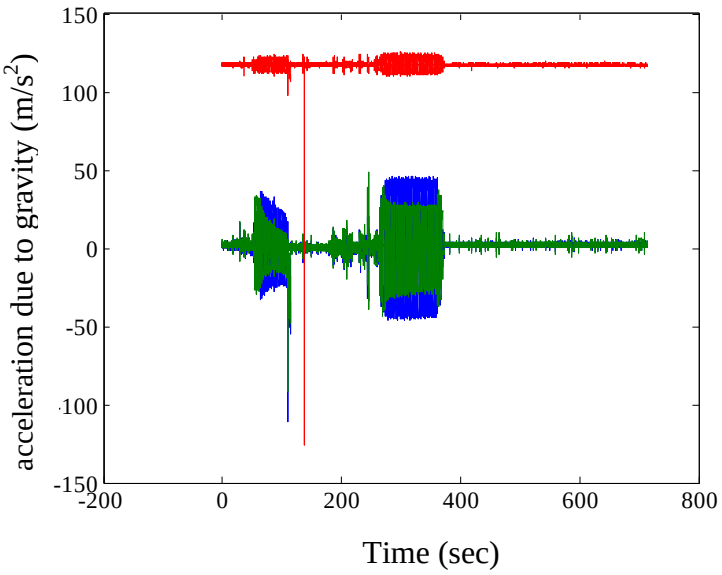

Figure 3.35Time recorded data from input (Sensor 4)

After taking the reading for model embedded in the wet soil, for the post surge condition the same test is repeated as displayed in Figure 3.35 shows time domain analysis as signal. The shaking response is considered for the cases in which the input has most disturbances. Using the time domain data those intervals are considered and corresponding FFT and Transfer function plots are plotted

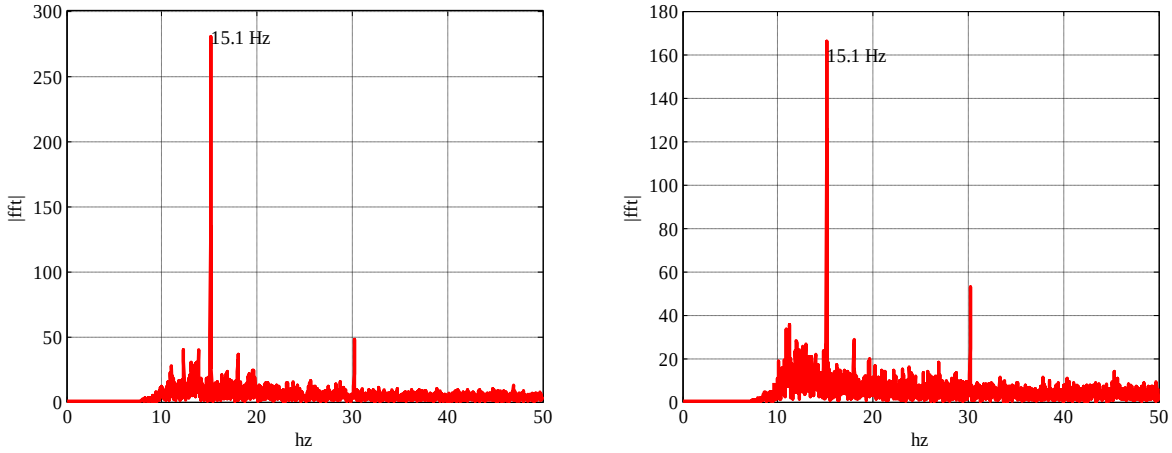

Figure 3.36 FFT plots for the input and the output for post - surge during strong disturbance in sensor 4 in the vertical direction for (a) input signal; (b) output signal

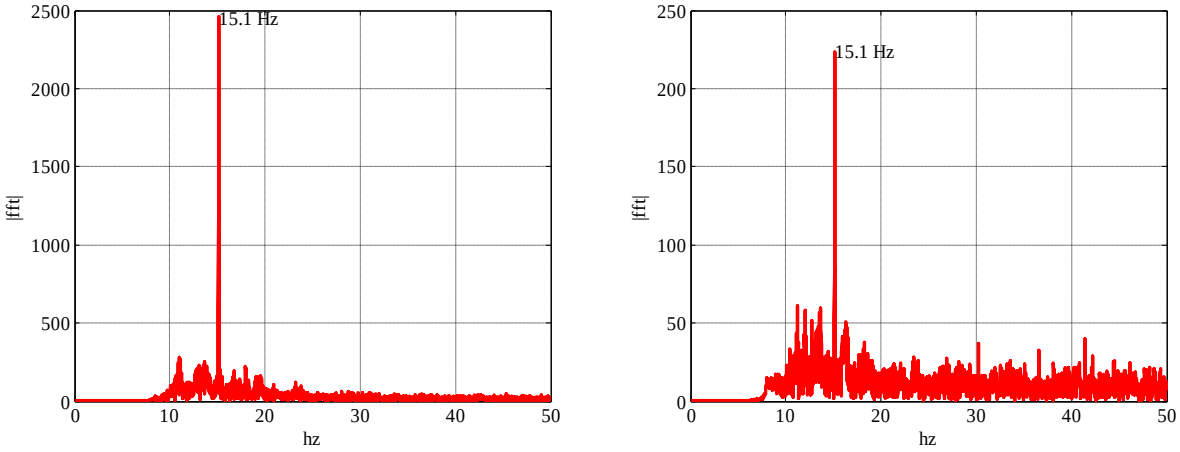

Figure 3.37 FFT plots for the input and the output for pre - surge during strong disturbance in sensor 4 in the lateral direction for (a) input signal; (b) output signal

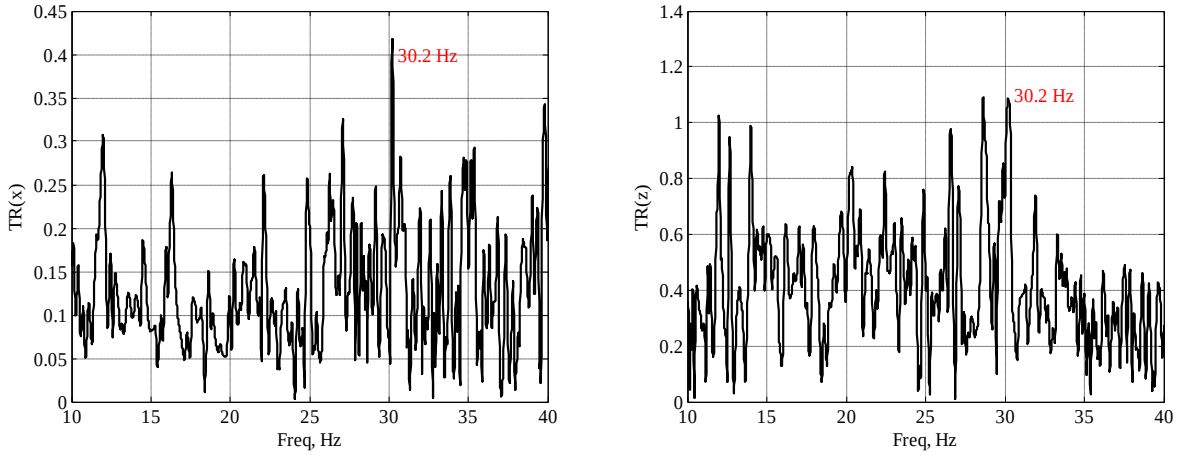

Figure 3.38Transfer Function between the input and the output for pre – surge during strong disturbance in sensor 4: (a) in the lateral direction; (b) in the vertical direction

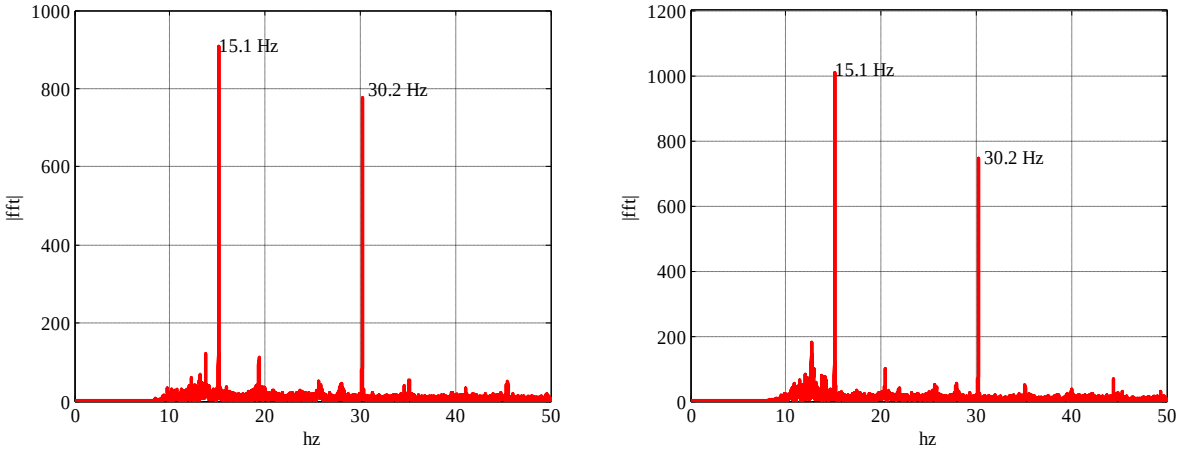

Figure 3.39 FFT plots for the input and the output for post - surge during strong disturbance in sensor 4 in the vertical direction for (a) input signal; (b) output signal.

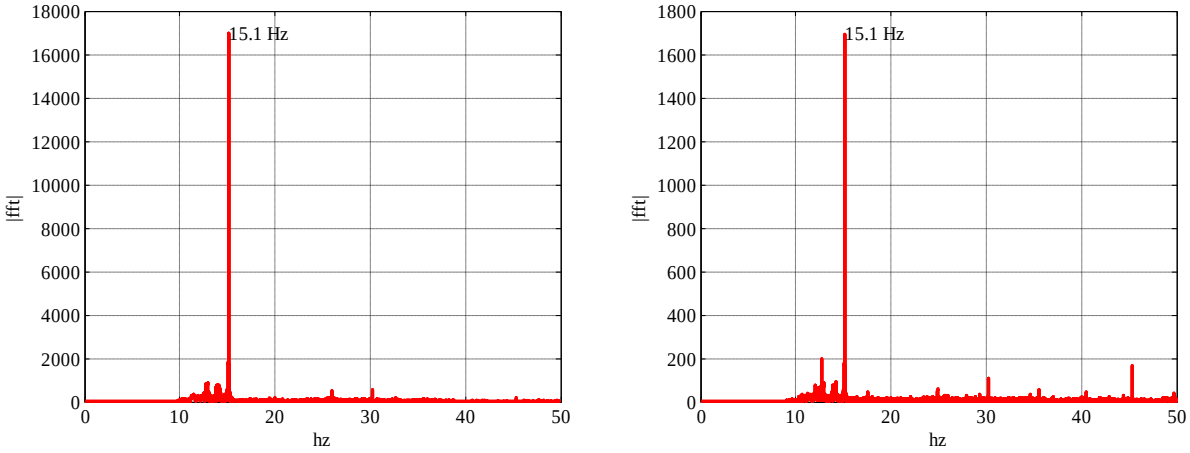

Figure 3.40 FFT plots for the input and the output for post - surge during strong disturbance in sensor 4 in the lateral direction for (a) input signal; (b) output signal

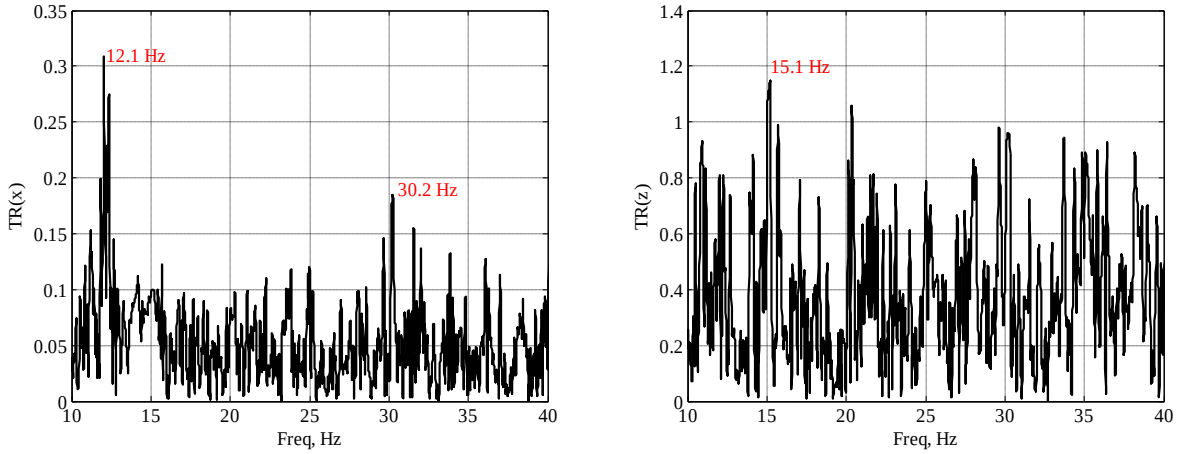

Figure 3.41Transfer Function between the input and the output for post – surge during strong disturbance in sensor 4: (a) in the lateral direction; (b) in the vertical direction

During this test, the first mode as displayed in Figure 3.38 shows frequency slightly decreases to 30.2 Hz in the lateral direction, and the random peaks at lower frequency might be because of the disturbances aroused from the noise or any other disturbance, it is interesting to observe the modal frequencies when the surge reaches maximum. The lateral mode as displayed in 3.41 shows decrease, this is primarily attributed to the fact that the accumulated scouring has weakened the lateral stiffness drastically.

3.4 Conclusion and Discussion

Flood and flood-induced scour have been long recognized as a leading cause of bridgefailure in the United States. Two other types of combined hydraulic impact and scour hazard that have drawn attention are due to storm surgewhose impact on buildings and bridges are discussed in Chapter 1and 2. Computational assessment of capturing the complex soil-structure interaction has been discussed by available soil-structure interaction models in chapter 2. Thus it has been tried to show the impact of storm surge on buildings and bridges along with soil-structure interaction. Chapter 3 introduces the proposed concept of soil-fluid-structure interaction presented in previous chapters. Due to the complexity in assessing the combined effects of flooding or storm surge and their respective scouring during and in the immediate aftermath of a storm, laboratory-scale testing of fluid-structure systems is performed and discussed in chapter 3 to capture the response of structures before and after a surging event which due to the combined soil-fluid-structure interaction is a complex multi-physics problem. By characterizing the structural properties of a small scale model structure subject to 1-g scale surging, it has been shown from the transfer function plots that the soil-fluid-foundation-structure model reduces in rigidity as the surge event occurs. Thus the soil stiffness decreases due to surging and leads to scouring. The hydraulic flume test results shed light for further conducting tests at full scale such as to establish both sophisticated and reduced-order computational modeling for soil-fluid-structure systems. In this regard for computational modeling of soil-fluid-structure model, chapter4 introduces the available material models used commercially for such analysis.

.

CHAPTER 4

SOIL MATERIAL MODELING AND VERIFICATION

In this chapter, the different soil material models are discussed that captures the material nonlinearity and predicts the behavior of soil under different loading conditions. These material models include Mohr-coulomb,Cam clay and Modified cam clay model, Duncan Chan model.

4.1 General Overview

Soil is a porous medium with open voids which contains water, air in the voids of the skeleton; to describe its behavior correctly soil has to be considered multiphase material that is influenced by the properties of each phase and interaction with each other.Depending on the permeability of the soil and velocity of the external loading in static loading conditions, excess pore water and time dependent deformations of the soil can occur. In dynamic loading conditions effects due to temporary decrease in the shear strength of the soil can occur. Liquefaction of the soil can cause great damage in the case of earthquake loadings [30].

Dynamic soil-structure interactions are based on equivalent single phase material models of the soil, it can be analyzed using two phase material, soil comprises of solid skeleton with interconnected pores filled with water. The two phase formulation of Biot (1956) helps in predicting the dynamic response of saturated soils.Poroelastic behavior involves solid to fluid coupling which occurs when change in applied stress produces change in fluid pressure. And fluid to solid coupling occurs when a change in fluid pressure produces change in the volume of the porous material.

4.2 Theoretical Background

The subsoil usually consists of three phases: solid particles, water and air. The resulting governing equation representing the soil behavior as a multiphase material consists of system of coupled partial differential equations: mass balance equations or continuity equations and linear momentum balance equations for each phase or for the multiphase medium [31].

The governing equation for coupled pore water soil problems can be derived from Biot's theory of saturated porous media, which is based on continuum mechanics. For liquefaction and consolidation analyses, a u-p formulation is adopted where displacement of solid and water pressure are used as the unknown variables [32].

Governing Equations for Fluid-Solid Two Phase Materials

The governing equation for coupled pore water-soil problems can be derived from Biot's theory of saturated porous media, which is based on continuum mechanics. For liquefaction and consolidation analyses, a u-p formulation is adopted where displacement of solid and water pressure are used as the unknown variables [33].

The following assumptions are adopted in the u-p formulation:

- An infinitesimal strain is assumed.
- The acceleration of the solid phase is much higher than that of the relative acceleration of the fluid phase.
- Grain particles of solid are incompressible
- The effect of temperature is disregarded.

The motion of multiphase medium is described by superposition of solid phase and fluid phase for fluid-solid two phase mixture; it is assumed that each point within the mixture is occupied simultaneously by two constituents.

The density of the mixture is described by

$$\rho_r = (1-n)\,\rho_s + n\,\rho_w \tag{4.1}$$

Where n is the porosity, ρ_s and ρ_w is the density of the solid grains and water. The linear momentum balance equation of the mixture of solid and water is given by

$$S^T\,\sigma_{tot} - \rho_r\,a_s + \rho_r\,b = 0 \tag{4.2}$$

$$S = \begin{bmatrix} \frac{\partial}{\partial x} & 0 & 0 \\ 0 & \frac{\partial}{\partial y} & 0 \\ 0 & 0 & \frac{\partial}{\partial z} \\ \frac{\partial}{\partial y} & \frac{\partial}{\partial x} & 0 \\ 0 & \frac{\partial}{\partial z} & \frac{\partial}{\partial y} \\ \frac{\partial}{\partial z} & 0 & \frac{\partial}{\partial x} \end{bmatrix} \tag{4.3}$$

Where:

S = differential operator

σ_{tot} =Total stress state

a_s = Acceleration of the solid grains

b = Body force per unit mass

Effective and partial stresses of the fluid-solid mixture

$$\sigma_{ij} = \sigma_{ij}^s + \sigma_{ij}^f \tag{4.4}$$

Where σ_{ij}^s , σ_{ij}^f is the partial stress tensor for the solid phase and the fluid phase.

The partial stresses for the fluid and solid phase are given by

$$\sigma_{ij}^{f} = -n\,p\,\delta_{ij},\ \ \sigma_{ij}^{s} = \sigma_{ij} - (1-n)\,p\,\delta_{ij} \tag{4.5}$$

Where, p is the pore water pressure, n is the porosity.

For the mixture of the solid and water phases the relation between strain and total stress is defined in an incremental formulation, furthermore, the effective stress is defined as

$$\sigma_{tot} = \sigma' - m\,n_w\,p_w \tag{4.6}$$

$$\delta\sigma_{tot} = k\,\delta\varepsilon - m(\delta p_w) \tag{4.7}$$

Where

σ' = Effective stress state

m = second- order unit tensor

n_w = Effective area coefficient

p_w = Pore water pressure

$\delta\sigma_{tot}$ = Total stress increment

K = Stiffness matrix of the soil skeleton

$\Delta\,\varepsilon$ = Strain increment

Δp_w = Pore water pressure increment

The continuity equation combined with a linear balance of momentum for the water phase is

$$\nabla^{T}\,\frac{\kappa}{\mu_w}(-\nabla p_w - \rho_w a_s + \rho_w b) + \alpha\,m\,\dot{\varepsilon}_s + \frac{\dot{p}_w}{Q} + \dot{s}_0 = 0 \tag{4.8}$$

$$\frac{1}{Q} = \frac{n}{K_w} + \frac{\alpha - n}{K_s} \tag{4.9}$$

And the Biot's constant

$$\alpha = 1 - \frac{K_T}{K_S} = 1 - \frac{\frac{E}{3-6\nu}}{K_S} \tag{4.10}$$

Where

κ = Intrinsic Permeability

μ_w = Dynamic viscosity of water

ε_s = Strain rate of the soil skeleton

S_0 = Rate of volume expansion of the solid

K_w = Bulk Modulus of water

K_s = Bulk modulus of the solid grains

K_T = Bulk Modulus of the soil skeleton

E = Young's Modulus of the soil skeleton

υ = poisson's ratio of the soil skeleton

4.3 Available Material Models

Mohr-Coulomb

Is a first order model used to model soil behavior and is an elastic-perfectly plastic model. Hooke's law is valid for the elastic range where the model's stress-strain behaves linearly in the elastic range with parameters from Hooke's law (E, V). It assumes that maximum shear stress controls failure and the failure shear stress depends on the normal stress. The Mohr-Coulomb criterion can be written as

$$\tau = c - \sigma \tan\phi \tag{4.11}$$

$$s = \frac{1}{2}(\sigma_1 - \sigma_3) \tag{4.12}$$

Where s is half the difference between the maximum and minimum principal stresses

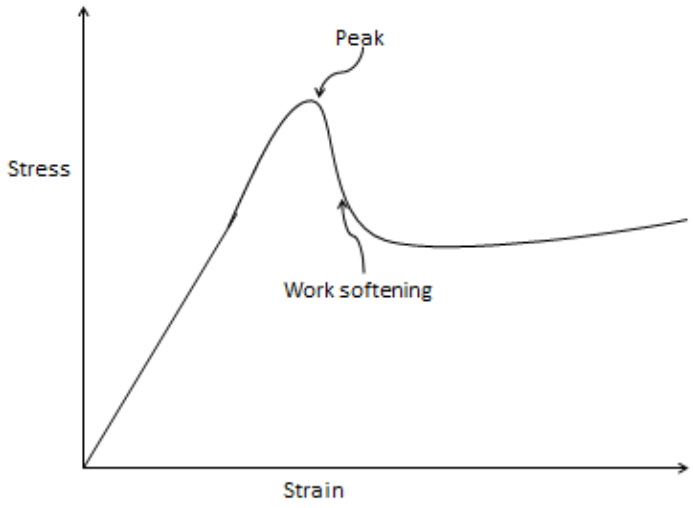

Figure 4.1 Elastic-perfectly plastic assumption of Mohr-Coulomb model [33]

Duncan-Chang Model

Soil inhibits stress dependent stiffness and behaves highly nonlinear. Stress dependent model is known as hyperbolic model, which approximates hyperbolae with high degree of accuracy for stress-strain curve in triaxial compression test of both clay and sand. Its failure criteria is based on Mohr-Coulomb's two strength parameters, and this model predicts the complex behavior of soil namely non-linearity, stress-dependent and inelastic behavior of cohesive and non-cohesive soil.

For plastic deformation to occur and to remain continue the state of stress must remain on the yield surface, corresponding loading should be, otherwise the stress must reduce below yield value and in this case no further plastic deformation occurs and all incremental deformations are elastic [34].

Cam-Clay and Modified-Cam Clay Critical State Strength Model

Cam Clay and Modified-Cam Clay soil model is formulated using three important aspects of soil behavior.

- Strength
- Compression or Dilatancy
- Critical State

Volume occupied by the soil mass consists of voids that are filled by fluids, due to which deformation in soil results volume change, and cap plasticity models have the ability to model volume changes more realistically [28].

In critical state mechanics, the state of a soil sample is characterized by three parameters:

- Effective stress
- Deviatoric (Shear stress)
- Specific volume

The mean pressure and deviatoric stress are related to the principal stresses as

$$p = \frac{1}{3}(\sigma_1 + \sigma_2 + \sigma_3) \tag{4.13}$$

$$q = \frac{1}{\sqrt{2}}\sqrt{(\sigma_1' - \sigma_2')^2 + (\sigma_2' - \sigma_3')^2 + (\sigma_3' - \sigma_1')^2} \tag{4.14}$$

The specific volume is defined as M = 1 + e, where e is the void ratio.

Virgin Consolidation Line and Swelling Lines

The model assumes that under isotropic stress condition and under perfectly drained condition if soft soil sample is slowly compressed, the relationship between specific volume and In p’ consists of a straight virgin consolidation line or normal compression line, and swelling

lines also called as unloading-reloading lines. The virgin consolidation line is defined by the equation.

$$v = N - \lambda \ln p' \tag{4.15}$$

The equation for the unloading-reloading lines

$$v = v_s - \kappa \ln p' \tag{4.16}$$

The slope of the normal compression line on v-ln p' plane, slope of the swelling line and N is the specific volume of normal compression line at unit pressure, and are the characteristic properties of a particular soil.

The Critical State line

At critical state, distortion of soil takes place at constant state of stress with no volume change. In p'-q plane the CSL is a straight line passing through the origin with the slope equal to M, one of the characteristic of the material.

Yield Functions

The yield functions for MCC models are represented as

$$\frac{q^2}{p'^2} + M^2 \left(1 - \frac{p_o'}{p'}\right) \tag{4.17}$$

In p'-q space the yield surface plots are elliptical curve.

4.4 Drained and Undrained Conditions

When saturated coarse grained soils are slowly loaded, volume change occurs, pore water pressure dissipate rapidly due to high permeability. This condition is called as Drained Loading. But when fine grained soils are loaded, they generate excess pore pressures that remain entrapped inside the pores because these soils have very low permeability. This is called as

undrained loading. Undrained condition means that there will be no volumetric change in the soil specimen.

In finite element methods, the drained behavior of a soil can be simulated using coupled analysis, where pore water pressure is calculated for a specific given load in each soil element and then subtracted from the total stresses to estimate the effective stresses in the element. These effective stresses govern the deformation and shear strength of the soil element according to the effective stress principle [35].

Four main boundary conditions must be considered for a successful finite element analysis of soils considering undrained behavior.

- Initial conditions of the soil strata which will determine the initial stiffness and strength of the soil strata, must be estimated carefully and implemented in the analysis.
- Boundary condition must be defined carefully: pervious or impervious.
- Long term strength parameters of the soil must be used in the soil model.
- Load should be applied fast which will not allow enough time for the pore water pressure to dissipate, as compared to drained condition where the loads is applied very slowly to avoid the generation of excess pore water pressure throughout the analysis.

  Similarly four main boundary conditions must be considered for a successful finite element analysis of soils considering drained behavior.

- Initial conditions of the soil strata such as initial geostatic stresses, initial pore water pressures, and initial void ratios which will determine the initial stiffness and strength of the soil strata, must be estimated carefully and implemented in the analysis.
- Boundary condition must be defined carefully: pervious or impervious.
- The long term strength parameters of the soil must be used in the soil model.

- Loads must be applied very slowly to avoid the generation of excess pore water pressure throughout the analysis.

4.5 Modified Cam Clay Soil Model and Verification

Consider a cylindrical soil specimen with diameter 5cm and height 5cm subjected to a 210 kPa confining pressure, the clay specimen is normally consolidated and has a constant permeability and initial void ratio. Assuming that the clay obeys poroelastic soil material model simulate the consolidated-undrained behavior of this soil.

Table 4.1Parameters input for analysis [35]

Parameters	Magnitude
Log of Bulk Modulus	0.1174
Stress ratio at critical state	1
Tensile limit	0
Mass density	3.8
Log of Bulk Modulus	.026
Poisson's ratio	.28
Void ratio	1.5

Finite Element Mesh

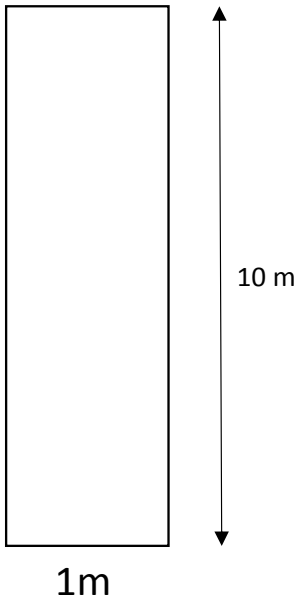

Figure 4.2 Column of Soil

A two dimensional axisymmetric mesh is used with one element chosen as pore fluid eight node axisymmetric quadrilateral element with biquadratic displacement, bilinear pore pressure, and reduced integration. The boundary conditions of the finite element mesh is as follows: The vertical component of displacement is fixed, the left hand side of the mesh is a symmetry line, on the top downward displacementof the loading plate is specified as 0.127 cm at a displacement rate of 1.27 x E 3 cm/s. This displacement along with impervious boundaries will cause the excess pore water pressure to generate.

Analysis

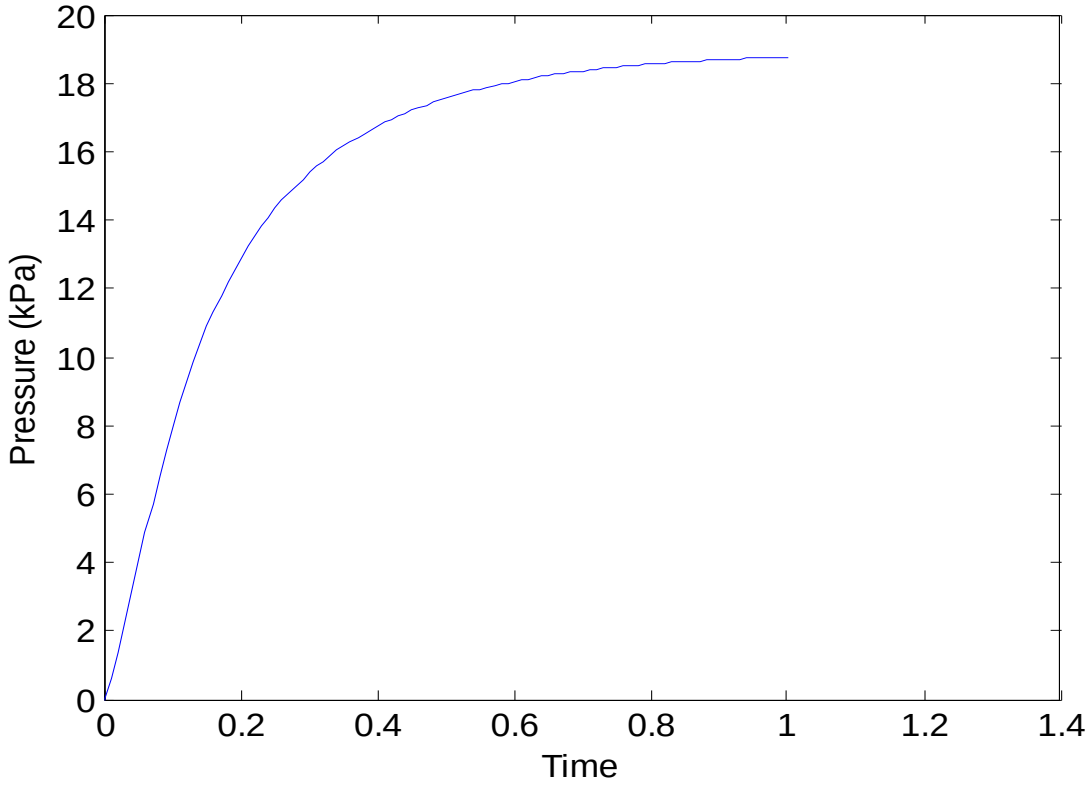

Figure 4.3 Variation of Pore water pressure with time

The problem of one dimensional consolidation is run in two steps,

The first step consists of consolidation step; an all-around confining pressure of 210 kPa is applied while drainage is permitted across the top surface. This step refers to geostatic step is used to make sure that equilibrium is satisfied within the soil layer. It also makes sure that the initial stress condition in any soil falls within the initial yield surface of the cam clay model. The second step consists of undrained shearing step, has duration of 100 seconds. In the beginning of this step the pervious boundary condition at the top surface is removed restricting the top surface to be impervious. The loading plate is forced to displace downward a distance of 0.127 cm at a displacement rate of 1.27 x E-3 cm/s. This rate of displacement along with impervious

boundaries will cause the excess pore water pressure to generate element falls within the initial yield surface of the Cam clay model

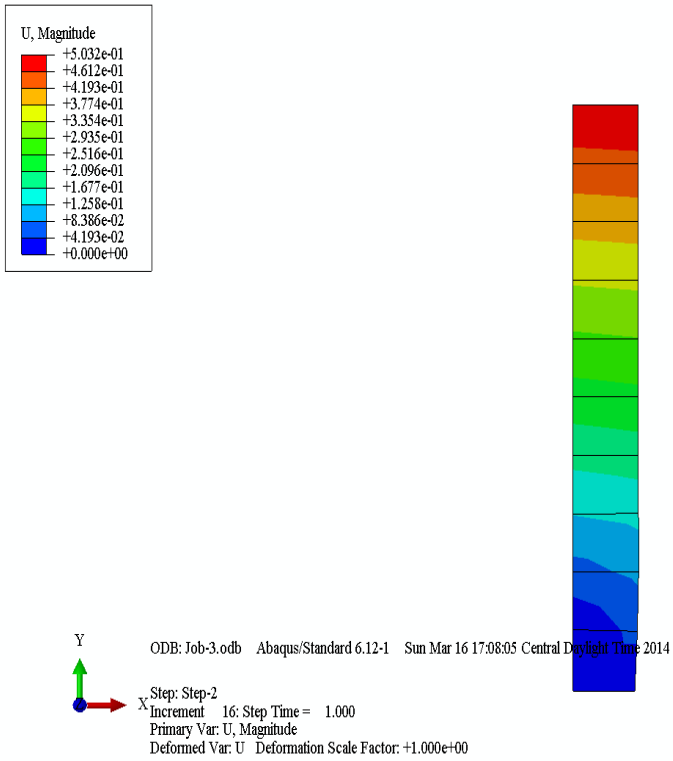

Figure 4.4 Displacement variations within the soil column

The whole analysis can be interpreted as during the undrained condition at the first stage of the analysis the soil model is subjected to a constant confining pressure, then in the second stage the soil model is subjected to the pressure stress while the drainage valve is closed that means there will be no volumetric change in the soil specimen, confirming the undrained condition. There will be no volume change in the soil specimen, in other words excess pore water pressure will be developed inside the soil specimen throughout the analysis.

4.6 Conclusion and Discussion

Chapter 4 discusses the properties of soil, which is a heterogeneous mixture of solid particles, water and air filling the pore space. Saturated soil has two components solid particles and water. Different soil models available computationally in finite element analysis (FEA) are discussed with regard to that soil model that can accurately model the response of soil material during storm activity. Modified cam clay soil material model showed better result as it can capture the pore water pressure in soil. The validation of modified cam clay model has been tested where due to undrained loading condition the pore water pressure increases in the soil mass and afterwards it decreases, predicting the actual behavior of saturated soil during loading condition. Chapter 5 introduces soil-structure modeling using the modified cam clay soil model, where static pushover analysis is performed computationally to provide realistic soil-structure interaction tool.

CHAPTER 5

PARAMETRIC SOIL-STRUCTURE MODELING USING ABAQUS CAE

In this chapter brief review is being done on the usage of commercial available finite element software abaqus. Using Abaqus software computational static pushover analysis is performed on a foundation embedded in the inelastic soil, and supported by a slender structure. The static horizontal force induces primarily an overturning moment and a secondary shear force in the foundation. The footing eventually uplifts from the soil, provoking strong inelastic soil response culminating in development of a bearing-capacity failure mechanism and progressive settlement. Parametric study is discussed through which the factors affecting the response of foundation are varied to note the

5.1 Abaqus Analysis

General Overview

Finite element models are created in Abaqus Cae using graphical user interface that can be analyzed in Abaqus Standard. The abaqus scripting uses python commands that are equivalent to the models and data used by Abaqus. The abaqus python scripting is an extension of the python object-oriented programming language. Commands are issued internally by Abaqus Cae when Abaqus Cae graphical user interface is used to create model and visualize the results. These commands represent the geometry and material properties created and assigned to the model. The commands issued by the GUI are sent to the Abaqus Cae Kernel, which interprets the commands to create internal representation of the model. The GUI is the interface between the user and the kernel.

The abaqus scripting interface directly interact with the kernel, without using the help of Graphical User Interface. The uses of scripting are following

- To automate repetitive tasks - Create a script that executes when a user starts an Abaqus Cae session which may represent script used to define a library of standard material, as a result when the user enters the property module, these materials will be available.
- To perform a parametric study – Create a script that incrementally modifies the geometry of a part and analyzes the resulting model. The same script can read the resulting output databases, and generate results.

Model Using GUI

Abaqus 6.12 is used to create a simple model using GUI,when model is created in Abaqus Cae, two files are automatically created in the work directory. The replay file records every action that is performed in CAE and also the mistakes that were made and corrected. This file can be run to note all the work that has been done on the model. The second files recover file records the minimum necessary commands to recreate the model. When a model is saved. abaqus cae uses the recover file to write a journal file. The journal file is the python script that shows al work saved on the model. Recover file is deleted when model is saved in Abaqus Cae and all commands are transferred to the Journal file. The easiest way to trace the python scripts is to create model in Abaqus Cae using GUI and then save the Python commands from the recover or Journal files as a separate script file [36].

- Create Part: Three dimensional, two dimensional parts can be created by sketching in Abaqus Cae GUI sketch.

- Create Material: Abaqus Cae allows a wide range of inbuilt material properties including elastic and in elastic materials. User defined materials can be assigned to the corresponding model but it requires significant coding to define User defined material.
- Create Assembly: Assembly module is used to create and modify the assembly. The model contains only one assembly, which is composed of instances of parts from the model.
- Create Step: Is used to define a sequence of convenient way to capture changes in the loading and boundary conditions of the model, changes in the way parts of the model interact with each other.
- Interaction Module: Is used to create interaction between regions of a model or between regions of a model and its surrounding model.
- Load Module: Is used to define and manage the prescribed conditions of loads, Boundary conditions, Predefined fields and Load Cases.
- Mesh Module: Allows generating meshes on parts and assemblies created within Abaqus Cae. Mesh attributes are assigned to the model such as seeds, mesh techniques, and element types.
- Job Module: After defining the geometry of the model, assigning section properties and defining contact, Job Module is used to analyze the model. It allows creating a job, submitting it for analysis and monitoring its progress.

Parametric Scripting

Parametric studies allow generating, executing and accumulating the results of multiple analyses that differ in the values of parameters used in place of input quantites. Parametric studies can be performed by creating a template parametrized input files from which different

parametric variations are generated. A parametric study is useful when multiple analyses are performed to provide information about the behavior of a structure or component at different design points in a design space. The inputs for these analyses are varied by assigning the parameters of a parameterized keyword input file. Parametric studies in Abaqus can be done by developing a Python script in a file with .psf extension that contains python commands to define the parametric study.

A parametric study is associated with a particular set of parameters that define the design space. Each parameter should be defined which to be has selected to be considered in a parametric study. Parameters are differentiated as either continuous or discrete in nature and may have a domain and reference value. Sample values for each parameter are specified through which design points in the design space are analyzed. An initial definition and sampling of the parameters in the parametric study must be given before any combinations of parameter can be specified. In summary parametric studies in Abaqus Cae are organized as follows:

- Create Parametric study
- Define Parameters
- Sample Parameters
- Combine Parameters
- Constrain designs
- Generate designs and job analysis
- Execute the job analysis for selected designs of the study
- Result gathering
- Report generation from gathered result

5.2 Static Pushover Analysis

Geometry

The finite element analysis was carried out with commercially available finite element software Abaqus v.6.12 (Dassault System). A 2 meter wide foundation supporting a 5 meter high mars, foundation being embedded in the soil.A series of two dimensional finite element analyses is reformed for SDOF oscillator on a foundation embedded in inelastic soil allowing uplift. The mars element, which allows the introduction of lumped mars at a point is located 5m above the foundation level and is connected to the footing using linear elastic beam elements. The modulus of elasticity of the beam is selected such as structure has a fixed base natural period. Horizontal displacement controlled load is applied on the mass element which causes foundation uplifting from the soil [37].

Mesh type and element property

The soil is modeled with continuum solid plane strain 4 noded bilinear elements. The interface of soil footing is modeled through advanced contact algorithm to encounter the potential uplifting of the foundation. The contact is further defined through node surface interaction for soil footing interaction with contact boundaries such as large coefficient of friction at the soil footing interface to prevent sliding of the footing and a hard contact pressure overcome relationship for normal behavior. The soil in the analysis is modeled with modified cam clay (MCC) constitutive model with the same material properties defined in chapter 3

The saturated unit weight of the soil is considered to be 18.4 KN/m3. Analysis is carried in two stages. The first stage consisted of creating the geostatic stress in the soil. The second stage consists of application of displacement controlled load on the mars element, which primarily induces shear force and overturning moment at the foundation.

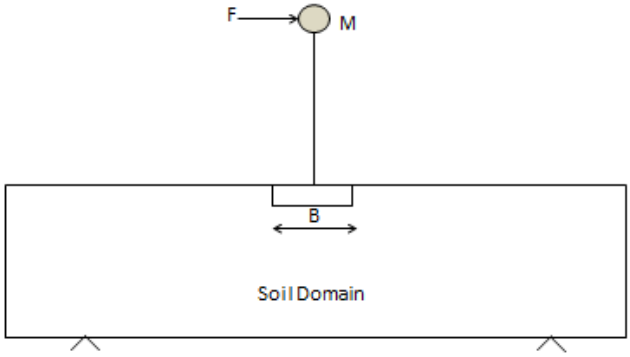

Figure 5.1Illustration of static pushover problem analyzed

- Geostatic Step:- The first step consist of creating the geostatic stresses in the soil by providing self-weight to the soil by considering the gravity load as a body force on the soil. Under equilibrium of stress conditions in the soil, shear strength profile of soil is obtained.
- Static Step: - Horizontal displacement controlled load is applied on the mass element.

Verification of bearing capacity

Meyerhof (1963) developed a generalized bearing capacity equation including correction factors for foundation depth, foundation shape and inclined loads.

$$q_u = c' N_c F_{cs} F_{cd} F_{ci} + q N_q F_{qs} F_{qd} F_{qi} + \frac{1}{2} \gamma B N_\gamma F_{\gamma s} F_{\gamma d} F_{\gamma i} \quad (5.1)$$

Where N_c, N_q are the bearing capacity factors:

$$N_q = \tan^2 (45 + \frac{\varphi'}{2}) e^{\pi \tan \phi'} \quad (5.2)$$

$$N_c = (N_q - 1) \cot \phi' \quad (5.3)$$

$$N_\gamma = 2(N_q + 1)\tan\phi' \tag{5.4}$$

For depth of footing/ Breath of footing less than 1 (Shallow Foundation)

$$F_{cd} = 1 + 0.4\frac{D_f}{B} \tag{5.5}$$

$$F_{qd} = 1 + 2\tan\phi'(1 - \sin\phi')^2\frac{D_f}{B} \tag{5.6}$$

Bearing capacity of a 2 m wide strip foundation on a 16 m thick homogeneous layer of sand underlain by bedrock. The foundation is subjected to an inclined loading, with the foundation depth of 1 m. The unit weight of soil is 19 kN/m^3.A layer of sand is loaded by a strip footing. The modified cam clay model is used to simulate the behavior of the sand. The concrete foundation assumed to be linear elastic foundation with a young's modulus of 1435 MPa and a Poission ratio of 0.2.

Reduced integration, bilinear, plane strain quadrilateral elements are used for the sand and the concrete foundation. The base of the sand layer is fixed in all direction. All vertical boundaries are fixed in the horizontal direction but free in the vertical direction. Mesh is finer in the vicinity of the foundation as this zone is the zone of stress concentration. Dimensions of the sand layer are chosen in a way that the boundary effect on foundation behavior is minimized. In the beginning of the analysis, gravity loads are applied to the sand layer. These loads are applied to maintain equilibrium before the start of analysis, and it determines the initial stresses in the soil elements. During this step geostatic step is invoked to make sure that the initial stress condition in any sand element falls within the initial yield surface of the cam clay model. An increasing point load having horizontal and vertical components is applied at the center of the foundation. The resultant of these two components is inclined at 15°angle from the vertical.

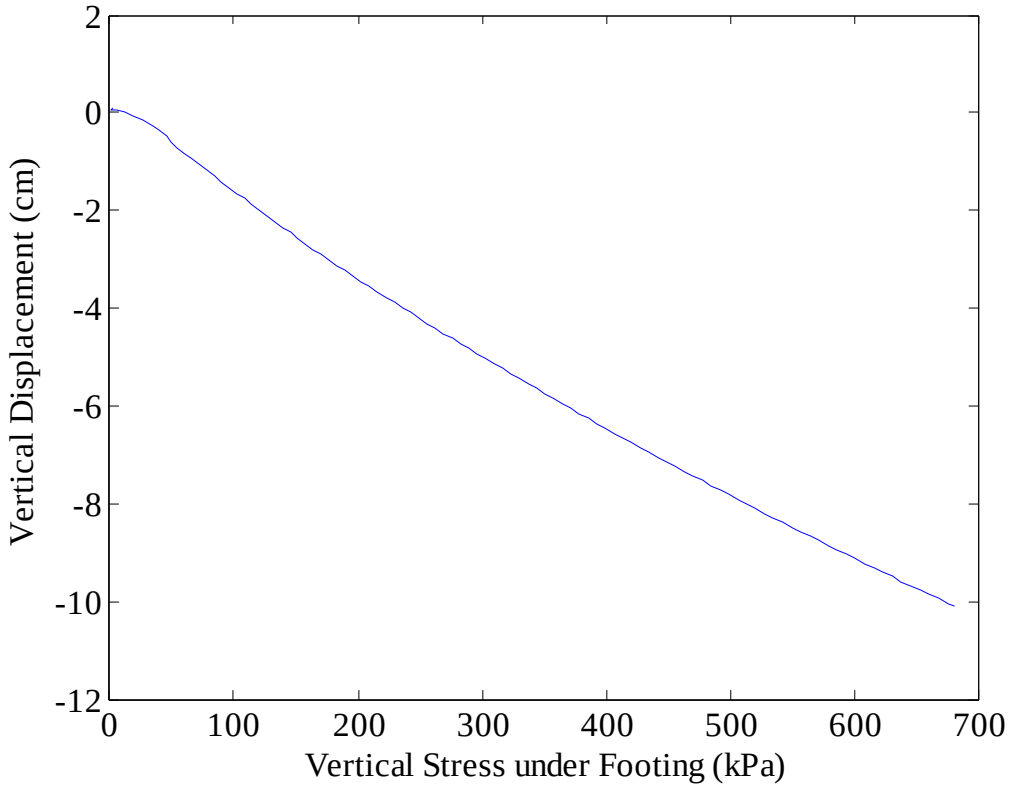

Figure 5.2 Load-displacement curve of footing with an inclined load

Load displacement relationship for the 2m wide shallow footing is established. The bearing capacity of the footing is predicted from the finite element analysis of approximately 675 kPa as compared to analytical result of bearing capacity of 738 kPa predicted from analytical solution of Meyerhof's equation.

5.3 Conclusion and Discussion

For the static pushover analysis displacement controlled horizontal force is applied to the mass of the superstructure. Parametric variation of factor of safety is performed aiming to achieve two different behaviors, that of a heavily loaded foundation where the failure mode is

related to the bearing capacity of the foundation and that of a typical conservatively designed , moderately to lightly loaded foundation for which uplift is the predominant failure mechanism.

Parametric study for system response parameters

The following section investigates the effect of key dimensionless parameters on the rocking response of SDOF system rocking on inelastic soil.

The system response depends on the following parameters:-

- Vertical foundation load in comparison with ultimate vertical capacity, the Nu, Expressed through the ratio $\chi=N/N_u$.
- Dimensionless frequency $a_o = \omega H / v_s$ where ω is the circular frequency of the fixed base structure, H is the height of superstructure and v_s is the shear wave velocity.

Three pairs of equivalent systems are examined, all having aspect ratio of 2. The factor of safety against vertical loads for the three pairs is 1.25, 2, 5, thus representing heavily loaded to lightly loaded foundations. Factor of safety plays a key role in the rocking response of the two systems. Plastic strain contours corresponding to two cases provides evidence for the soil plasticization taking place underneath the footing, leading to mobilization of a bearing capacity mechanism failure.

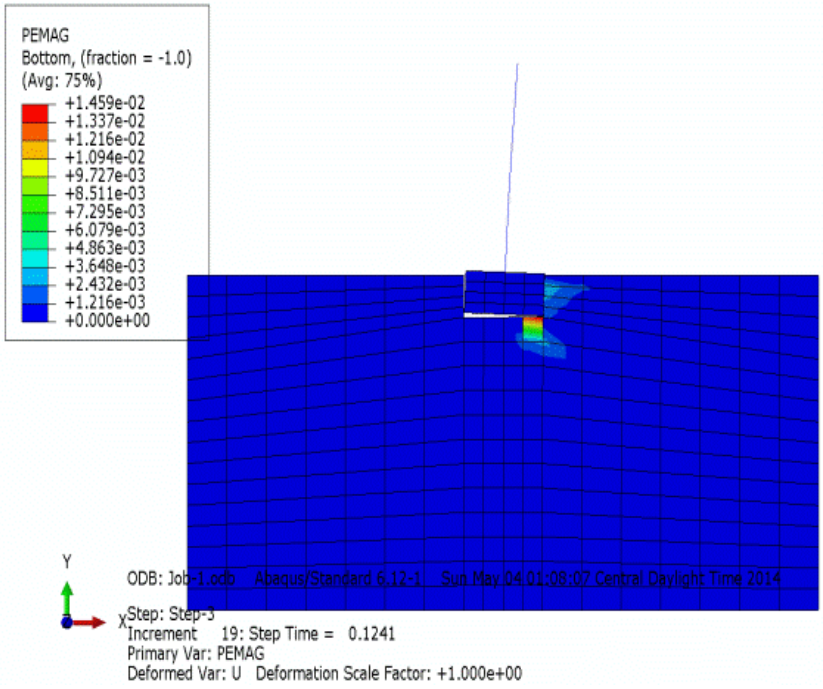

(a)

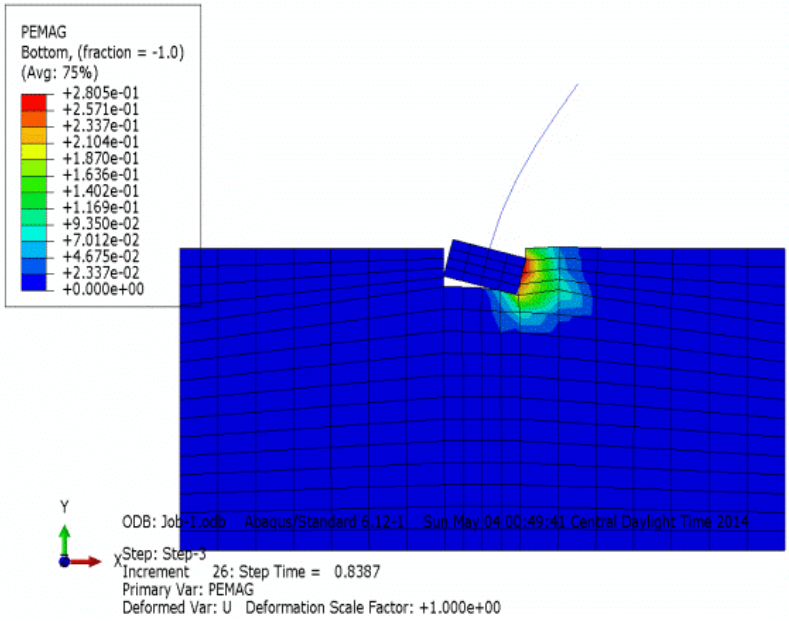

(b)

Figure 5.3 Plastic deformation contours corresponding to (a) lightly loaded foundation (b) heavily loaded foundation

The factor of safety plays a key role in the rocking response of the lightly and heavily loaded foundation systems as evidenced from the plastic strain contours in the case of heavily loaded foundation extensive soil plastification takes place underneath the footing leading to mobilization of bearing capacity failure mechanism. But in case of lightly loaded foundation very limited soil plastification takes place underneath the edge of footing. The ultimate moment-rotation curve corresponding to the two systems is

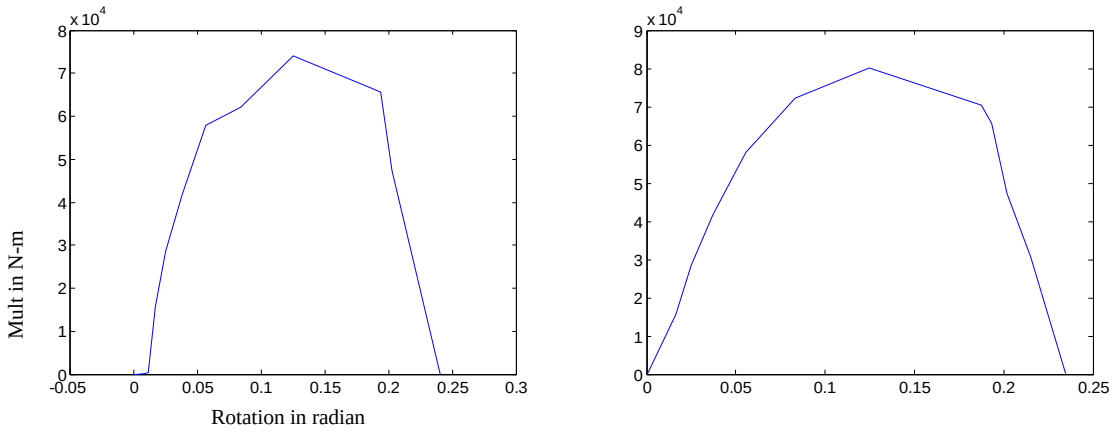

(a) (b)

Figure 5.4 Moment rotation curve corresponding to (a) lightly loaded foundation (b) heavily loaded foundation

The ultimate moment-rotation response of the two systems shows that the moment capacity of heavily loaded foundation is slightly greater than the moment capacity for the lightly loaded foundation.

Table 5.1Dimensionless products of three pairs of equivalent systems

Dimensionless product	Symbol	Range
Inverse of factor of safety. $1/FS_v$	x	0.2 0.5 0.85
Dimensionless frequency	a_o	0.3 0.6 1

To better understand the response of foundation, both the key response parameters are appropriately changed using the python script of abaqus cae model. Dependence of moment capacity of the foundation on the three safety factor and three dimensionless frequencies has been plotted.

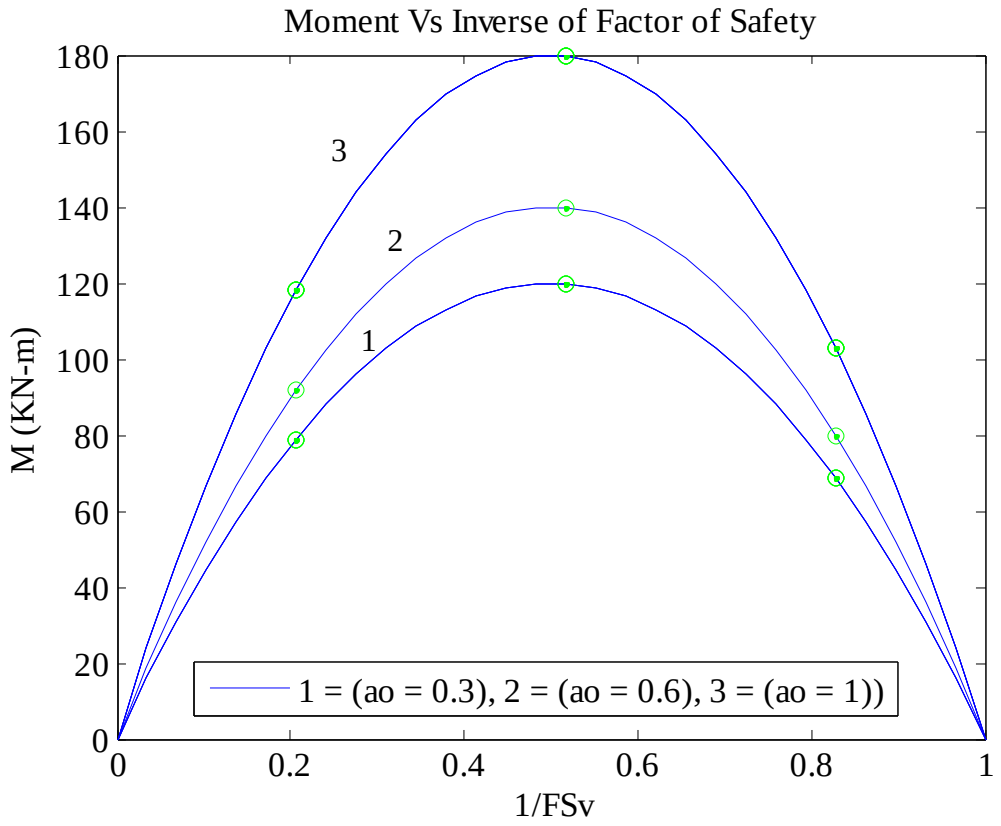

Figure 5.5 Dependence of moment capacity of foundation on dimensionless products (χ , a_o)

For the static pushover analysis the (Moment- $1/FS_v$) curve for the three range of the factor of safety along with the $a_o$is shown in the above figure, the largest value of moment capacity is reached for a static safety factor of about 2.By varying the value of a_o i.e. the stiffness of the structure the value of moment also varied.In Figure 6.5 curve 1 shows the variation of (Moment- $1/FS_v$) when the value of a_o is 0.3, as the value of a_o increases the maximum moment capacity also increases. From the curve it is clear that maximum moment is achieved when FS_v is 2. And for lightly and heavily loaded foundation the moment achieved is less.Curve 2 shows the same variation when the value of $a_o$is varied, again the value of maximum moment is achieved at FS_v 2 but the curve has been shifted up. Same observation can be seen for curve 3.

CHAPTER 6

CONCLUSIONS AND FUTURE WORK

The following conclusions can be drawn from the work done in this thesis on the physical modeling and system identification that proves the observation of hydraulic wave and scour impacts and computational modeling using simplified soil-structure model that proves the feasibility of developing a realistic order-reduced soil-structure modeling tool.

- From the hydraulic flume experiment it has been shown that the soil-fluid-foundation structure model reduces in rigidity as the surge event occurs as observed in the lateral transfer function plots.
- System identification has been performed to assess all the peaks of the frequency plots, and experimental test has been validated by the scour formation and observed deflection.
- From the computational simplified soil-structure model the behavior of an uplifting foundation of a relatively tall structure is affected by the magnitude of the normal force compared with the vertical bearing capacity of the foundation (i.e., the static factor of safety) and the non-dimensional frequency as an index of the structure-to-soil stiffness ratio.
- By parametrically increasingly varying the vertical load, initially the increased static settlement of the foundation delays the initiation of uplifting and leads to a higher value of maximum moment that can be achieved for any value of vertical load and it corresponds to factor of safety 2. At this loading best combination of uplifting and soil plastification is achieved. As the vertical load is further

increased the maximum moment starts decreasing as a result of the increased rate of plastification. The ultimate rotation also continues to decrease.

- By parametrically varying the dimensionless frequency which depends on the structure to soil stiffness the maximum moment decreases as the stiffness of the superstructure decreases.
- A Python language based scripting interface is developed to perform the parametric study by varying the key response parameters to note the change in structural response and predicts rapid hazard assessment.
- Rapid field-field based assessment and decision making can be made through the implementation of client based Python-code in terms of mobile applications.

Based on the research conducted the following recommendations are made on the future work related to the inelastic response of shallow foundation supporting a slender structure.

- Study the effect of varying other material and geometric properties of soil and foundation supporting structure to capture the modification in response of system as a whole.
- Perform cyclic pushover analysis and study the difference of structural response and compare it with static pushover analysis.
- Perform seismic analysis to study the difference in structural behavior and compare it with static and cyclic pushover analysis.
- Study and revise current seismic design which according to results shown is uneconomical and leads to very conservative seismic solutions. Also it transmits large inertial forces to superstructure during earthquake events.

APPENDIX A

Matlab code to plot transfer function

```
g = 9.807;

filename1a = './TestDataDec28/DryConditionBeforeTest1.txt'; %
dry Test1
% filename1b = './TestDataDec28/Test1_data.txt'; % Test 1
filename2a =
'./TestDataDec28/Test2_Data_before_flowing_of_water.txt'; % Wet
Condition Test 2
filename2b = './TestDataDec28/Test2_data_during_flow.txt'; %
Test 2 During water flowing
filename3a =
'./TestDataDec28/Test3_Data_before_flowing_of_water.txt';% Wet
Condition Test 3
filename3b = './TestDataDec28/Test3_Data_during_flow.txt'; %
Test 3 During water flowing


filename = filename3b; flag = 31;
[t1, sensor1, t2, sensor2, t3, sensor3, t4, sensor4] = ...
    data_read(filename);

switch flag
    case 10
        ix = t1<250&t1>180; % for filename1a
    case 20
        ix = t1<240&t1>170; % for filename2a
    case 21
        % ix = t1<240&t1>170; % for filename2b   % need to split
the data file (which is too large)
    case 30
        ix = t1<280&t1>200; % for filename3a
    case 31
        ix = t1<360&t1>280; % for filename3b
end

t1a = t1(ix); t1a = t1a-t1a(1);
t2a = t2(ix); t2a = t2a-t2a(1);
t3a = t3(ix); t3a = t3a-t3a(1);
t4a = t4(ix); t4a = t4a-t4a(1);
sensor1 = sensor1(ix, :);
sensor2 = sensor2(ix, :);
sensor3 = sensor3(ix, :);
sensor4 = sensor4(ix, :);
% obtain calibrated and detrended sensor data
```

```
Csensor1 = detrend_new(sensor1 / cf1 - ones(size(sensor1, 1), 1)
* [0 0 g]);
Csensor2 = detrend_new(sensor2 / cf2 - ones(size(sensor2, 1), 1)
* [0 0 g]);
Csensor3 = detrend_new(sensor3 / cf3 - ones(size(sensor3, 1), 1)
* [0 0 g]);
Csensor4 = detrend_new(sensor4 / cf4 - ones(size(sensor4, 1), 1)
* [0 0 g]);

% creaet a time vector (with a constant time interval, 0.01 sec);
ts0 = max([t1a(1) t2a(1) t3a(1) t4a(1)]);
ts1 = min([t1a(end) t2a(end) t3a(end) t4a(end)]);
tv = ts0:0.01:ts1;
% perform resampling
CS1 = resample_new(Csensor1, t1a, tv);
CS2 = resample_new(Csensor2, t2a, tv);
CS3 = resample_new(Csensor3, t3a, tv);
CS4 = resample_new(Csensor4, t4a, tv);
tv1a = tv - tv(1);



% -- psl resolve CS4 --- transform it so the data are in X-, Y,
and Z
% plot calibrated, detrendedm, and resampled data
% figure;
 subplot(4, 1, 1); plot(tv, CS1); xlabel('sec'); grid on;
title('Base Sensor 1');
% subplot(4, 1, 2); plot(tv, CS2); xlabel('sec'); grid on;
title('Base Sensor 2');
% subplot(4, 1, 3); plot(tv, CS3); xlabel('sec'); grid on;
title('Base Sensor 3');
% subplot(4, 1, 4); plot(tv, CS4); xlabel('sec'); grid on;
title('Top Sensor 4');

dt = 0.01; fs = 100;

 figure, fftPlots(CS1, fs); subplot(3, 1, 1); title('Sensor 1');
% figure, fftPlots(CS2, fs); subplot(3, 1, 1); title('Sensor 2');
% figure, fftPlots(CS3, fs); subplot(3, 1, 1); title('Sensor 3');
% figure, fftPlots(CS4, fs); subplot(3, 1, 1); title('Sensor 4');



% illustration of transfer function in the Z- driection
 input_z = CS4(:, 3);
 output_z = CS3(:, 3);
```

```
[TR, coh, freq] = FRF_Coherence(input_z, output_z, fs, 1);
%  plot the transfer function to identify the modal freq in the
z-direction
figure, plot(freq, abs(TR),'linewidth', 2, 'color', 'k'); grid
on;
 % figure, plot(freq, coh, 'linewidth', 2, 'color', 'r'); grid
on;
set(gca, 'xlim', [10 40]);%, 'xtick', [10, 15, 20, 25, 30, 35,
40]);
xlabel('Freq, Hz'); ylabel('TR(z)');


% illustration of transfer function in the X- driection
input_X = CS4(:, 1) * cos(pi/4) + CS4(:, 2) * sin(pi/4);
  % output_X =  (CS3(:,1)+CS2(:,2))/2;
output_X = CS3(:, 1);


% filter out the any frequences lower than 10 hz
fn = 50; band = 10 / fn;
[b, a] = butter(10, band, 'high');
input_X = filter(b, a, input_X);
output_X = filter(b, a, output_X);
% figure; plot(tv, input_X , 'r-'); % hold on; plot(tv, CS2(:,
1), 'k-');
% figure; plot(tv, output_X , 'r-'); % hold on; plot(tv, CS4(:,
2), 'k-');
% figure; fftPlots(input_X,  100); %%% please study why there is
a dominant
% frequencey about 15.1 hz in the input
% figure; fftPlots(output_X, 100);
[TR, coh, freq] = FRF_Coherence(input_X, output_X, fs, 1);
% plot the transfer function to identify the modal freq in the
z-direction
 figure, plot(freq, abs(TR), 'linewidth', 2, 'color', 'k'); grid
on;
set(gca, 'xlim', [10 40]);%, 'xtick', [10, 15, 20, 25, 30, 35,
40]);
 % figure, plot(freq, coh, 'linewidth', 2, 'color', 'r'); grid
on;
```

Figure A.1 Matlab code to plot transfer function

Matlab code to calculate fast fourier transform

```
function [ff, fA] = fftPlots(pX, samplerate)
```

```
% figure(gcf);
nT = length(pX);
maxFreq = samplerate;
f = (0: 1/nT: 1 - 1/nT)' * maxFreq;


n = size(pX, 2);
col = {'r', 'g', 'b', 'c', 'm', 'k', 'y', 'g', 'b', 'c', 'm',
'k','y', 'g', 'b', 'c', 'm', 'k','y', 'g', 'b', 'c', 'm', 'k'};
for i = 1 : n
fD1 = fft(pX(:, i));
nn = floor(nT / 2);

ff = f(1:nn-1);
fA = fD1(1:nn-1);
if nargout == 0
subplot(n,1,i); h = plot(f(1:nn-1), abs(fD1(1:nn-1)), col{i});
set(h, 'LineWidth', 2.5);
xlabel('hz'); ylabel('|fft|');
grid;
end
end
```

Figure A.2 Matlab code to calculate fast fourier transform

APPENDIX B

Python code for Abaqus based model

```
from part import *
from material import *
from section import *
from assembly import *
from step import *
from interaction import *
from load import *
from mesh import *
from optimization import *
from job import *
from sketch import *
from visualization import *
from connectorBehavior import *
mdb.models['Model-1'].ConstrainedSketch(name='__profile__',
sheetSize=20.0)
mdb.models['Model-
1'].sketches['__profile__'].rectangle(point1=(-2.5, 2.0),
    point2=(3.5, -1.5))
mdb.models['Model-1'].Part(dimensionality=TWO_D_PLANAR,
name='Part-1', type=
    DEFORMABLE_BODY)
mdb.models['Model-1'].parts['Part-1'].BaseShell(sketch=
    mdb.models['Model-1'].sketches['__profile__'])
del mdb.models['Model-1'].sketches['__profile__']
mdb.models['Model-1'].ConstrainedSketch(gridSpacing=0.89,
name='__profile__',
    sheetSize=35.77)
mdb.models['Model-1'].parts['Part-
1'].projectReferencesOntoSketch(filter=
    COPLANAR_EDGES, sketch=mdb.models['Model-
1'].sketches['__profile__'])
mdb.models['Model-
1'].sketches['__profile__'].rectangle(point1=(4.45, 6.5),
    point2=(7.12, 5.34))
mdb.models['Model-
1'].sketches['__profile__'].VerticalDimension(textPoint=(
    3.3086953163147, 5.38225603103638), value=1.0, vertex1=
    mdb.models['Model-1'].sketches['__profile__'].vertices[4],
vertex2=
    mdb.models['Model-1'].sketches['__profile__'].vertices[5])
mdb.models['Model-1'].parts['Part-1'].Cut(sketch=
    mdb.models['Model-1'].sketches['__profile__'])
del mdb.models['Model-1'].sketches['__profile__']
mdb.models['Model-1'].ConstrainedSketch(name='__profile__',
sheetSize=20.0)
mdb.models['Model-
1'].sketches['__profile__'].rectangle(point1=(-1.0, 0.5),
```

```
    point2=(0.625, -0.5))
mdb.models['Model-1'].Part(dimensionality=TWO_D_PLANAR,
name='foundation',
    type=DEFORMABLE_BODY)
mdb.models['Model-1'].parts['foundation'].BaseShell(sketch=
    mdb.models['Model-1'].sketches['__profile__'])
del mdb.models['Model-1'].sketches['__profile__']
mdb.models['Model-
1'].parts['foundation'].DatumPointByMidPoint(point1=
    mdb.models['Model-1'].parts['foundation'].vertices[1],
point2=
mdb.models['Model-1'].parts['foundation'].vertices[0])
mdb.models['Model-
1'].parts['foundation'].DatumPointByOffset(point=
    mdb.models['Model-1'].parts['foundation'].datums[2],
vector=(0.0, 5.0,
    0.0))
mdb.models['Model-1'].ConstrainedSketch(gridSpacing=0.31,
name='__profile__',
    sheetSize=12.64)
mdb.models['Model-
1'].parts['foundation'].projectReferencesOntoSketch(filter=
    COPLANAR_EDGES, sketch=mdb.models['Model-
1'].sketches['__profile__'])
mdb.models['Model-
1'].sketches['__profile__'].VerticalConstraint(addUndoState=
    False, entity=mdb.models['Model-
1'].sketches['__profile__'].geometry[6])
mdb.models['Model-1'].parts['foundation'].Wire(sketch=
    mdb.models['Model-1'].sketches['__profile__'])
del mdb.models['Model-1'].sketches['__profile__']
mdb.models['Model-1'].parts['foundation'].Set(name='Set-1',
vertices=
    mdb.models['Model-
1'].parts['foundation'].vertices.getSequenceFromMask((
    '[#1 ]', ), ))
mdb.models['Model-
1'].parts['foundation'].engineeringFeatures.PointMassInertia(
    alpha=0.0, composite=0.0, mass=1.0, name='Inertia-1',
region=
    mdb.models['Model-1'].parts['foundation'].sets['Set-1'])
mdb.models['Model-1'].parts['foundation'].Set(edges=
    mdb.models['Model-
1'].parts['foundation'].edges.getSequenceFromMask((
    '[#1 ]', ), ), name='Set-2')
mdb.models['Model-
1'].parts['foundation'].assignBeamSectionOrientation(method=
```

```
    N1_COSINES, n1=(0.0, 0.0, -1.0), region=
    mdb.models['Model-1'].parts['foundation'].sets['Set-2'])
mdb.models['Model-1'].Material(name='beam')
mdb.models['Model-1'].materials['beam'].Density(table=((10.0, ),
))
mdb.models['Model-
1'].materials['beam'].Elastic(table=((1000000.0, 0.2), ))
mdb.models['Model-1'].Material(name='foundation')
mdb.models['Model-
1'].materials['foundation'].Density(table=((1923.0, ), ))
mdb.models['Model-
1'].materials['foundation'].Elastic(table=((3000000000000.0,
    0.2), ))
mdb.models['Model-1'].Material(name='Soil')
mdb.models['Model-1'].materials['Soil'].Density(table=((1923.0,
), ))
mdb.models['Model-
1'].materials['Soil'].ClayPlasticity(intercept=None, table=((
    0.174, 1.0, 58.0, 1.0, 1.0), ))
mdb.models['Model-
1'].materials['Soil'].Permeability(inertialDragCoefficient=
    0.142887, specificWeight=9.81, table=((2.5e-09, 0.889), ))
mdb.models['Model-
1'].materials['Soil'].PorousElastic(table=((0.026, 0.28,
    0.0), ))
mdb.models['Model-1'].RectangularProfile(a=1.0, b=1.0,
name='Profile-1')
mdb.models['Model-1'].BeamSection(consistentMassMatrix=False,
integration=
    DURING_ANALYSIS, material='beam', name='Section-1',
poissonRatio=0.0,
    profile='Profile-1', temperatureVar=LINEAR)
mdb.models['Model-1'].parts['foundation'].Set(edges=
    mdb.models['Model-
1'].parts['foundation'].edges.getSequenceFromMask((
    '[#1 ]', ), ), name='Set-3')
mdb.models['Model-
1'].parts['foundation'].SectionAssignment(offset=0.0,
    offsetField='', offsetType=MIDDLE_SURFACE, region=
    mdb.models['Model-1'].parts['foundation'].sets['Set-3'],
sectionName=
    'Section-1', thicknessAssignment=FROM_SECTION)
mdb.models['Model-
1'].HomogeneousSolidSection(material='foundation', name=
    'Section-2', thickness=None)
mdb.models['Model-1'].parts['foundation'].Set(faces=
```

```
    mdb.models['Model-
1'].parts['foundation'].faces.getSequenceFromMask((
    '[#1 ]', ), ), name='Set-4')
mdb.models['Model-
1'].parts['foundation'].SectionAssignment(offset=0.0,
    offsetField='', offsetType=MIDDLE_SURFACE, region=
    mdb.models['Model-1'].parts['foundation'].sets['Set-4'],
sectionName=
    'Section-2', thicknessAssignment=FROM_SECTION)
mdb.models['Model-1'].HomogeneousSolidSection(material='Soil',
name='Section-3'
    , thickness=None)
mdb.models['Model-1'].HomogeneousSolidSection(material='Soil',
name='Section-4'
    , thickness=None)
mdb.models['Model-1'].parts['Part-1'].Set(faces=
    mdb.models['Model-1'].parts['Part-
1'].faces.getSequenceFromMask(('[#1 ]',
    ), ), name='Set-1')
mdb.models['Model-1'].parts['Part-
1'].SectionAssignment(offset=0.0,
    offsetField='', offsetType=MIDDLE_SURFACE, region=
    mdb.models['Model-1'].parts['Part-1'].sets['Set-1'],
sectionName=
    'Section-4', thicknessAssignment=FROM_SECTION)
mdb.models['Model-1'].rootAssembly.DatumCsysByDefault(CARTESIAN)
mdb.models['Model-1'].rootAssembly.Instance(dependent=ON,
name='Part-1-1',
    part=mdb.models['Model-1'].parts['Part-1'])
mdb.models['Model-1'].rootAssembly.Instance(dependent=ON,
name='foundation-1',
    part=mdb.models['Model-1'].parts['foundation'])
mdb.models['Model-
1'].rootAssembly.translate(instanceList=('foundation-1', ),
    vector=(5.5, 6.0, 0.0))
mdb.models['Model-
1'].rootAssembly.translate(instanceList=('Part-1-1', ),
    vector=(0.0, -4.0, 0.0))
mdb.models['Model-1'].GeostaticStep(name='Step-1',
previous='Initial')
mdb.models['Model-1'].StaticStep(name='Step-2', previous='Step-
1')
mdb.models['Model-1'].parts['Part-1'].Surface(name='Surf-1',
side1Edges=
    mdb.models['Model-1'].parts['Part-
1'].edges.getSequenceFromMask(('[#c1 ]',
    ), ))
```

```
mdb.models['Model-1'].parts['foundation'].Surface(name='Surf-2',
side1Edges=
    mdb.models['Model-
1'].parts['foundation'].edges.getSequenceFromMask((
    '[#38 ]', ), ))
mdb.models['Model-1'].rootAssembly.regenerate()
mdb.models['Model-1'].ContactProperty('IntProp-1')
mdb.models['Model-1'].interactionProperties['IntProp-
1'].TangentialBehavior(
    dependencies=0, directionality=ISOTROPIC,
elasticSlipStiffness=None,
    formulation=PENALTY, fraction=0.005,
maximumElasticSlip=FRACTION,
    pressureDependency=OFF, shearStressLimit=None,
slipRateDependency=OFF,
    table=((0.3, ), ), temperatureDependency=OFF)
mdb.models['Model-
1'].SurfaceToSurfaceContactStd(adjustMethod=NONE,
    clearanceRegion=None, createStepName='Initial',
datumAxis=None,
    enforcement=NODE_TO_SURFACE, initialClearance=OMIT,
interactionProperty=
    'IntProp-1', master=
    mdb.models['Model-1'].rootAssembly.instances['Part-1-
1'].surfaces['Surf-1']
    , name='Int-1', slave=
    mdb.models['Model-1'].rootAssembly.instances['foundation-
1'].surfaces['Surf-2']
    , sliding=FINITE, smooth=0.2, supplementaryContact=NEVER,
surfaceSmoothing=
    NONE, thickness=OFF)
mdb.models['Model-
1'].rootAssembly.translate(instanceList=('Part-1-1', ),
    vector=(0.0, 4.0, 0.0))
mdb.models['Model-1'].TabularAmplitude(data=((0.0, 0.0), (0.01,
1.0)), name=
    'Amp-1', smooth=SOLVER_DEFAULT, timeSpan=STEP)
mdb.models['Model-1'].rootAssembly.Set(faces=
    mdb.models['Model-1'].rootAssembly.instances['Part-1-
1'].faces.getSequenceFromMask(
    mask=('[#1 ]', ), )+\
    mdb.models['Model-1'].rootAssembly.instances['foundation-
1'].faces.getSequenceFromMask(
    mask=('[#1 ]', ), ), name='Set-1')
mdb.models['Model-1'].BodyForce(amplitude='Amp-1', comp2=75.4,
createStepName=
    'Step-1', name='Load-1', region=
```

```
    mdb.models['Model-1'].rootAssembly.sets['Set-1'])
mdb.models['Model-1'].loads['Load-1'].setValues(comp2=-75.4)
mdb.models['Model-1'].rootAssembly.Set(name='Set-2', vertices=
    mdb.models['Model-1'].rootAssembly.instances['foundation-
1'].vertices.getSequenceFromMask(
    ('[#1 ]', ), ))
mdb.models['Model-1'].ConcentratedForce(cf1=1.0,
createStepName='Step-2',
    distributionType=UNIFORM, field='', localCsys=None,
name='Load-2', region=
    mdb.models['Model-1'].rootAssembly.sets['Set-2'])
mdb.models['Model-1'].rootAssembly.Set(edges=
    mdb.models['Model-1'].rootAssembly.instances['Part-1-
1'].edges.getSequenceFromMask(
    ('[#8 ]', ), ), name='Set-3')
mdb.models['Model-1'].DisplacementBC(amplitude=UNSET,
createStepName='Initial',
    distributionType=UNIFORM, fieldName='', localCsys=None,
name='BC-1',
    region=mdb.models['Model-1'].rootAssembly.sets['Set-3'],
u1=SET, u2=SET,
    ur3=SET)
mdb.models['Model-1'].rootAssembly.Set(edges=
    mdb.models['Model-1'].rootAssembly.instances['Part-1-
1'].edges.getSequenceFromMask(
    ('[#4 ]', ), ), name='Set-4')
mdb.models['Model-1'].DisplacementBC(amplitude=UNSET,
createStepName='Initial',
    distributionType=UNIFORM, fieldName='', localCsys=None,
name='BC-2',
    region=mdb.models['Model-1'].rootAssembly.sets['Set-4'],
u1=SET, u2=SET,
    ur3=SET)
mdb.models['Model-1'].rootAssembly.Set(edges=
    mdb.models['Model-1'].rootAssembly.instances['Part-1-
1'].edges.getSequenceFromMask(
    ('[#10 ]', ), ), name='Set-5')
mdb.models['Model-1'].DisplacementBC(amplitude=UNSET,
createStepName='Initial',
    distributionType=UNIFORM, fieldName='', localCsys=None,
name='BC-3',
    region=mdb.models['Model-1'].rootAssembly.sets['Set-5'],
u1=SET, u2=UNSET,
    ur3=SET)
mdb.models['Model-1'].boundaryConditions['BC-
2'].setValues(u2=UNSET)
mdb.models['Model-1'].rootAssembly.Set(faces=
```

```
    mdb.models['Model-1'].rootAssembly.instances['Part-1-
1'].faces.getSequenceFromMask(
    mask=('[#1 ]', ), )+\
    mdb.models['Model-1'].rootAssembly.instances['foundation-
1'].faces.getSequenceFromMask(
    mask=('[#1 ]', ), ), name='Set-6')
mdb.models['Model-1'].GeostaticStress(lateralCoeff1=1.0,
lateralCoeff2=None,
    name='Predefined Field-1', region=
    mdb.models['Model-1'].rootAssembly.sets['Set-6'],
stressMag1=-75.4,
    stressMag2=-75.5, vCoord1=-1.5, vCoord2=6.5)
mdb.models['Model-1'].rootAssembly.Set(edges=
    mdb.models['Model-1'].rootAssembly.instances['Part-1-
1'].edges.getSequenceFromMask(
    mask=('[#c5 ]', ), )+\
    mdb.models['Model-1'].rootAssembly.instances['foundation-
1'].edges.getSequenceFromMask(
    mask=('[#38 ]', ), ), faces=
    mdb.models['Model-1'].rootAssembly.instances['Part-1-
1'].faces.getSequenceFromMask(
    mask=('[#1 ]', ), )+\
    mdb.models['Model-1'].rootAssembly.instances['foundation-
1'].faces.getSequenceFromMask(
    mask=('[#1 ]', ), ), name='Set-7', vertices=
    mdb.models['Model-1'].rootAssembly.instances['Part-1-
1'].vertices.getSequenceFromMask(
    mask=('[#81 ]', ), )+\
    mdb.models['Model-1'].rootAssembly.instances['foundation-
1'].vertices.getSequenceFromMask(
    mask=('[#30 ]', ), ))
mdb.models['Model-1'].VoidsRatio(distributionType=UNIFORM, name=
    'Predefined Field-2', region=
    mdb.models['Model-1'].rootAssembly.sets['Set-7'],
variation=CONSTANT_RATIO,
    voidsRatio1=0.889)
mdb.models['Model-
1'].parts['foundation'].seedPart(deviationFactor=0.1,
    minSizeFactor=0.1, size=0.5)
mdb.models['Model-
1'].parts['foundation'].seedPart(deviationFactor=0.1,
    minSizeFactor=0.1, size=0.3)
mdb.models['Model-
1'].parts['foundation'].setElementType(elemTypes=(ElemType(
    elemCode=CPE4R, elemLibrary=STANDARD,
secondOrderAccuracy=OFF,
```

```
    hourglassControl=DEFAULT, distortionControl=DEFAULT),
ElemType(
    elemCode=CPE3, elemLibrary=STANDARD)), regions=(
    mdb.models['Model-
1'].parts['foundation'].faces.getSequenceFromMask((
    '[#1 ]', ), ), ))
mdb.models['Model-
1'].parts['foundation'].setElementType(elemTypes=(ElemType(
    elemCode=B21, elemLibrary=STANDARD), ), regions=(
    mdb.models['Model-
1'].parts['foundation'].edges.getSequenceFromMask((
    '[#1 ]', ), ), ))
mdb.models['Model-1'].parts['foundation'].generateMesh()
mdb.models['Model-1'].parts['foundation'].deleteMesh()
mdb.models['Model-
1'].parts['foundation'].seedPart(deviationFactor=0.1,
    minSizeFactor=0.1, size=0.5)
mdb.models['Model-1'].parts['foundation'].generateMesh()
mdb.models['Model-1'].ConstrainedSketch(gridSpacing=0.89,
name='__profile__',
    sheetSize=35.77, transform=
    mdb.models['Model-1'].parts['Part-1'].MakeSketchTransform(
    sketchPlane=mdb.models['Model-1'].parts['Part-1'].faces[0],
    sketchPlaneSide=SIDE1, sketchOrientation=RIGHT, origin=(5.5,
2.444444,
    0.0)))
mdb.models['Model-1'].parts['Part-
1'].projectReferencesOntoSketch(filter=
    COPLANAR_EDGES, sketch=mdb.models['Model-
1'].sketches['__profile__'])
mdb.models['Model-1'].sketches['__profile__'].Line(point1=(-1.0,
3.055556),
    point2=(-8.0, 3.055556))
mdb.models['Model-
1'].sketches['__profile__'].HorizontalConstraint(
    addUndoState=False, entity=
    mdb.models['Model-1'].sketches['__profile__'].geometry[10])
mdb.models['Model-
1'].sketches['__profile__'].PerpendicularConstraint(
    addUndoState=False, entity1=
    mdb.models['Model-1'].sketches['__profile__'].geometry[2],
entity2=
    mdb.models['Model-1'].sketches['__profile__'].geometry[10])
mdb.models['Model-
1'].sketches['__profile__'].CoincidentConstraint(
    addUndoState=False, entity1=
```

```
    mdb.models['Model-1'].sketches['__profile__'].vertices[8],
entity2=
    mdb.models['Model-1'].sketches['__profile__'].geometry[4])
mdb.models['Model-1'].sketches['__profile__'].Line(point1=(1.0,
3.055556),
    point2=(8.0, 3.055556))
mdb.models['Model-
1'].sketches['__profile__'].HorizontalConstraint(
    addUndoState=False, entity=
    mdb.models['Model-1'].sketches['__profile__'].geometry[11])
mdb.models['Model-
1'].sketches['__profile__'].PerpendicularConstraint(
    addUndoState=False, entity1=
    mdb.models['Model-1'].sketches['__profile__'].geometry[8],
entity2=
    mdb.models['Model-1'].sketches['__profile__'].geometry[11])
mdb.models['Model-
1'].sketches['__profile__'].CoincidentConstraint(
    addUndoState=False, entity1=
    mdb.models['Model-1'].sketches['__profile__'].vertices[9],
entity2=
    mdb.models['Model-1'].sketches['__profile__'].geometry[6])
mdb.models['Model-1'].sketches['__profile__'].Line(point1=(-1.0,
3.055556),
    point2=(-1.0, -3.94444400001124))
mdb.models['Model-
1'].sketches['__profile__'].VerticalConstraint(addUndoState=
    False, entity=mdb.models['Model-
1'].sketches['__profile__'].geometry[12])
mdb.models['Model-
1'].sketches['__profile__'].ParallelConstraint(addUndoState=
    False, entity1=mdb.models['Model-
1'].sketches['__profile__'].geometry[2],
    entity2=mdb.models['Model-
1'].sketches['__profile__'].geometry[12])
mdb.models['Model-
1'].sketches['__profile__'].CoincidentConstraint(
    addUndoState=False, entity1=
    mdb.models['Model-1'].sketches['__profile__'].vertices[10],
entity2=
    mdb.models['Model-1'].sketches['__profile__'].geometry[5])
mdb.models['Model-1'].sketches['__profile__'].Line(point1=(1.0,
3.055556),
    point2=(1.0, -3.94444400001124))
mdb.models['Model-
1'].sketches['__profile__'].VerticalConstraint(addUndoState=
```

```
    False, entity=mdb.models['Model-
1'].sketches['__profile__'].geometry[13])
mdb.models['Model-
1'].sketches['__profile__'].ParallelConstraint(addUndoState=
    False, entity1=mdb.models['Model-
1'].sketches['__profile__'].geometry[8],
    entity2=mdb.models['Model-
1'].sketches['__profile__'].geometry[13])
mdb.models['Model-
1'].sketches['__profile__'].CoincidentConstraint(
    addUndoState=False, entity1=
    mdb.models['Model-1'].sketches['__profile__'].vertices[11],
entity2=
    mdb.models['Model-1'].sketches['__profile__'].geometry[5])
mdb.models['Model-
1'].sketches['__profile__'].ArcByCenterEnds(center=(0.0,
    4.005), direction=CLOCKWISE, point1=(-1.78,
4.05555600000001), point2=(
    1.78, 4.05555600000001))
mdb.models['Model-
1'].sketches['__profile__'].CoincidentConstraint(
    addUndoState=False, entity1=
    mdb.models['Model-1'].sketches['__profile__'].vertices[12],
entity2=
    mdb.models['Model-1'].sketches['__profile__'].geometry[3])
mdb.models['Model-
1'].sketches['__profile__'].CoincidentConstraint(
    addUndoState=False, entity1=
    mdb.models['Model-1'].sketches['__profile__'].vertices[13],
entity2=
    mdb.models['Model-1'].sketches['__profile__'].geometry[7])
mdb.models['Model-1'].sketches['__profile__'].undo()
mdb.models['Model-1'].sketches['__profile__'].undo()
mdb.models['Model-1'].sketches['__profile__'].redo()
mdb.models['Model-
1'].sketches['__profile__'].ArcByCenterEnds(center=(0.0,
    4.005), direction=COUNTERCLOCKWISE, point1=(-1.78,
4.05555600000001),
    point2=(1.78, 4.05555600000001))
mdb.models['Model-
1'].sketches['__profile__'].CoincidentConstraint(
    addUndoState=False, entity1=
    mdb.models['Model-1'].sketches['__profile__'].vertices[12],
entity2=
    mdb.models['Model-1'].sketches['__profile__'].geometry[3])
mdb.models['Model-
1'].sketches['__profile__'].CoincidentConstraint(
```

```
    addUndoState=False, entity1=
    mdb.models['Model-1'].sketches['__profile__'].vertices[13],
entity2=
    mdb.models['Model-1'].sketches['__profile__'].geometry[7])
mdb.models['Model-
1'].sketches['__profile__'].ArcByCenterEnds(center=(0.0,
    4.005), direction=COUNTERCLOCKWISE, point1=(-2.67,
4.05555600000001),
    point2=(2.67, 4.05555600000001))
mdb.models['Model-
1'].sketches['__profile__'].CoincidentConstraint(
    addUndoState=False, entity1=
    mdb.models['Model-1'].sketches['__profile__'].vertices[15],
entity2=
    mdb.models['Model-1'].sketches['__profile__'].geometry[3])
mdb.models['Model-
1'].sketches['__profile__'].CoincidentConstraint(
    addUndoState=False, entity1=
    mdb.models['Model-1'].sketches['__profile__'].vertices[16],
entity2=
    mdb.models['Model-1'].sketches['__profile__'].geometry[7])
mdb.models['Model-
1'].sketches['__profile__'].ArcByCenterEnds(center=(0.0,
    4.005), direction=COUNTERCLOCKWISE, point1=(-3.56,
4.05555600000001),
    point2=(3.56, 4.05555600000001))
mdb.models['Model-
1'].sketches['__profile__'].CoincidentConstraint(
    addUndoState=False, entity1=
    mdb.models['Model-1'].sketches['__profile__'].vertices[17],
entity2=
    mdb.models['Model-1'].sketches['__profile__'].geometry[3])
mdb.models['Model-
1'].sketches['__profile__'].CoincidentConstraint(
    addUndoState=False, entity1=
    mdb.models['Model-1'].sketches['__profile__'].vertices[18],
entity2=
    mdb.models['Model-1'].sketches['__profile__'].geometry[7])
mdb.models['Model-
1'].sketches['__profile__'].ArcByCenterEnds(center=(0.0,
    4.005), direction=COUNTERCLOCKWISE, point1=(-4.5, 4.055556),
point2=(4.5,
    4.055556))
mdb.models['Model-
1'].sketches['__profile__'].CoincidentConstraint(
    addUndoState=False, entity1=
```

```
    mdb.models['Model-1'].sketches['__profile__'].vertices[19],
entity2=
    mdb.models['Model-1'].sketches['__profile__'].geometry[3])
mdb.models['Model-
1'].sketches['__profile__'].EqualDistanceConstraint(
    addUndoState=False, entity1=
    mdb.models['Model-1'].sketches['__profile__'].vertices[1],
entity2=
    mdb.models['Model-1'].sketches['__profile__'].vertices[2],
midpoint=
    mdb.models['Model-1'].sketches['__profile__'].vertices[19])
mdb.models['Model-
1'].sketches['__profile__'].CoincidentConstraint(
    addUndoState=False, entity1=
    mdb.models['Model-1'].sketches['__profile__'].vertices[20],
entity2=
    mdb.models['Model-1'].sketches['__profile__'].geometry[7])
mdb.models['Model-
1'].sketches['__profile__'].EqualDistanceConstraint(
    addUndoState=False, entity1=
    mdb.models['Model-1'].sketches['__profile__'].vertices[5],
entity2=
    mdb.models['Model-1'].sketches['__profile__'].vertices[6],
midpoint=
    mdb.models['Model-1'].sketches['__profile__'].vertices[20])
mdb.models['Model-
1'].sketches['__profile__'].ArcByCenterEnds(center=(0.0,
    4.005), direction=CLOCKWISE, point1=(-6.23,
4.05555600000001), point2=(
    6.23, 4.05555600000001))
mdb.models['Model-
1'].sketches['__profile__'].CoincidentConstraint(
    addUndoState=False, entity1=
    mdb.models['Model-1'].sketches['__profile__'].vertices[21],
entity2=
    mdb.models['Model-1'].sketches['__profile__'].geometry[3])
mdb.models['Model-
1'].sketches['__profile__'].CoincidentConstraint(
    addUndoState=False, entity1=
    mdb.models['Model-1'].sketches['__profile__'].vertices[22],
entity2=
    mdb.models['Model-1'].sketches['__profile__'].geometry[7])
mdb.models['Model-1'].sketches['__profile__'].undo()
mdb.models['Model-
1'].sketches['__profile__'].ArcByCenterEnds(center=(0.0,
    4.005), direction=COUNTERCLOCKWISE, point1=(-6.23,
4.05555600000001),
```

```
    point2=(6.23, 4.05555600000001))
mdb.models['Model-
1'].sketches['__profile__'].CoincidentConstraint(
    addUndoState=False, entity1=
    mdb.models['Model-1'].sketches['__profile__'].vertices[21],
entity2=
    mdb.models['Model-1'].sketches['__profile__'].geometry[3])
mdb.models['Model-
1'].sketches['__profile__'].CoincidentConstraint(
    addUndoState=False, entity1=
    mdb.models['Model-1'].sketches['__profile__'].vertices[22],
entity2=
    mdb.models['Model-1'].sketches['__profile__'].geometry[7])
mdb.models['Model-
1'].sketches['__profile__'].ArcByCenterEnds(center=(0.0,
    4.005), direction=COUNTERCLOCKWISE, point1=(-8.0, 4.055556),
point2=(8.0,
    4.055556))
mdb.models['Model-1'].parts['Part-
1'].PartitionFaceBySketch(faces=
    mdb.models['Model-1'].parts['Part-
1'].faces.getSequenceFromMask(('[#1 ]',
    ), ), sketch=mdb.models['Model-1'].sketches['__profile__'])
del mdb.models['Model-1'].sketches['__profile__']
mdb.models['Model-1'].parts['Part-
1'].seedEdgeByNumber(constraint=FINER, edges=
    mdb.models['Model-1'].parts['Part-
1'].edges.getSequenceFromMask((
    '[#800000 ]', ), ), number=3)
mdb.models['Model-1'].parts['Part-
1'].seedEdgeByNumber(constraint=FINER, edges=
    mdb.models['Model-1'].parts['Part-
1'].edges.getSequenceFromMask((
    '[#800000 ]', ), ), number=2)
mdb.models['Model-1'].parts['Part-
1'].seedEdgeByNumber(constraint=FINER, edges=
    mdb.models['Model-1'].parts['Part-
1'].edges.getSequenceFromMask((
    '[#0:2 #80000 ]', ), ), number=2)
mdb.models['Model-1'].parts['Part-
1'].seedEdgeByNumber(constraint=FINER, edges=
    mdb.models['Model-1'].parts['Part-
1'].edges.getSequenceFromMask((
    '[#0 #80000000 ]', ), ), number=2)
mdb.models['Model-1'].parts['Part-
1'].seedEdgeByNumber(constraint=FINER, edges=
```

```
    mdb.models['Model-1'].parts['Part-
1'].edges.getSequenceFromMask(('[#2 ]',
    ), ), number=2)
mdb.models['Model-1'].parts['Part-
1'].seedEdgeByNumber(constraint=FINER, edges=
    mdb.models['Model-1'].parts['Part-
1'].edges.getSequenceFromMask((
    '[#0:2 #8000 ]', ), ), number=4)
mdb.models['Model-1'].parts['Part-
1'].seedEdgeByNumber(constraint=FINER, edges=
    mdb.models['Model-1'].parts['Part-
1'].edges.getSequenceFromMask((
    '[#80000000 ]', ), ), number=4)
mdb.models['Model-1'].parts['Part-
1'].seedPart(deviationFactor=0.1,
    minSizeFactor=0.1, size=1.0)
mdb.models['Model-1'].parts['Part-
1'].setElementType(elemTypes=(ElemType(
    elemCode=CPE8RP, elemLibrary=STANDARD),
ElemType(elemCode=CPE6MP,
    elemLibrary=STANDARD)), regions=(
    mdb.models['Model-1'].parts['Part-
1'].faces.getSequenceFromMask((
    '[#ffffffff #f ]', ), ), ))
mdb.models['Model-1'].parts['Part-1'].generateMesh()
mdb.models['Model-1'].rootAssembly.regenerate()
mdb.models['Model-1'].parts['Part-1'].deleteMesh(regions=
    mdb.models['Model-1'].parts['Part-
1'].faces.getSequenceFromMask((
    '[#0 #1 ]', ), ))
mdb.models['Model-1'].parts['Part-
1'].seedEdgeBySize(constraint=FINER,
    deviationFactor=0.1, edges=
    mdb.models['Model-1'].parts['Part-
1'].edges.getSequenceFromMask((
    '[#0:2 #8000 ]', ), ), size=0.5)
mdb.models['Model-1'].parts['Part-1'].deleteMesh(regions=
    mdb.models['Model-1'].parts['Part-
1'].faces.getSequenceFromMask(('[#400 ]',
    ), ))
mdb.models['Model-1'].parts['Part-
1'].seedEdgeBySize(constraint=FINER,
    deviationFactor=0.1, edges=
    mdb.models['Model-1'].parts['Part-
1'].edges.getSequenceFromMask((
    '[#80000000 ]', ), ), size=0.5)
mdb.models['Model-1'].parts['Part-1'].deleteMesh()
```

```
mdb.models['Model-1'].ConstrainedSketch(gridSpacing=0.89,
name='__profile__',
    sheetSize=35.77, transform=
    mdb.models['Model-1'].parts['Part-1'].MakeSketchTransform(
    sketchPlane=mdb.models['Model-1'].parts['Part-1'].faces[1],
    sketchPlaneSide=SIDE1, sketchOrientation=RIGHT,
origin=(12.594699, 5.99924,
    0.0)))
mdb.models['Model-1'].parts['Part-
1'].projectReferencesOntoSketch(filter=
    COPLANAR_EDGES, sketch=mdb.models['Model-
1'].sketches['__profile__'])
mdb.models['Model-1'].sketches['__profile__'].Line(point1=(-
8.094699, -0.49924)
    , point2=(-15.094699, -7.49924))
mdb.models['Model-1'].sketches['__profile__'].Line(point1=(-
6.094699, -0.49924)
    , point2=(0.905301, -7.49924))
mdb.models['Model-1'].parts['Part-
1'].PartitionFaceBySketch(faces=
    mdb.models['Model-1'].parts['Part-
1'].faces.getSequenceFromMask((
    '[#ffffff9e #f ]', ), ), sketch=
    mdb.models['Model-1'].sketches['__profile__'])
del mdb.models['Model-1'].sketches['__profile__']
mdb.models['Model-1'].parts['Part-1'].generateMesh()
mdb.models['Model-1'].rootAssembly.regenerate()
mdb.models['Model-1'].parts['foundation'].deleteMesh(regions=
    mdb.models['Model-
1'].parts['foundation'].faces.getSequenceFromMask((
    '[#1 ]', ), ))
mdb.models['Model-
1'].parts['foundation'].seedEdgeByNumber(constraint=FINER,
    edges=mdb.models['Model-
1'].parts['foundation'].edges.getSequenceFromMask((
    '[#10 ]', ), ), number=7)
mdb.models['Model-1'].parts['foundation'].deleteMesh(regions=
    mdb.models['Model-
1'].parts['foundation'].edges.getSequenceFromMask((
    '[#1 ]', ), ))
mdb.models['Model-
1'].parts['foundation'].seedEdgeByNumber(constraint=FINER,
    edges=mdb.models['Model-
1'].parts['foundation'].edges.getSequenceFromMask((
    '[#7 ]', ), ), number=7)
mdb.models['Model-1'].parts['foundation'].generateMesh()
mdb.models['Model-1'].rootAssembly.regenerate()
```

```
mdb.models['Model-1'].parts['foundation'].deleteMesh(regions=
    mdb.models['Model-
1'].parts['foundation'].faces.getSequenceFromMask((
    '[#1 ]', ), ))
mdb.models['Model-
1'].parts['foundation'].seedEdgeByNumber(constraint=FINER,
    edges=mdb.models['Model-
1'].parts['foundation'].edges.getSequenceFromMask((
    '[#10 ]', ), ), number=5)
mdb.models['Model-1'].parts['foundation'].deleteMesh(regions=
    mdb.models['Model-
1'].parts['foundation'].edges.getSequenceFromMask((
    '[#1 ]', ), ))
mdb.models['Model-
1'].parts['foundation'].seedEdgeByNumber(constraint=FINER,
    edges=mdb.models['Model-
1'].parts['foundation'].edges.getSequenceFromMask((
    '[#7 ]', ), ), number=5)
mdb.models['Model-1'].parts['foundation'].generateMesh()
mdb.models['Model-1'].parts['foundation'].deleteMesh(regions=
    mdb.models['Model-
1'].parts['foundation'].faces.getSequenceFromMask((
    '[#1 ]', ), ))
mdb.models['Model-
1'].parts['foundation'].seedEdgeByNumber(constraint=FINER,
    edges=mdb.models['Model-
1'].parts['foundation'].edges.getSequenceFromMask((
    '[#4 ]', ), ), number=3)
mdb.models['Model-
1'].parts['foundation'].seedEdgeByNumber(constraint=FINER,
    edges=mdb.models['Model-
1'].parts['foundation'].edges.getSequenceFromMask((
    '[#2 ]', ), ), number=3)
mdb.models['Model-
1'].parts['foundation'].seedEdgeByNumber(constraint=FINER,
    edges=mdb.models['Model-
1'].parts['foundation'].edges.getSequenceFromMask((
    '[#10 ]', ), ), number=6)
mdb.models['Model-1'].parts['foundation'].generateMesh()
```

Figure B.1 Python code for soil-foundation interaction model

Python script to change the vertical force on superstructure.

```
        import section
        import regionToolset
```

```
        import part
        import material
        import assembly
        import step
        import interaction
        import load
        import mesh
        import optimization
        import job
        import sketch
        import visualization
        import xyPlot
        import displayGroupOdbToolset as dgo
        import connectorBehavior
        mdb.models['Model-1'].loads['Load-
3'].setValues(cf1=1600, cf2=-76885.0,)
```

Figure B.2 Typical Python script to change the Vertical force on the structure

Python Script to extract moment and rotation data at a particular node

```
        import section
```

```
        import regionToolset
        import displayGroupMdbToolset as dgm
        import part
        import material
        import assembly
        import step
        import interaction
        import load
        import mesh
        import optimization
        import job
        import sketch
        import visualization
        import xyPlot
        import displayGroupOdbToolset as dgo
        import connectorBehavior
        session.xyDataListFromField(odb=odb,
outputPosition=NODAL, variable=(('RM3',
            NODAL),), nodeSets=('SET-6', ))
        xyList = xyPlot.xyDataListFromField(odb=odb,
outputPosition=NODAL, variable=((
            'RM3', NODAL),), nodeSets=('SET-6', ))
        xyp = session.xyPlots['XYPlot-1']
        chartName = xyp.charts.keys()[0]
        chart = xyp.charts[chartName]
        curveList = session.curveSet(xyData=xyList)
        chart.setValues(curvesToPlot=curveList)
        session.viewports['Viewport:
1'].setValues(displayedObject=xyp)
            session.viewports['Viewport:
1'].setValues(displayedObject=odb)
        session.viewports['Viewport:
1'].odbDisplay.display.setValues(plotState=(
            CONTOURS_ON_DEF,))
```

Figure B.3 Python script to process and save moment and rotation

REFERENCES

[1]Klein, R. J., Nicholls, R. J., Ragoonaden, S., Capobianco, M., Aston, J., and Buckley, E. N. (2001). Technological options for adaptation to climate change in coastal zones. *Journal of Coastal Research*, 531-543.

[2] Michener, W. K., Blood, E. R., Bildstein, K. L., Brinson, M. M., and Gardner, L. R. (1997). Climate change, hurricanes and tropical storms, and rising sea level in coastal wetlands. *Ecological Applications*, *7*(3), 770-801.

[3] Savonis, M. J., Burkett, V. R., and Potter, J. R. (2008). *Impacts of climate change and variability on transportation systems and infrastructure*: Gulf Coast study, phase I: US Climate Change Science Program.

[4] FEMA. (April 2006). *Summary Report on Building Performance, Hurricane Katrina 2005*, Federal Emergency Management Agency report 548.

[5] FEMA. (2006a). *Hurricane Katrina in the Gulf Coast Summary: Observations, recommendations, and technical guidance*, Federal Emergency Management Agency549, March.

[6] FEMA. (2006b). *Summary report on building performance: Hurricane Katrina 2005*, Federal Emergency Management Agency548.

[7] Padgett, J., DesRoches, R., Nielson, B., Yashinsky, M., Kwon, O.-S., Burdette, N., and Tavera, E. (2008*). Bridge damage and repair costs from hurricane katrina*. *Journal of Bridge Engineering*, *13*(1), 6-14.

[8] Kaufman, A., and Gallaher, T. (2008). *Deflecting the wave: Can coastal vegetation assist in mitigating Tsunami and Storm surge damage*: The Tropical Landscape and Human Interaction Lab, University of Hawaii.

[9] Coastal Change hazards: Hurricanes and Extreme Storms, Hurricane Sandy. (2012). Retrieved April 15, 2014, from http://coastal.er.usgs.gov/hurricanes/sandy/

[10] Hashash, Y. M. A., Nikolaou, S., Sukumaran, B., Sacks, A., Burlingame, M., Baxter, C., . . . O'Rourke, T. (2013). *Field Reconnaissance of Geotechnical Aspects of October 2012 Hurricane Sandy along the US East Coast*, Geo-Engineering Extreme Events Reconnaissance (GEER) Association, Report No. GEER-032, Version 1.

[11] Caraballo-Nadal, N. C., Zapata-Lopez, R. E., and Pagan-Trinidad, I. (2006). Building damage estimation due to riverine floods, storm surges and tsunamis: A proposed methodology. Proceeding of the 4th LACCEI International Latin American and Caribbean Conference for Engineering and Technology (LACCET'2006)"Breaking Frontiers and Barriers in Engineering: Education, Research and Practice.

[12] ORNL (Oakridge National Laboratory), (2011). Floodproof Construction: Working for Coastal Communities, SERRI (Southeast Region Research Initiative) Report 80024.

[13] Richardson, E. V., and Davis, S. R. (2001). Evaluating Scour at Bridges. Federal Highway Administration, Hydraulic Engineering Circular No. 18. *Publication FHWA NHI*, 01-001.

[14] Mylonakis, G., Nikolaou, S., and Gazetas, G. (2006). Footings under seismic loading: Analysis and design issues with emphasis on bridge foundations. *Journal ofSoil Dynamics and Earthquake Engineering, 26*(9), 824-853.

[15] Tileylioglu, S.(2008) "*Evaluation of soil-structure interaction effects from field performance data,"* Doctoral Dissertation, University of California Los Angeles, 2008: ProQuest.

[16] Chopra, A. K. (1995). *Dynamics of structures* (Vol. 3): Prentice Hall New Jersey.

[17] Veletsos, A. S., and Meek, J. W. (1974). Dynamic behaviour of building‐foundation systems.*Journal of Earthquake Engineering and Structural Dynamics*, 3(2), 121-138.

[18] Chen, Z., Trombetta, N., Hutchinson, T., Mason, H., Bray, J., and Kutter, B. (2013). Seismic System Identification Using Centrifuge-based Soil-Structure Interaction Test Data. *Journal of Earthquake Engineering, 17*(4), 469-496.

[19] Luco, J. E., Trifunac, M. D., and Wong, H. L. (1987). On the apparent change in dynamic behavior of a nine-story reinforced concrete building. Bulletin of the Seismological Society of America, 77(6), 1961-1983.

[20] Pitilakis, K. D. (2007). Earthquake Geotechnical Engineering: 4th International Conference on Earthquake Geotechnical Engineering-Invited Lectures, Springer.

[21] Stewart, J. P., Fenves, G. L., and Seed, R. B. (1999). Seismic soil-structure interaction in buildings. I: Analytical methods. *Journal of Geotechnical and Geoenvironmental Engineering, 125*(1), 26-37.

[22] Meek, J. W., & Wolf, J. P. (1994). Cone models for embedded foundation.*Journal of Geotechnical Engineering*, *120*(1), 60-80.

[23] Gerolymos, N., and Gazetas, G. (2006a). Development of Winkler model for static and dynamic response of caisson foundations with soil and interface nonlinearities. *Journal ofSoil Dynamics and Earthquake Engineering*, *26*(5), 363-376.

[24] Gerolymos, N., and Gazetas, G. (2006b). Static and dynamic response of massive caisson foundations with soil and interface nonlinearities—validation and results. *Journal ofSoil Dynamics and Earthquake Engineering*, *26*(5), 377-394.

[25] Taciroglu, E., Rha, C., and Wallace, J. W. (2006). A robust macroelement model for soil–pile interaction under cyclic loads. *Journal of Geotechnical and Geoenvironmental Engineering, 132*(10), 1304-1314.

[26] Cremer, C., Pecke. Cyclic macro−element for soil–structure interaction: material and geometrical non−linearities. *International Journal for Numerical and Analytical Methods in Geomechanics, 25*(13), 1257-1284.

[27] Khodabakhshi, P., Jahankhah, H., and Ghannad, M. (2011). A discrete model for response estimation of soil-structure systems with embedded foundations. *Journal of Earthquake Engineering and Engineering Vibration, 10*(2), 263-276.

[28] Description of Cam-Clay and Modified-Cam-Clay Critical State Strength Models". (2014). from http://www.rocscience.com/help/phase2/webhelp/pdf_files/theory/CamClay.pdf.

[29] Homles, R., Chen, Z., Tripathi, R., and Chen, J. *1-g Scale Hydraulic Flume-based Soil-Fluid-Structure Model Testing and Evaluation of Surging and Scouring Effects.* Paper presented at the Structures Congress 2013@ sBridging Your Passion with Your Profession.

[30] Hamann, T., and Grabe, J. (2013). A simple dynamic approach for the numerical modelling of soil as a two-phase material. *geotechnik, 36*(3), 180-191.

[31] Zienkiewicz, O. C., Chan, AHC., Pastor, M., Schrefler, BA., and Shiomi, T (1999). Computational geomechanics, Wiley Chichester.

[32] Qin, X., Chen, S., andZeng, X. "Analysis of fluid-saturated porous media in two dimensions under earthquake load."

[33] Oka, F. and S. Kimoto (2012). *Computational modeling of multiphase geomaterials*, CRC Press.

[34]Ti, K. S., Huat, B. B., Noorzaei, J., Jaafar, M. S., and Sew, G. S.(2009). "A review of basic soil constitutive models for geotechnical application." Electronic Journal of Geotechnical Engineering **14**: 1-18.

[35] Helwany, S. (2007). Applied soil mechanics with ABAQUS applications, John Wiley & Sons.

[36] "Systèmes, D. (2012). "Abaqus 6.12 Theory Manual." Dassault Systèmes Simulia Corp., Providence, Rhode Island.

[37] Gazetas, G., Panagiotidou, A. I., and Gerolymos, N. (2010). Pushover and inelastic-seismic response of shallow foundations supporting a slender structure. Proceedings of the 5th international conference on recent advances in geotechnical earthquake engineering and soil dynamic, San Diego, CA.

VITA

Rahul Tripathi was born in Udaipur, India in 1987. He attended University College of Engineering, Kota, India for his Bachelor's degree in Civil Engineering. Following graduation he worked as faculty member in engineering and diploma colleges.

He joined University of Missouri-Kansas City in fall semester 2012 to pursue his Master's in Civil Engineering with a focus on Structural Engineering. He was awarded graduate research assistantship from the Civil Engineering Department to identify surge and scour impact on Civil structures, along with small-scale testing, identification and soil-fluid-structure simulation. He is currently working on practical training as a structural engineer with Sterling Engineering Group of Compaines in St.Louis, Missouri.

He plan to utilize his research and educational knowledge and past professional experience in pursuing a career in Structural Engineering.